Synthesis of a Novel Fluorescent Optical pH Sensor

Maryam Norouzbahari

Submitted to the
Institute of Graduate Studies and Research
in partial fulfillment of the requirements for the Degree of

Master of Science
in
Chemistry

Eastern Mediterranean University
August 2011
Gazimağusa, North Cyprus

Approval of the Institute of Graduate Studies and Research

Prof. Dr. Elvan Yılmaz
Director

I certify that this thesis satisfies the requirements as a thesis for the degree of Master of Science in Chemistry.

Prof. Dr. Mustafa Halilsoy
Chair, Department of Chemistry

We certify that we have read this thesis and that in our opinion it is fully adequate in scope and quality as a thesis for the degree of Master of Science in Chemistry.

Prof. Dr. Huriye İcil
Supervisor

Examining Committee

1. Prof. Dr. Huriye İcil
2. Assoc. Prof. Dr. Hamit Caner
3. Asst. Prof. Dr. Nur Paşaoğulları Aydınlık

ABSTRACT

In today's high technological applications organic materials were widely employed in many sensing architectures. Plenty of ongoing research shows the importance and necessity of smart organic compounds with profound optical, photophysical, and electrochemical properties to apply in the industry.

Perylene dyes are well known dyes with unique optical properties in conjunction with outstanding stabilities and are widely applied in many photonic applications. Benzopurpurin 4B is a purpurin derivative known as a textile dye has a pH sensing ability. The combination of these two interesting materials led to an excellent fluorescent optical pH sensor with great characteristics.

Here in, we report the design, synthesis and characterization of a novel fluorescent optical pH sensing perylene derivative (Di-*N*-(4-hydroxyphenyl)-3,4,9,10-perylenetetracarboxy monoimide chrmophores containing benzopurpurin-4B) based on a perylene monoimide, N-(4-Hydroxyphenyl)-3, 4, 9, 10-perylene tetracarboxylic-3, 4-anhydride-9, 10-imide (OH-PMI), and benzopurpurin 4B. The synthesized compound was well characterized by FTIR, Mass, Elemental, UV-vis, Emission, DSC, and TGA techniques.

BP-OHPDI has shown interesting pH sensing property in addition to the high thermal stability. It has shown mostly two colors at day light; violet in acidic solutions (pH=1–3) and pink-violet in organic solvents with a gradual increase in pH (up to 9). On the other hand, in sulfuric acid (pH=0) the color of the solution is dark blue. Under UV light at 365 nm, except in acidic solutions the color was mostly fluorescent yellow and fluorescent greenish-yellow. Interestingly, in acidic solutions

under 365 nm, the color was intense orange. On the other hand, in sulfuric acid intense red color was observed.

Keywords: Perylene, benzopurpurine 4B, pH sensor, plasma stain

ÖZ

Perilen boyaları eşsiz optik özelliklerinin yanında, olağanüstü kararlılıkları ile özellikle fotonik uygulamalarda oldukça yaygın olarak kullanılan boyar maddelerdir. Bir purpurin türevi olan ve tekstil boyası olarak bilinen Benzopurpurin 4B aynı zamanda pH algılama özelliğine de sahiptir. İlgi çekici olan bu iki boyar maddenin birleştirilmesi önemli karakteristik özelliklere sahip mükemmel bir fluoresans optik pH algılayıcı elde edilmesine neden olmuştur.

Bu çalışmada, perilen monoimit, N-(4-Hidroksifenil)-3,4,9,10-perilentetrakarboksilik-3,4-anhidrit-9,10-imit (OH-PMI), ve benzopurpurin 4B kullanılarak tasarlanan yeni bir fluoresans optik pH algılayıcı perilen türevi (Di-*N*-(4-hydroxyphenyl)-3,4,9,10-perylenetetracarboxy monoimide chrmophores containing benzopurpurin-4B) sentezlenmiş ve karakterize edilmiştir. Sentezlenen bu madde FTIR, elementel analiz, UV-vis, emisyon, DSC ve TGA teknikleri ile tanımlanmıştır.

BP-OH-PDI yüksek termal kararlılığının yanında ilgi çekici pH algılayıcı özellik göstermiştir. Özellikle gün ışığında iki renk vermektedir. Asidik çözgenlerde (pH=1–3) menekşe renk verirken organik çözücülerde aşamalı artırılan pH'lerde (pH=9'a kadar) pembe-menekşe renk vermektedir. Buna karşılık, sülfürik asitte (pH=0) çözeltinin rengi koyu mavidir. 365 nm UV ışığı altında asidik çözeltiler hariç fluoresans sarı ve fluoresans yeşil-sarı renk vermektedir. İlgi çekici olarak, 365 nm'de asidik çözeltilerdeki rengi yoğun turuncudur. Buna karşılık, sülfürik asitte yoğun kırmızı renk gözlemlenmiştir.

Anahtar Kelimeler: Perilen, benzopurpurine 4B, pH algılayıcı, plazma renklendirici

To My Lovely Family

ACKNOWLEDGMENTS

First and foremost, I would like to state my great thanks to my supervisor **Prof. Dr. Huriye İcil** for her tireless and ongoing support during my Master thesis and research. Her supervision aided me in all the time of research and writing of this thesis.

The pleasure, enthusiasm, patience she has for research has always been motivational for me. I could never imagine such a scientist and at the same time she is friendly and open heart lady being a supervisor of my thesis. In fact it is an honor for me to work with her.

I would like to thank my fellow group-mates in Organic Chemistry group of Eastern Mediterranean University: Dr. Jagadeesh Babu Bodapati, Dr. Duygu Uzun, Dr. Süleyman Aşır, Hürmüs Refiker, Abimbola A. Ololade, İlke Yücekan, and Maryam Pakseresht for several perceptive and stimulating discussions and conversations during this thesis, for the times we spent together, and for all the memorable funs we have had during last two years.

I would like to give my grateful acknowledgement to the funding sources (TUBITAK Organization) which made my Master work possible by supporting our research group.

Last but not the least, I would like to thank my family; my parents for supporting me throughout my life.

TABLE OF CONTENTS

LIST OF TABLES

LIST OF FIGURES

LIST OF ILLUSTRATION

LIST OF SYMBOLS/ABBREVIATIONS

Å:	Armstrong
A:	Absorption
AU:	Arbitrary unit
Bp- 4B:	Benzopurpurin 4B
C:	Concentration
Calcd.:	Calculated
DMAc:	Dimethylacetamid
DMF:	Dimethylformamide
DMSO:	Dimethyl sulfoxide
DSSC:	Dye sensitized solar cells
ε:	Molar absorption coefficient
$\varepsilon_{max:}$	Maximum Extinction coefficient / Molar absorptivity
$E_{1/2}$:	Half- Wave potential
F:	Oscillator Strength
FT – IR:	Fourier transform infrared spectroscopy
h:	Hour
HOMO:	Highest occupied molecular orbital
IR:	Infrared spectrum/ spectroscopy
k_d:	Rate constant of radiationless deactivation
k_f :	Fluorescent
l:	path length
LUMO:	Lowest unoccupied molecular orbital

M:	Molar concentration
max:	Maximum
min:	Minimum
mmol:	Millimole
mol:	Mole
NMP:	*N*-methylpyrrolidinone
Φ_f:	Fluorescence quantum yield
PDA:	Perylene 3, 4, 9, 10-tetracarboxylic dianhydride
PDI:	perylene diimide
Std. :	Standard
τ_0:	Theoretical radiative lifetime
t:	Time
TCE:	1,1,2,2-tetrachloroethane
TFAc:	Trifluoroacetic acid
TGA:	Thermogravimetric analysis
THF:	Tetrahydrofuran
UV:	Ultraviolet
UV-vis:	Ultraviolet visible light absorption
$\bar{\vartheta}$:	Wavenumber
$\Delta\upsilon_{1/2}$:	Half-width (of the selected absorption)
$\bar{\upsilon}_{max}$:	Maximum wavenumber
λ:	Wavelength
λ_{exc}:	Excitation wavelength
λ_{em}:	Emission wavelength

Chapter 1

INTRODUCTION

For the first time, Kardos discovered the perylene dyes in 1913. They have a great potential towards several applications, in general, in paints industry, textiles, plastics, molecular architectures, electronic devices and solar cells, etc. In conjunction with the high quality applicabilities, perylene dyes, in general, are having high fluorescent quantum yields making them useful in many photonic applications. Keeping all the potential applications, perylene dyes are termed as 'functional dyes' (Langhals, H., PUST, T., 2005). The extremely fluorescence character of a perylene diimide was not revealed until 1959 by Geissler and Remy (Posch H.E, Wolfbeis O.S 1998) as a result of their low solubility founded by the strong π-π stacking interactions (Figure 1.1). Later, it was found that the substituents at the nitrogen can control the solubility of the dyes and thus optical properties. However, the subjects of inertness and low solubility of perylene dyes are also advantageous in pigment applications.

Briefly, the perylene dyes can be defined as the universal building blocks of synthesis (especially for the synthesis of multichromophoric materials) because of possessing several unique properties and stabilities.

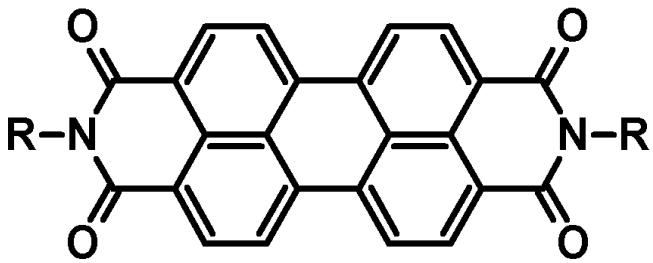

Figure 1.1: A General Structure of a Symmetrical Perylene Diimide

High fluorescence quantum yields, high photo stability, high thermal stability (in general higher than 550°C), electrochemical stability and reversibility, photochemical stability and chemical inertness are demonstrated by perylene dyes. The anhydride groups present in the structure of perylene give the opportunity to tailor the compounds by the substitution and thus forming imide functional groups. The substituents attaching at the nitrogen atoms can control the solubility of the dyes and other properties. The modification of the dyes provides several interesting opto-, photo- physical properties and are still searched in detail for design and preparation of molecular and opto- electronic devices. Bathochromic shift is related to the electronic interface of the π-systems and therefore light emitting property of perylene dyes and their attached backbone π-systems provide different colorful compounds by the emission of different colors. It is therefore of prime interest to obtain easily prepared perylene dyes with high fluorescent quantum yields (Icil H, Arslan, E., 2001). Novel research illustrates that perylene dyes have usage as indicators of relative humidity in optical sensors as well (Posch H.E, Wolfbeies O.S 1998).

Benzopurpurin-4B shown in Figure 1.2 is well known as a red acid and textile dye. It has a pH sensing ability by showing different colored solutions at different pH values. It is also known as an effective staining agent. Stains are frequently used in biology and medicine to highlight structures in biological tissues for viewing, often with the aid of different microscopes (Mckitterick, C. B., et al).

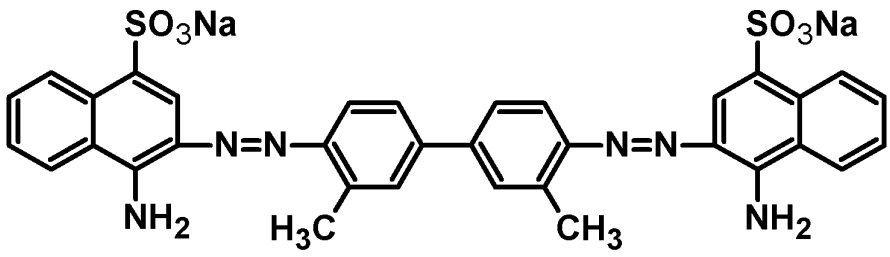

Figure 1.2: Structure of Benzopurpurin – 4B

Due to their outstanding applications in biological sciences and technologies, ecology, and medicine; the design and development of optical sensors have grown rapidly with great interest. Moreover, the research proved (Misra and et al. 2000) that they are useful in diagnosing cancer as the sensor has a capability of indicating the cancerous cells. Optical pH sensors are one of the greatest devices that can differentiate the damaged cells from the healthy cells as the level of acidity differs. The first fluorescence based pH sensors were reported in 1982 by Saari. Peterson in 1990 reported the initial optical pH sensors. The sensors made of the absorbance dye, phenol red was applied for evaluation in blood pH in-vivo and in vitro (Misra and et al. 2000).

Several research papers indicate the design and importance of optical fluorescent pH sensors. Acriflavine and Rhodamine 6G combination and their excitation energy transfer studies leading to the pH sensing ability was discussed by Misra and et al. in 2000, and a similar study based on nafion film was reported in 2002 (Misra, V., et al. 2000, 2002). A Fiber-optic pH sensor was developed and evaluated based on excitation of evanescent wave (Xiong, Y., et al. 2010). The pH sensing range was limited to the range of pH 2.09 to 8.85, where as the linear range was reported as 3.25 to 8.85. A novel optical pH sensor for high and low pH values was reported by Safavi and Bagheri (Safavi, A., Bagheri, M., 2003). A pH sensing fluorescent dye as a probe for proton uptake in photosynthetic reactions was studied by Agostiano and et al (Agostiano., A., et al. 2004),(Shi, W., et al.2010) reported the optical pH sensor based on fluorescein intercalated double layered hydroxide. Some pH sensors were also developed on the basis of sol-gel doping method (Austin, E., and et al. 2002), (Ahmad, M., Tan, T.W., 2001), (Wencel, D., et al. 2007), and (Lee, S.T., et al. 2001). Some solid-state pH sensor was also developed by Lau and et al (Lau, K.T., et al. 2006).

In previous researchs, it is affirmed that among the most promising studied, manufactured and tested sensing elements for an optical sensor is based on Benzopurpurin-4B to monitor the acidity of solutions for etching electronic boards. On the other hand, perylene dyes and derivatives were also proved as most promising fluorescent materials with diverse optical properties in conjunction with stabilities. Therefore, a combination of perylene derivative and purpurin derivative can lead to a potential fluorescent optical pH sensor.

It is the goal of this project to design and characterize the molecular architecture of a novel fluorescent optical pH sensing material based on a perylene monoimide derivative and a dye molecule, benzopurpurin 4B. The potential pH sensing product (BP-OHPDI) was characterized in detail by IR, elemental, UV-vis, emission, excitation, DSC, and TGA measurements.

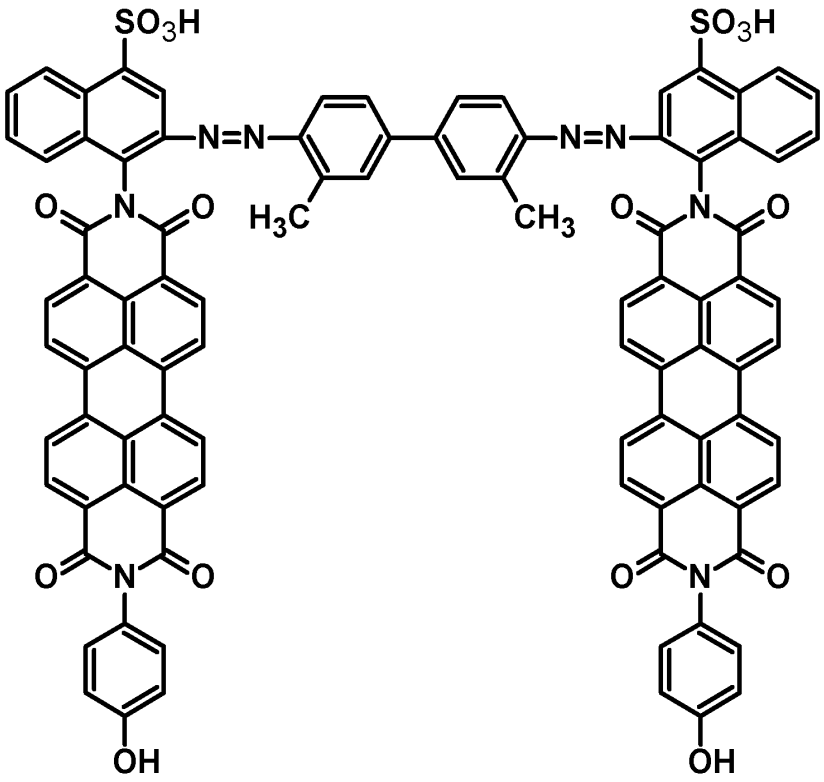

Figure 1.3: Chemical Structure of a Novel Fluorescent Optical pH Sensor [(Di-*N*-(4-hydroxyphenyl)-3,4,9,10-perylenetetracarboxy monoimide chrmophores containing benzopurpurin-4B (BP-OHPDI)] Based on Perylene and Benzopurpurin

Chapter 2

THEORETICAL

2.1 Perylene Dyes

Perylene dyes have got distinctive attention due to their outstanding characteristics like very high lightfastness, strong fluorescence, excellent photoluminescence (corresponds to fluorescence quantum yield near unity), and wide absorption encompassing visible to near infrared. They are capable of light conversion and collection which are the key factors relating to photovoltaics and therefore making the perylene dyes applicable in organic photovoltaic cells, artificial photosynthesis and dye sensitized solar cells (DSSCs) (Heinz Langhals and Tim Pust 2010), (Wen-Ke F et al. 2010). In fact, perylene dyes are having numerous high status applications industrially; as red vat dyes, as pigments most particularly in automotive finishes, in many molecular and electronics and in organic photonics, etc (Würthner, F., 2004), (Ahrens, M.J., et al. 2003).

Because of their above potential applications in various fields resulting from their unusual favorable combinations of optical and redox properties, unique thermal, mechanical, photochemical, and electrochemical stabilities; diverse derivatives of perylene dianhydride (both symmetrical and unsymmetrical) including perylene-3, 4, 9, 10-bis (dicarboximides) [perylene diimides (PDIs)], perylene monoimides and perylene polyimides have been investigated with great interest in recent years. It will not be an exaggeration to conclude that the perylene mono-, di- imides are the best

fluorophores available for single molecule spectroscopy at present (Würthner, F., 2004).

In addition to the conventional utilizes in high technological applications, perylene derivatives are employed in photodynamic therapy and in stabilization of G-quadruplex DNA (Dinçalp, H., et al. 2007).

2.1.1 Structural Properties

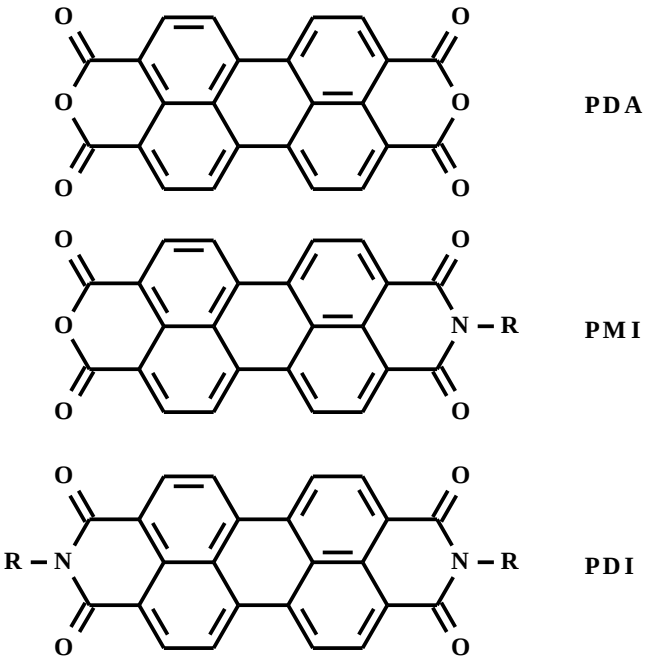

Figure 2.1: Chemical Structures of a Perylene Dianhydride (PDA), A General Perylene Monoimide (PMI), and A General Perylene Diimide (PDI)

The chemical structure of perylene-3,4,9,10-tetracarboxylic dianhydride (PDA) reveals the possibility of synthesizing various perylene derivatives where the dianhydride carbonyls can be converted to imide- carbonyls (shown in the structure of PDI) by using different amine functional group substituents. Therefore, the properties can be changed according to the necessity by the easy tailoring of substituents.

As shown in the general chemical structure of a PDI, the four carbonyls present bring the electron accepting property and hence perylene derivatives/dyes undergo rapid electron transfer and acts like a substantial electron acceptor (Wen-Ke, F., et al . 2010). The electron accepting property together with high stabilities mentioned of these compounds made them superior in the field of electronics. Recent studies indicate that they are the best *n*-type semiconductors available. Therefore, perylene dyes are thus promising for electronic applications such as organic field effect transistors (OFETs) due to the electron affinity of these compounds.

The photophysical/optical properties arise from the π-π interactions of the conjugated perylene ring and related attached back bone of perylene are exciting and even fluorescence quantum yields near unity were recorded. The high fluorescence has provided extensive research on perylene dyes to explore the photo/light- induced electron and energy transfer processes. The light emitting capacity of these dyes make them applicable in laser dyes, organic light emitting diodes (OLEDs), and fluorescent light collectors. Multichromophoric perylene dyes are much more exciting with great optical properties. The systems that are possessing matching electron-donating and electron-withdrawing groups are highly favorable in the production of dye sensitized solar cells because of promising photoinduced energy and electron transfer processes.

Dyads with suitable electron donor compounds, electron acceptor perylene compounds are promising light harvesting systems and nowadays a plenty of research is going on. One of the important critical factors concerning these dyads is the rate of photoinduced electron-transfer. This factor is influenced by some parameters like the matching of donor and acceptor energy levels (HOMO/LUMO),

the molecules configuration, length and conjugation of the bridges, and the solvent environment (Wen-Ke F, et al. 2010). Charge separation and charge injection processes are the key factors in DSSCs and are related to the HOMO/LUMO energy distributions. In order to improve the photovoltaic performance of the dye, there should be an optimum HOMO/LUMO orbital separation which can help to enforce charge injection immediately from the excited state of dye to the conduction band of metal oxide (Dinçalp, H., et al. 2010).

Light emitting capacity with different colors and high fluorescence quantum yields of perylene dyes opened the doors of photonics applications. According to Asir and co-authors, a balance should be established between the solubility and stack forming ability caused by the extended overlap of intermolecular π orbitals of perylene dyes to better find applications in the field of photonics. The tailoring of the compounds should not omit corresponding photochemical, electrochemical, and thermal stabilities while concentrating the optical properties so that the perylene derivatives will bring bright future in the field of photonics (Asir, S., et al. 2010).

Perylene bisimide dyes show the properties of self-assembly and can form the supramolecular architectures. The feature article of Würthner reveals complete details of perylene bisimides and their supramolecular organization (Würthner, F., 2004). Moreover, Chen and co-authors expressed the increasing interest on ordered PDI assemblies based on non-covalent interactions instead of the covalent linkages. Non-covalent interactions such as static electronic interactions, hydrogen bonding, van der Waals forces, metal-ligand coordinations and intermolecular/intramolecular π-π interactions greatly govern the supramolecular ordered perylene-diimides assemblies and their respective characteristics (Chen Y, et al . 2009).

2.2 Benzopurpurin (Bp-4B)

An azo dye, Benzopurpurin 4B is also known as 'Direct Red 2' (shown in Figure 2.2) which has two nitrogen double bonded (N=N) groups and a sulfonic group in its chemical structure. Bp-4B has a great adsorbent potential as it comes under the category of direct adsorbent dye class and therefore it can be employed to deposit on the fibers directly without any assistance of other chemical compounds.

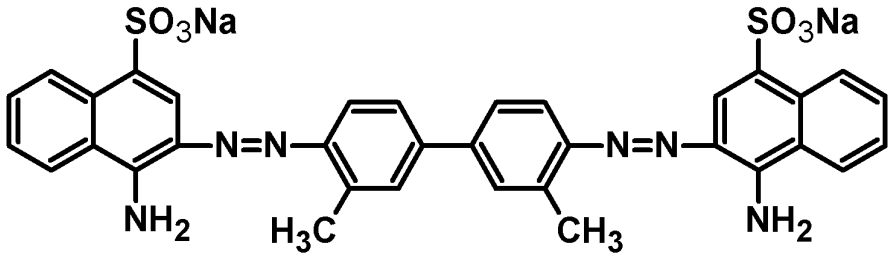

Figure 2.2: Chemical Structure of Benzopurpurin 4B – A Planar View

Considering different azo group of dyes, likely mono-, di-, tri-, and poly- azo, are said to be the largest group of dyes exist currently. As an approximate number, it is estimated about 26000 dyes exist by 2008. In fact, azo compounds were proved as carcinogenic and several experiments conducted on animals supported the carcinogenetic property of these dyes. It was reported that they are carcinogenic toward human being as well. Specifically, direct azo dyes were in wide spread use in textile and related industries which causes environmental concern. The degradation of these dyes delivers the toxic aromatic amines and especially the removal rate during aerobic waste treatment is very low. Environment and human health are interconnected and related to adsorption by solids. The final result could be

detrimental towards life and hence there is necessity to produce adsorbents that are relatively cheap and can be applied to water pollution control (Zohra, B., et al. 2008). Rashwan and et al. stressed the adverse antinutagenicity and genotoxic effects of purpurin and related naturally available derivatives of purpurin (Rashwan, F.A., et al. 2005).

2.2.1 Properties of Bp-4B

The two sulfonic groups present in the chemical structure of Bp-4B provide the solubility of the compound in aqueous medium. The solubility in aqueous medium in combination with the adsorption property, Bp-4B was used as a model compound in many adsorption studies. Zohra and et al. studied the adsorption and desorption properties of organic molecules (includes benzopurpurin) in the clays. In their study, their model organoclay posses low surface areas and in fact acts as a separation media in the sorption. By increasing the temperature, the adsorption of the dye benzopurpurin 4B tends to increase showing that the adsorption occurs chemically. This behavior most likely supports the chemisorption principle which explains the relation between rate of adsorption and temperature, where it states that increase in temperature causes increase in amount of dye due to the decrease in corresponding desorption mechanism (Zohra, B., et al. 2008).

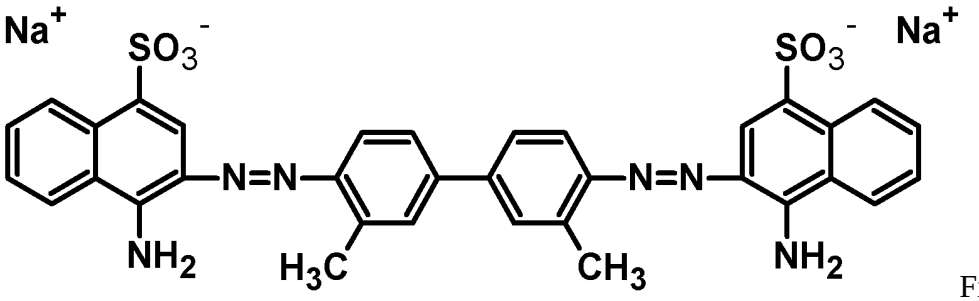

Figure 2.3: A Chromonic Liquid Crystal – Benzopurpurin- 4B and its Molecular Structure

Benzopurpurin-4B is also a chromonic liquid crystal and as shown in Figure 2.3, the shape of the crystal is in general a plank or disk shape rather than a rod shape. As shown in the figure, either end of the molecule does not possess clustered hydrophilic or hydrophobic groups.

According to the simple general theory where any two molecules can bond together and begin to form aggregates, chromonic molecules do the same with no exception. They do form aggregates at low concentrations and therefore different sizes of aggregates are possible. Furthermore, changes in enthalpy and entropy in association with intermolecular bonding interactions encourage the aggregate formation, especially, entropy catalyzes aggregate formation of amphiphillic and enthalpy promotes aggregation of chromonic molecules.

The aggregate formation ability of chromonic liquid crystals even at low concentrations can cause the solution to have anisotropic aggregates, but they may not align and form a macroscopically anisotropic phase. Thus the phase transition will only occur when aggregates grow large enough that interactions between aggregates force them to align (Figure 2.4).

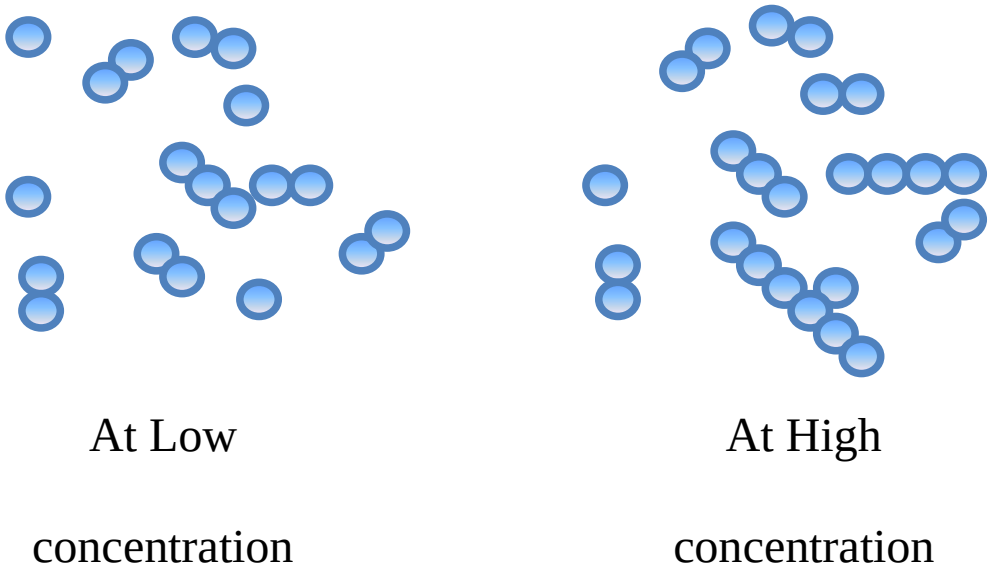

Figure 2.4: Formation of Aggregates at Low and High concentrations in a Traditional Chromonic Liquid Crystal

At lower concentration, formation of aggregates occurs but do not form the liquid crystal phase. At higher concentration, the formed aggregates align together as they are large enough to align, but there exists ‘a range’ of aggregate sizes in both cases (Figure 2.4) (McKitterick C.B., et al. 2010). The authors (Mckitterick, C.B., et al. 2010) reported that benzopurpurin 4B forms micrometer sized aggregates even at low concentrations in aqueous solutions. They (Mckitterick, C.B., et al. 2010) reported that a chromonic liquid crystal phase in general is stable below the concentrations as low as 0.4 wt% at room temperature only if the formed aggregates contain an ample amount of water (Mckitterick, C.B., et al. 2010).

Bp-4B acts as a pH sensor and the pH studies were reported in many papers. Shtykov and et al. reported the protolytic properties of Bp-4B in both water and in surfactant solutions as it is a well known amphoteric compound and exhibits both acidic and basic properties in the pH range 1-6 (Shtykov S. N., et al. 2004). They focused on

the preparation of a sensing element of Bp-4B for an optical sensor. Zohra, B., et al. studied the pH dependent color change of Bp-4B. It was reported that initially prepared dye solutions and their initial pH values considerably affect the chemistry of dye molecule. Among the solutions with pH range 2-13, the color of the solutions and their absorbance data were stable and unchanged over the pH range 3-11 after passing 1 hr of preparation of solutions. At pH below 3 and above 11, the color and the form of solutions were changed indicating the change in molecular form of Bp-4B; where below pH 3, the color was changed from dark red to dark blue with a suspension containing lot of fine particles and above pH 11, there was a change in degree of original red color. A similar result was also reported by Acemioglu (Acemioglu, 2004).

2.2.2 Applications of Bp-4B

The pH sensing ability, direct dying and adsorption ability, and chromonic liquid crystalline properties of Bp-4B were widely used industrially. Fabrication of a sensing element of Bp-4B for an optical sensor and thereby controlling acidity of various solutions for etching electronic boards was already discussed (Shtykov S. N., et al. 2004).

Maruthamuthu M., et al. explained the binding properties of dyes such as Bp-4B, Evans Blue, and Trypan Blue and their practical relevance as they are possessed some biological applications such as- in staining of plasma (especially Bp-4B was used), in determination of blood volume (especially Evans Blue was used), and in staining of reticuloendothelial system (especially trypan Blue was used) (Maruthamuthu M., et al. 1990).

In the study of Bhat and et al., they have explained the applicability of benzopurpurin and its related compounds and their inhabitance binding of gp120 to galactosyl sulfatide/ceramide and immunodeficiency virus infection of human (Bhat, S., et al. 1994).

2.3 Introduction to Fluorescence

In general, fluorescence is referred to the emission of bright light with a particular color. In the scientific language, photochemistry explains the process of fluorescence as a radiative method of deactivation of energy of a molecule from an electronically excited singlet state to the ground state (shown in Figure 2.6, Jablonski Diagram). The color of the emitted light depends on the wavelength of emission. In the following picture, Figure 2.5, a fire fly delivers natural fluorescent emission with colors yellow, green and light-red.

Figure 2.5: Fire fly, an example of natural fluorescence; which gives yellow, green, or pale-red with wavelengths from 510-670 nm (medgadget.com)

It is a well known fact that the fluorescence and its related colored light emissions of the compounds could find applications everywhere. Especially in biology, fluorescence is widely employed for deep tissue imaging, fluorescence labeling, and in several biological medical diagnostics applications. Spectral characterization of various biological/synthetic/natural materials and their modified systems by fluorescence spectroscopy and time-resolved fluorescence techniques became one of the most important research tools in several research areas. Applicability of fluorescent materials and their corresponding ongoing research in electronic and molecular systems can be declared as most exciting research fields emerging with great interest industrially. To name a few other important applications of fluorescence and fluorescent materials include forensics, DNA sequencing, flow cytometry, and genetic analysis (Lakwicz J. R., 2006).

In 18^{th} century, some scientific reports were reported on luminescence by Sir J. F. W. Herschel and Sir G. G. Stokes. Stokes found that the light emitted by quinine has a longer wavelength than the corresponding absorption wavelength, which is later termed as Stokes' shift and considered the concept as a fundamental property of fluorescence.

After a long 70 years, a new theoretical understanding on Stoke's result was developed by A. Jablonski, who was considered as father of fluorescence for all of his efforts on developing the concept of fluorescence and anisotropy. His investigations helped the development of various concepts of photophysics. The famous Jablonski diagram shown in Figure 2.6 explains the fundamental terms and various important photophysical processes, all embedded in one single diagram to understand better.

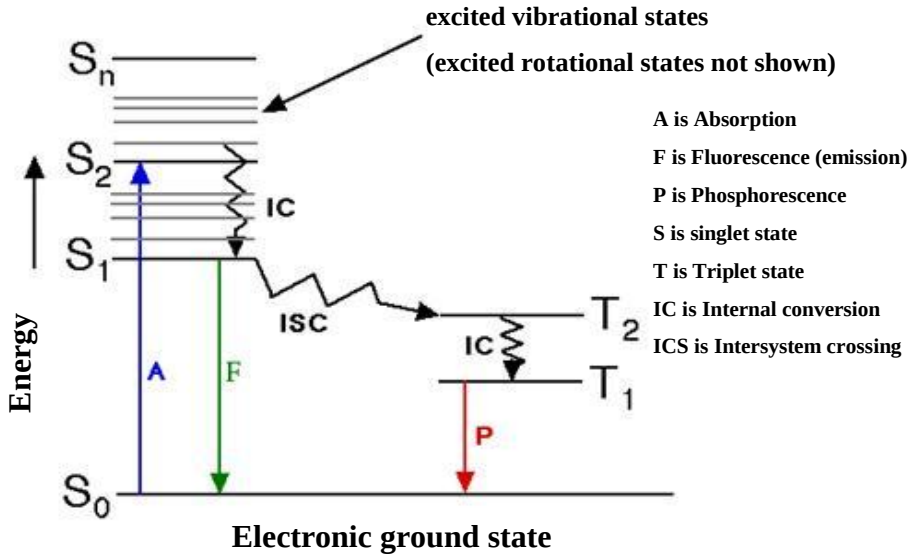

Figure 2.6: Jablonski Diagram

Jablonski diagram mainly explains the important photophysical processes- electronic absorption and emission/fluorescence of the molecules. If the molecule absorbs enough energy as electromagnetic radiation, it can be excited to either of the excited electronic single states (S_1 or S_2, etc.) from ground state S_0. The process of absorption is shown as 'A' in the diagram. Although higher vibrational energy levels are not in general populated according to the statistics of Boltzmann (less than 1%), the population of vibrational levels of S_1 or S_2 depends on the magnitude of absorption energy. By the process of internal conversion, the excited molecules relax to the lowest vibrational state of the first excited state (S_1). Therefore, a molecule can return to its ground state from the lowest vibrational state of the first excited state (S_1), which is known as Kasha's rule and it can be also concluded that the resulting fluorescence spectrum thus does not actually depend on the excitation wavelength. Among many ways of returning to the ground state from the excited state (in general by radiative and non-radiative path ways), releasing a photon by radiative path way

is termed as fluorescence and the transition occurs among states of the same spin state (for instance S_1--> S_0). On the other hand, the term phosphorescence is given if the spin states of the initial and final energy levels differ and the relaxation occurs from triplet excited state to the ground state after the process of intersystem crossing, shown on the diagram (Figure 2.6).

Since phosphorescence includes intersystem crossing, fluorescence much more likely occurs statistically and therefore fluorescence life times are in general very short and in contrary, phosphorescence is much longer comparing to fluorescence. Excitation to an excited state, absorption, internal conversion, fluorescence, intersystem crossing, and phosphorescence; all these processes completes the electronic transitions of a molecule. An important point to be noted is the nonradiative pathway of deactivation includes internal conversion, intersystem crossing and vibrational relaxation. Similar to the processes of fluorescence and phosphorescence, corresponding radiationless transition between energy states that have the same spin is called internal conversion and that of transition between energy states with different spin is named as intersystem crossing by definition. Another radiationless pathway, vibrational relaxation, most likely occurs very rapidly.

2.3.1 Fluorescent optical pH sensors

Nowadays, many technological applications include both molecular and electronic devices. Ongoing research (Safavi, A., et al. 2003) still indicates that there is a great necessity of cheap and effective materials in many areas of industry and fluorescent optical sensors have a significant importance. Shortly, it can be explained (Safavi, A., et al. 2003) that ‘where there is a sensitive pH measurement in any industrial field, there is a need and capability of producing a pH sensor.

The benefits of optical sensors include low cost, safety, absence of any electrical interference and also capability of remote sensing. Because of their potential uses, pH sensitive optodes found applications in clinical and environmental analyses and process control. The pH sensing ability depends on the pH of the solution and its affect on the optical properties of the compound. If the absorbance and fluorescence properties are showing variation greatly by changing the pH, such a compound acts as pH sensing element and can be termed as pH sensitive optode (Safavi, A., et al. 2003).

2.3.2 The critical properties of optical pH sensors

As a matter of fact, the sensing ability of pH sensors are solely depend on the pH of the solution and its corresponding optical properties, therefore, a broad range of pH sensitivity could not be easily possible and the research (Safavi, A., et al. 2003) indicates that most dyes are possessed the sensing ability for a very short range of pH, 2 – 4. According to the report paper of Safavi and co-authors, the pH sensing ability of a pH sensor can be extended to a bigger range (2.51 to 9.76) by a calibration method involving multivariate artificial neural network (Safavi, A., et al. 2003). Because of the fact that optodes are in general based on acid-base indicators, some more methods were attempted by employing different kinds of indicators, for example, fluorescent indicators, two acidic groups containing indicators, two different acidic constants possessed indicators, and by employing Fourier transform methods to increase the pH sensing range of an optode. Much higher fluorescence of the material designed gives much better sensing ability of a pH sensor. Therefore, there is a groom for developing the pH sensitive optodes.

Chapter 3

EXPERIMENTAL

3.1 Materials

Chemicals used were purchased and directly employed in the experiments without any purification. Some solvents according to the necessity were distilled by standard literature procedures (Armarego and perrin, 1980). For spectroscopic analyses, pure spectroscopic grade solvents were directly used.

Perylene -3,4,9,10-tetracarboxylic dianhydride, Benzopurpurin4B, 4-aminophenol Hydrochloride, potassium hydroxide, potassium carbonate, zinc acetate, *m*-cresol, isoquinoline were obtained from sigma Aldrich.

3.2 Instruments

Infrared spectra

FT-IR spectra were measured with KBr pellets in solid-state using Mattson FT-IR spectrophotometer. Evaluation of IR analyses for the compounds gave consistent results for structural characteristics.

Elemental Analysis

Elemental analyses were performed on a Carlo Erba-1106 C, Hand N analyzer.

Emission Spectra

Emission spectra and fluorescence quantum yield measurements for the synthesized compounds were studied using Varian Cary Eclipse Spectrophotometer.

Ultraviolet Absorption Spectra (UV)

Ultraviolet Absorption Spectra in solutions were measured on a Varian–Cary 100 Spectrophotometer. Thin films were prepared to obtain UV spectra in solid state and were measured using a Perkin –Elmer UV/VIS/NIR Lambda 19 spectrophotometer that is equipped with required solid-state accessories.

Differential Scanning Calorimeter (DSC)

Thermal analyses were carried out on a Diamond Differential Scanning Calorimeter at a heating rate of 10 ^{o}C. min $^{-1}$ in nitrogen.

Thermogravimetric Analyses (TGA)

Thermogravimetric thermograms were obtained on a Tg-Ms: Simultane TG-DTA/DSC apparatus STA 449 Jupiter from Netzsch, equipped with Balzers Quadstar 422 Vat a heating rate 10 ^{o}C. min $^{-1}$ in nitrogen.

3.3 Methods of syntheses

In this segment, the syntheses methods of N-(4-Hydroxyphenyl)-3, 4, 9, 10-perylene tetracarboxylic-3, 4-anhydride-9, 10-imide (OH-PMI) and synthesis of BP-OHPDI were presented.

N-(4-Hydroxyphenyl)-3, 4, 9, 10-perylene tetracarboxylic-3, 4-anhydride-9, 10-imide (OH-PMI) was synthesized and purified according to the previously reported procedure (Pasaogullari N, et al. 2005).

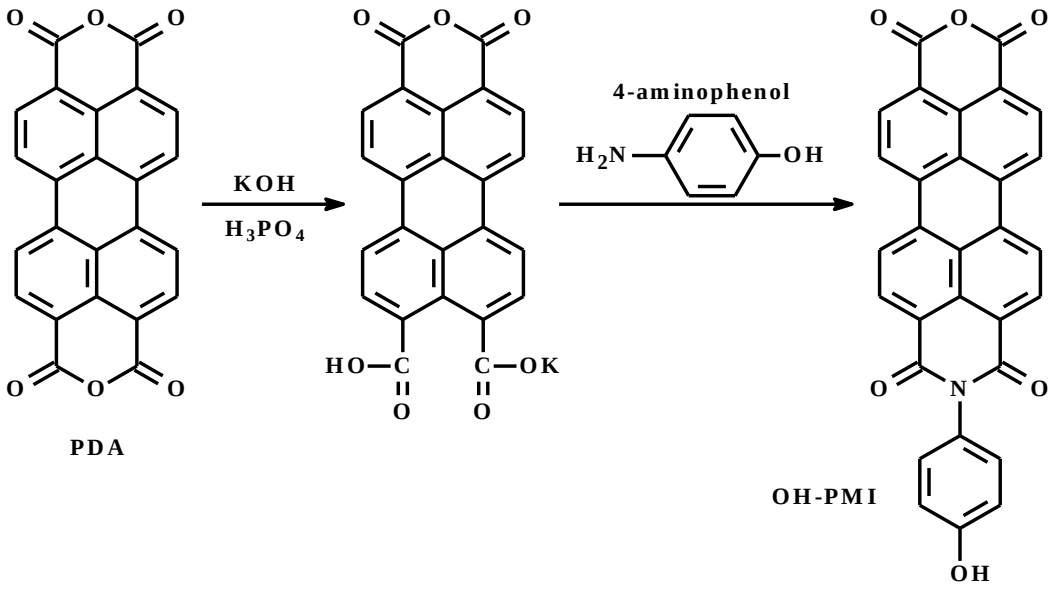

Scheme 3.1: Synthesis of N-(4-Hydroxyphenyl)-3, 4, 9, 10-perylene tetracarboxylic-3, 4-anhydride-9, 10-imide (OH-PMI) (Pasaogullari N, et al. 2005).

Finally, a novel fluorescent optical pH sensor (BP-OHPDI) was successfully synthesized from N-(4-Hydroxyphenyl)-3, 4, 9, 10-perylene tetracarboxylic-3, 4-anhydride-9, 10-imide (OH-PMI) and benzopurpurin 4B in presence of isoquinoline as a solvent shown below (Scheme 3.2).

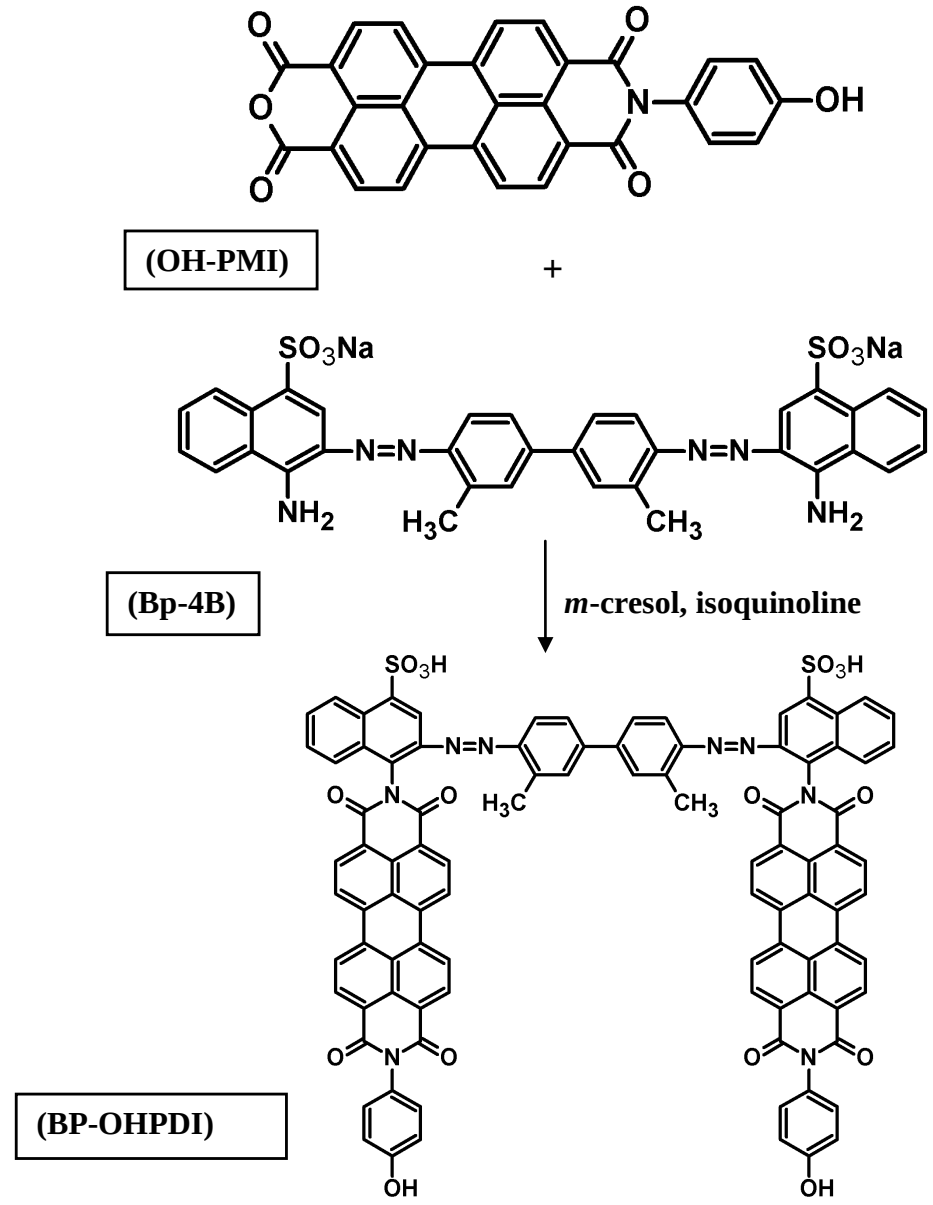

Scheme 3.2: Synthesis of Di-*N*-(4-hydroxyphenyl)-3,4,9,10-perylenetetracarboxy monoimide chrmophores containing benzopurpurin-4B (BP-OHPDI)

3.4 Synthesis of OH-PMI

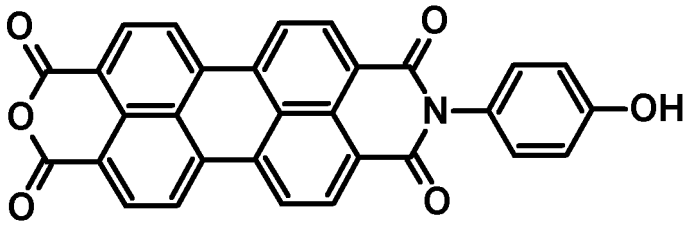

N-(4-Hydroxyphenyl)-3, 4, 9, 10-perylene tetracarboxylic-3, 4-anhydride-9, 10-imide (OH-PMI) was synthesized and purified according to the previously reported procedure (Pasaogullari N, et al. 2005).

3.5 Synthesis of BP-OHPDI

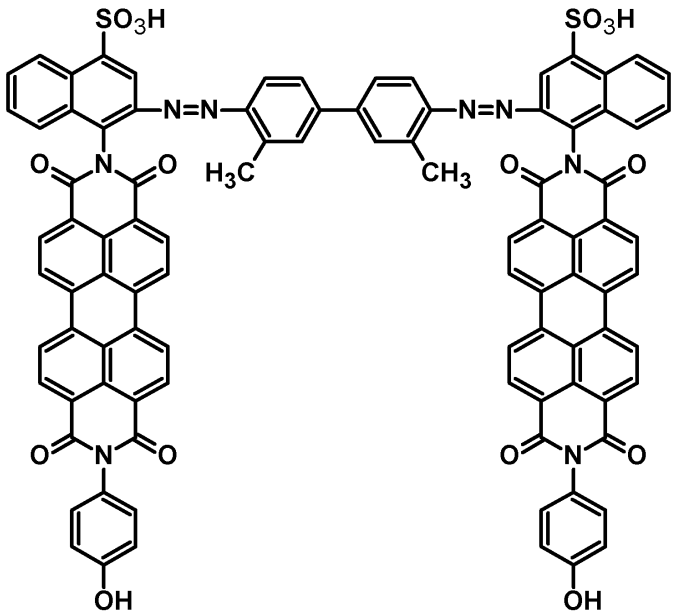

N-(4-Hydroxyphenyl)-3, 4, 9, 10-perylene tetracarboxylic-3, 4-anhydride-9, 10-imide (0.5014 g, 1.048 mmol) , benzopurpurin 4B (0.451 g, 0.622 mmol) and isoquinoline (30 mL) were stirred under argon gas very well, heated reaction mixture gradually at 100 °C for 3 h, 150 °C for 5 h, 180 °C for 5 h, 200°C for 8 h and finally at 220°C for 12 h.

The warm solution (60 °C) was poured into acetone (250 mL). The precipitate was then filtered by suction, washed with acetone and water, and then purified by soxhlet apparatus with water and methanol. The product was dried under vacuum at 110 °C.

Yield: 60 % (0.5g); **color:** Black powder

IR (KBr, cm^{-1}): υ= 3450, 2920, 1700, 1666, 1593, 1500, 1357, 1250, 810, 750

UV-vis ($CHCl_3$) (λ_{max} / nm; (ε_{max} / $L.mol^{-1}.cm^{-1}$)): 462 (27500), 490 (45100), 526 (58000)

Fluorescence ($CHCl_3$) (λ_{max} / nm): 535, 575, 625; Φ_f = 0.25

calcd. for $C_{94}H_{50}N_8O_{16}S_2$ (M_W, 1611.60): **C**, 70.06% **H**, 3.13%, **N,** 6.95%. **Found: C**, 72.06% **H**, 3.13%, **N,** 7.15%

3.6 General Reaction Mechanism of a Perylene Diimide

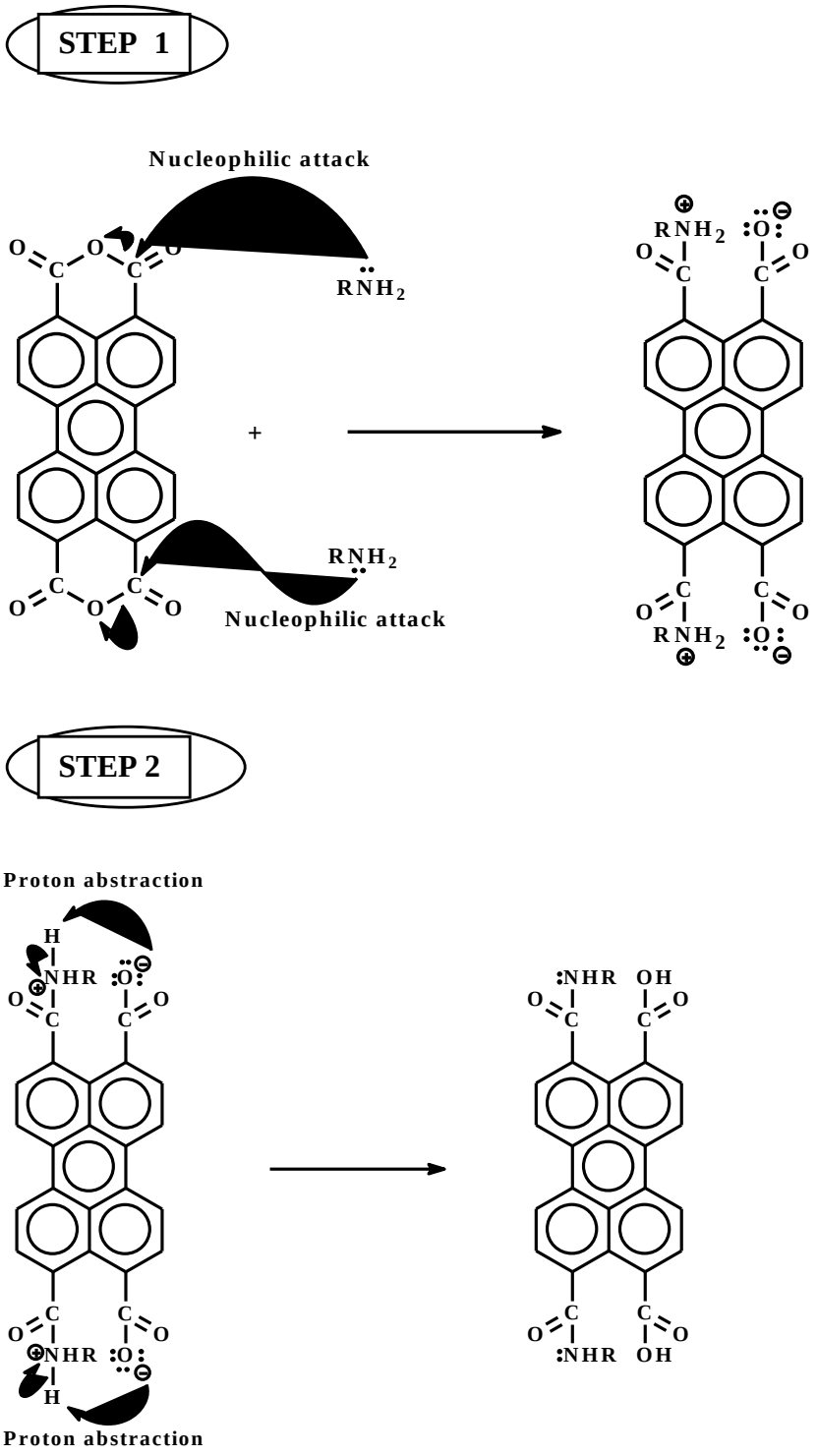

STEP 3

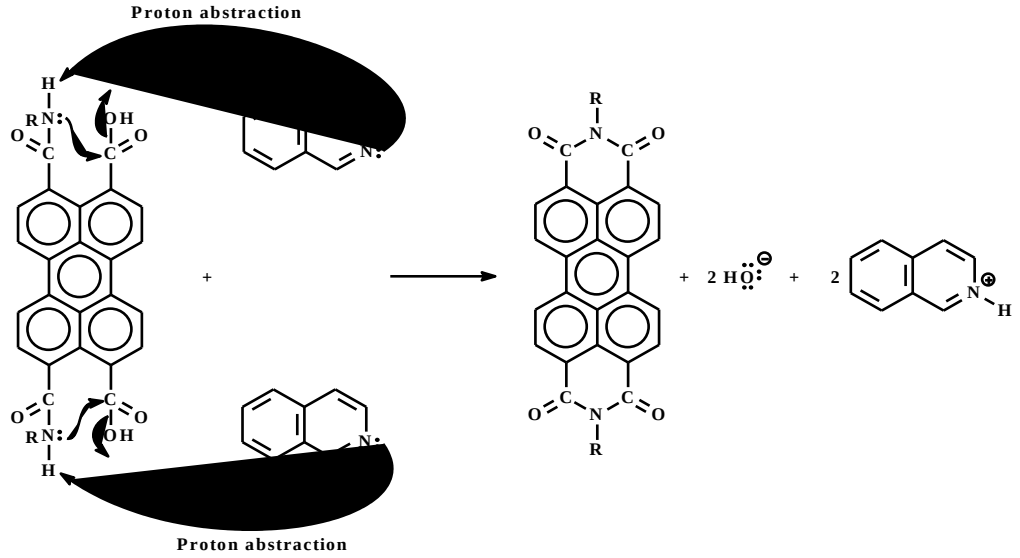

STEP4

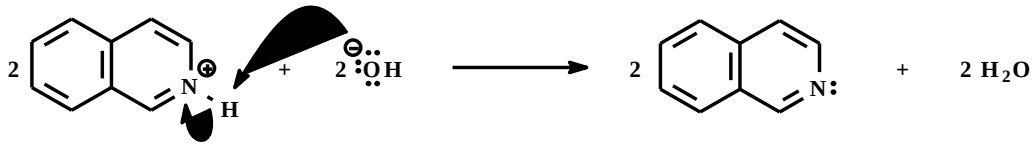

Chapter 4

DATA AND CALCULATIONS

4.1 Theoretical Aspects of Quantum Yield

The primary quantum yield of a photochemical reaction is the number of reactant molecules producing specified primary products per photon of light absorbed. These primary products (atoms or ions) might serve as chain carriers and lead to more than one molecule of additional atoms or ions of product. The overall quantum yield (**Φ**) is the number of molecules reacting per photons absorbed.

$$\ddot{\mathbf{O}} = \frac{\text{number of moles (molecules)of product formed}}{\text{number of photons of radiation absorbed}}$$

The differential quantum yield is;

$$\mathbf{\Phi} = \frac{\mathrm{d[x]/dt}}{\mathrm{n}}$$

Where d(x) / dt is the rate of change of a measurable quantity, and (n) the amount of photons (mole or its equivalent Einstein) absorbed per unit time. Φ can be used for photochemical reactions or photophysical processes.

High quantum yields are desirable for the application of photochemical reactions in organic syntheses. Quantum yield values fall in the range of 0 to 1.0, although in some specific situations a higher value for chemical reaction may be observed (Scaiano, J.C., 1989).

4.2 Method of Measurement of Fluorescence Quantum Yield

An energetically excited state will be formed when a fluorophore absorbs enough amount of energy from the electromagnetic radiation of light. Among many other deactivation processes of energy, fluorescence is the main radiative process where the deactivation of energy occurs by emitting a photon. The likelihood of the above mentioned process depends on the nature of the fluorophore and its environment around it. However, deactivation is the final result and the molecules must return to the ground state. Some deactivation processes to be listed are fluorescence that is yielding energy through photon emission, internal conversion, vibrational relaxation and intersystem crossing, etc.

Fluorescence is the main radiative process where the deactivation occurs via photon emission. Other cataloged processes are related to non- radiative processes of deactivation of energy, that is, by loss of energy in terms of heat to the surroundings.

The fluorescence quantum yield (Φ_f) is defined as the ratio of the absorbed photons to the emitted ones by florescence. The most reliable method for recording Φ_f is the comparative method of Williams et al.; this method uses well characterized standard samples for which Φ is known. In fact, standard and test samples solution that possess equal amount of absorbance in the same excitation wavelength are considered to absorb equal number of photons. The quantum yield values are obtained by the ratio of intensities of integrated fluorescence of the two solutions. The test sample Φ is calculated base on the known value of the standard sample Φ.

$$\mathbf{\Phi_f\,(U)} = \frac{A_{std}}{A_u} \times \frac{S_u}{S_{std}} \times \left[\frac{n_u}{n_{std}}\right]^2 \times \Phi_{std}$$

(Eqn.4.1)

Φ_f (U): Fluorescence quantum yield of unknown

A_{std}: Absorbance of the reference at the excitation wavelength

A_u: Absorbance of the unknown at the excitation wavelength

$S_{std:}$ The integrated emission area across the band of reference

$S_{u:}$ The integrated emission area across the band of unknown

n_{std}: Refractive index of reference solvent

$n_{u:}$ Refractive index of unknown solvent

Φ_{std}: Fluorescence quantum yield of reference (Scaiano, J.C., 1989).

The N, N-bis (dodecyl)-3, 4, 9, 10-perylenebis (discarboximide) in chloroform (Φ_f = 1) (Icil, 1997) was used as reference for the Fluorescence quantum yield measurements of perylene dyes. The perylene dyes reported were excited at the wavelength, λ_{exc} = 485 nm similar to the reference.

4.2.1 Fluorescence Quantum Yield (Φ_f) calculations of BP-OHPDI

Φ_f calculation of BP-OHPDI IN $CHCl_3$

N, N-bis (dodecyl)-3, 4, 9, 10-perylenebis (discarboximide) was used as reference (Icil 1997).

Φ_{std} = 1 when the solvent is chloroform

A_{std} = 0.1073

A_u = 0.1063

Su = 1549.7

S_{std} = 6231

$$\Phi_f = \frac{0.1073}{0.1063} \times \frac{1549.7}{6231} \times 1 \times 1$$

Φ_f = 0.25

The fluorescence quantum yield of BP-OHPDI was measured by the method described above in three different kinds of solvents and they were tabulated below (Table 4.1).

Table 4.1: Fluorescence Quantum Yields of BP-OHPDI

Solvent	**BP-OHPDI**
	Φ_f
$CHCl_3$	0.250
DMF	0.157
H_2SO_4	0.062

4.3 Calculation of Molar Absorption Coefficients

The following equation 4.2 is used to calculate the absorption coefficients of the compounds (Scaiano, J.C., 1989).

$$\boldsymbol{\varepsilon_{max} = \frac{A}{CL}}$$

(Eqn.4.2)

Where ε_{max} : Molar absorption coefficient

A: absorbance

C: concentration

L: cell length

ε_{max} Calculation of $CHCl_3$:

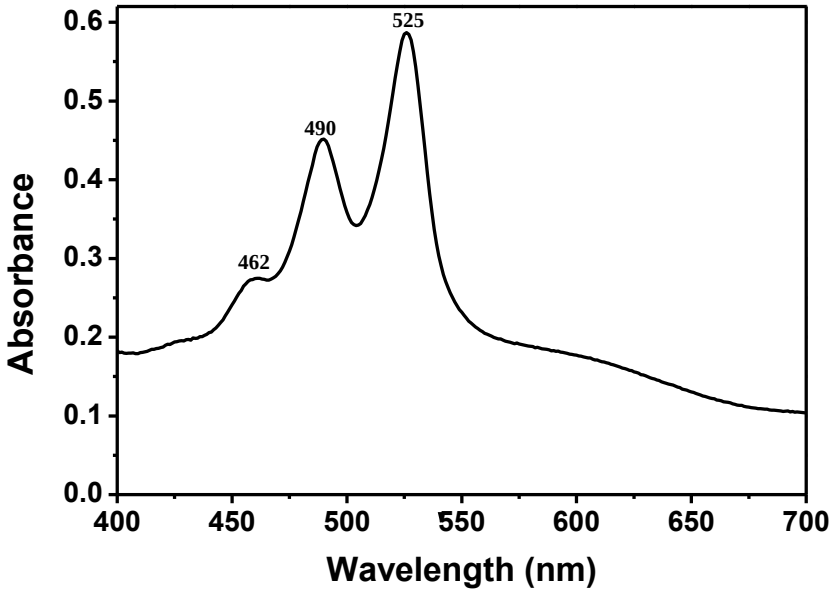

Figure 4.1: Absorption Spectrum of Chloroform at $1x10^{-5}$ M

ε_{max} Calculation of $CHCl_3$:

C = 5.00×10^{-5} M in Chloroform; L = 1cm

at λ_{max} = 525 nm, A = 0.58

$$\boldsymbol{\varepsilon_{max} = \frac{0.58}{1x10^{-5}\ M\ X\ 1cm} = 58000\ L\ mol^{-1}\ cm^{-1}}$$

In the similar way, the molar absorptivity of the compound (BP-OHPDI) was calculated in different solvents where the compound has shown solubility and the resulting values were tabulated in the following table (Table 4.2).

Table 4.2: Molar absorptivity data of BP-OHPDI in different solvents

Solvent	λ_{max} (nm)	ε_{max}(L.mol^{-1}.cm^{-1})
$CHCl_3$	525	58000
NMP	524	90900
DMF	524	130000
DMSO	542	100000
TCE	532	60000
THF	518	25000
DMAc	524	99800
H_2SO_4	607	26700
CH_3COOH	524	12400
TFAc	520	25600
H_3PO_4	552	11000
1,4-dioxane	526	34400

4.4 Theoretical Radiative Lifetimes (τ_o) Calculations

The following equation is used to calculate the theoretical radiative lifetime. It can be pointed out that the calculated theoretical radiative lifetime value is related to excited molecule in the absence of radiationless transitions (Bodapati J B 2005).

$$\tau_0 = \frac{3.5\times10^8}{\upsilon^2_{max}\times\varepsilon_{max}\times\Delta\upsilon_{1/2}} \qquad \textbf{(Eqn.4.3)}$$

Where

τ_o: Theoretical radiative lifetime in seconds

υ_{max} = Wavenumbers in cm $^{-1}$

ε_{max} : The maximum extinction coefficient at the selected adsorption wavelength.

$\Delta\upsilon_{1/2}$: Half-width of the selected absorption in units of cm^{-1}

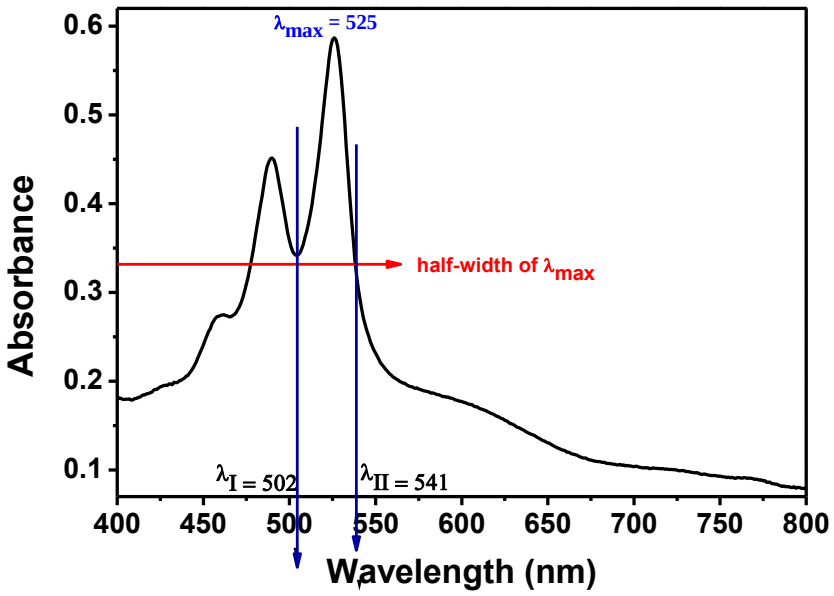

Figure 4.2: Absorption Spectrum of BP-OHPDI in $CHCl_3$ and a Representative Figure to Calculate the Half-width of the Selected Absorption of BP-OHPDI

τ_0 calculation of BP-OHPDI in $CHCl_3$:

λ_{max}= 525 nm **ε_{max}**= 58000 L mol^{-1} cm^{-1}

$\lambda_{max} = 525\text{nm} \times \frac{10^{-9}\ \text{m}}{1\text{nm}} \times \frac{100\text{cm}}{1\text{m}} = 5.25 \times 10^{-5}$ cm

$\bar{\upsilon}_{max} = \frac{1}{\lambda_{max}} = \frac{1}{5.25\times10-5_{\text{cm}}} = 19047.61\text{cm}^{-1}$

$\bar{\upsilon}^2_{max} = (19047.61\text{cm}^{-1})^2 = 3.628\times10^8\ \text{cm}^{-2}$

$\Delta\bar{\upsilon}_{1/2} = \bar{\upsilon}_{II} - \bar{\upsilon}_{I}$

λ_I = 502 nm

$\bar{\upsilon}_I = \frac{1}{\lambda_I} = \frac{1}{5.02\times10-5_{\text{cm}}} = 19920.31\text{cm}^{-1}$

λ_{II} = 541 nm

$\bar{\upsilon}_{II} = \frac{1}{\lambda_{II}} = \frac{1}{5.41\times10-5_{\text{cm}}} = 18484.28\text{cm}^{-1}$

$\Delta\bar{\upsilon}_{1/2} = \bar{\upsilon}_{II} - \bar{\upsilon}_{I}$= 19920.31$cm^{-1}$ – 18484.28 cm^{-1} = 1436.03 cm^{-1}

$\hat{o}_0 = \frac{3.5\times10^8}{3.628\times10^8\ \text{cm}^{-2}\times58000\times1436.03\text{cm}^{-1}} = 1.158\times10^{-8}$ sec

$\hat{o}_0 = 11.58\times10^{-9}$ sec

$\tau_0 = 11.58\times10^{-9}\ \text{sec} \times \frac{1\text{ns}}{10-9_{\text{sec}}} = 11.58$ ns

According to this method of calculation, theoretical radiative lifetimes were calculated for the compound in different solvents and the resulting values were tabulated in the following table (Table 4.3).

Table 4.3: Theoretical radiative lifetimes of BP-OHPDI in different solvents

Solvent	λ_{max} (nm)	$å_{max}$(L.mol^{-1}.cm^{-1})	$\bar{\upsilon}^2_{max}$ (cm^{-2})	$\Delta\bar{\upsilon}_{1/2}$ (cm^{-1})	$\hat{o}_0$(ns)
$CHCl_3$	525	58000	3.628 x 10^8	1436.03	11.58
NMP	524	90900	3.642 x10^8	1619.53	6.53
DMF	524	130000	3.642 x10^8	1307.09	5.66
DMSO	542	100000	3.404 x 10^8	1358.34	7.57
TCE	532	60000	3.533 x 10^8	1417.29	11.65
THF	518	25000	3.727 x 10^8	2398.92	15.66
DMAc	524	99800	3.642 x10^8	1439.06	6.69
H_2SO_4	607	26700	2.714 x 10^8	1617.47	29.86
CH_3COOH	524	12400	3.642 x10^8	1403.08	55.24
TFAc	520	25600	3.698 x 10^8	1363.11	27.12
H_3PO_4	552	11000	3.282 x10^8	3064.40	31.64
1,4-dioxane	526	34400	3.614 x 10^8	1465.52	19.21

4.5 Calculation of Theoretical Fluorescence Lifetime (τ_f)

Fluorescence lifetimes were calculated using formula 4.4 shown below and it refers to the theoretical average time of the molecule stays in the excited state before fluorescence (emitting a photon) (Turro, 1965).

$$\tau_f = \tau_0 . \Phi_f \qquad \textbf{(Eqn.4.4)}$$

Where, τ_f: Fluorescence lifetime in nano seconds

τ_0: Theoretical radiative lifetime in nano seconds

Φ_f: Fluorescence quantum yield

τ_f Calculation of BP-OHPDI in $CHCl_3$:

$\tau_f = \tau_0 . \Phi_f$

τ_f = 11.58 ns x 0.25 = 0.29 ns

According to this method of calculation, theoretical fluorescence lifetime (τ_f) was calculated for the compounds in different solvents and the resulting values were tabulated in the following table (Table 4.4).

Table 4.4: Theoretical Fluorescence Lifetimes (τ_f) of BP-OHPDI in different solvents

Solvent	Φ_f	$\tau_{0\ (ns)}$	τ_f (ns)
$CHCl_3$	0.250	11.58	2.9
DMF	0.157	5.66	0.9
H_2SO_4	0.062	29.86	1.9

4.5.1 Calculations of Theoretical Fluorescence Rate constant (k_f)

The theoretical fluorescence rate constant for the compounds can be calculated by using Turro's equation 4.5 given below.

$$k_f = \frac{1}{\tau_0} \qquad \textbf{(Eqn.4.5)}$$

Where, k_f: fluorescence rate constant in s^{-1}

τ_0: Theoretical radiative lifetime in s $\quad k_f = \frac{1}{11.58\times10^{-9}} = 8.63 \times 10^8\ s^{-1}$

k_f calculation of BP-OHPDI in $CHCl_3$:

The theoretical fluorescence rate constant were calculated in the similar manner for BP-OHPDI in different solvents and the values were given in the following table.

Table 4.5: fluorescence rate constants data of BP-OHPDI in different solvents

Solvent	$\tau_{0\ (ns)}$	$K_f\ (s^{-1})$
$CHCl_3$	11.58	8.64 x 10^7
NMP	6.53	1.53 x 10^8
DMF	5.66	1.77 x 10^8
DMSO	7.57	1.32 x 10^8
TCE	11.65	8.58 x 10^7
THF	15.66	6.39 x 10^7
DMAc	6.69	1.49 x 10^8
H_2SO_4	29.86	3.35 x 10^7
CH_3COOH	55.24	1.81 x 10^7
TFAc	27.12	3.69 x 10^7
H_3PO_4	31.64	3.16 x 10^7
1,4-dioxane	19.21	5.21 x 10^7

4.5.2 Calculation of singlet Energy (E_s)

The following equation given by Turro can be used to calculate the singlet energy, (is the minimum amount of energy required for a chromophore to get excited from ground state to an excited state).

$$E_s = \frac{2.86 \times 10^5}{\lambda_{max}} \qquad \textbf{(Eqn.4.6)}$$

Where, E_s: singlet energy in kcal mol^{-1}

λ_{max}: The maximum absorption wavelength in Å

E_s calculation of BP-OHPDI IN $CHCl_3$

$E_s = \frac{2.86 \times 10^5}{\lambda_{max}} = \frac{2.86 \times 10^5}{5260} = 54.48$ kcal mol^{-1}

Table 4.6: E_s data of BP-OHPDI in different solvents

Solvent	λ_{max} (nm)	E_s
$CHCl_3$	525	54.48
NMP	524	54.58
DMF	524	54.58
DMSO	542	52.77
TCE	532	53.76
THF	518	55.21
DMAc	524	54.58
H_2SO_4	607	47.12
CH_3COOH	524	54.58
TFAc	520	55.00
H_3PO_4	552	51.81
1,4-dioxane	526	54.37

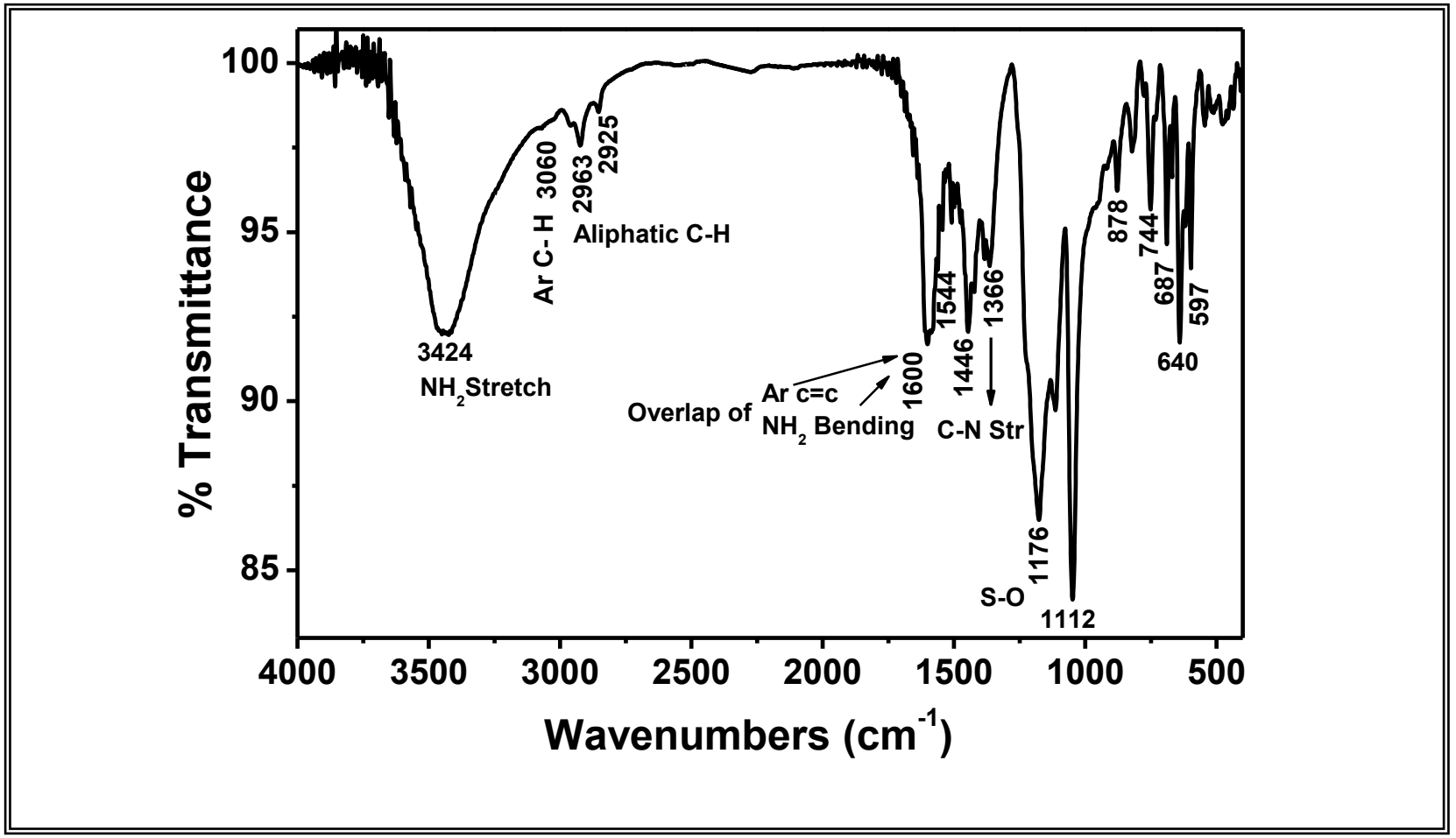

Figure 4.3 FT-IR Spectrum of Bp-4B

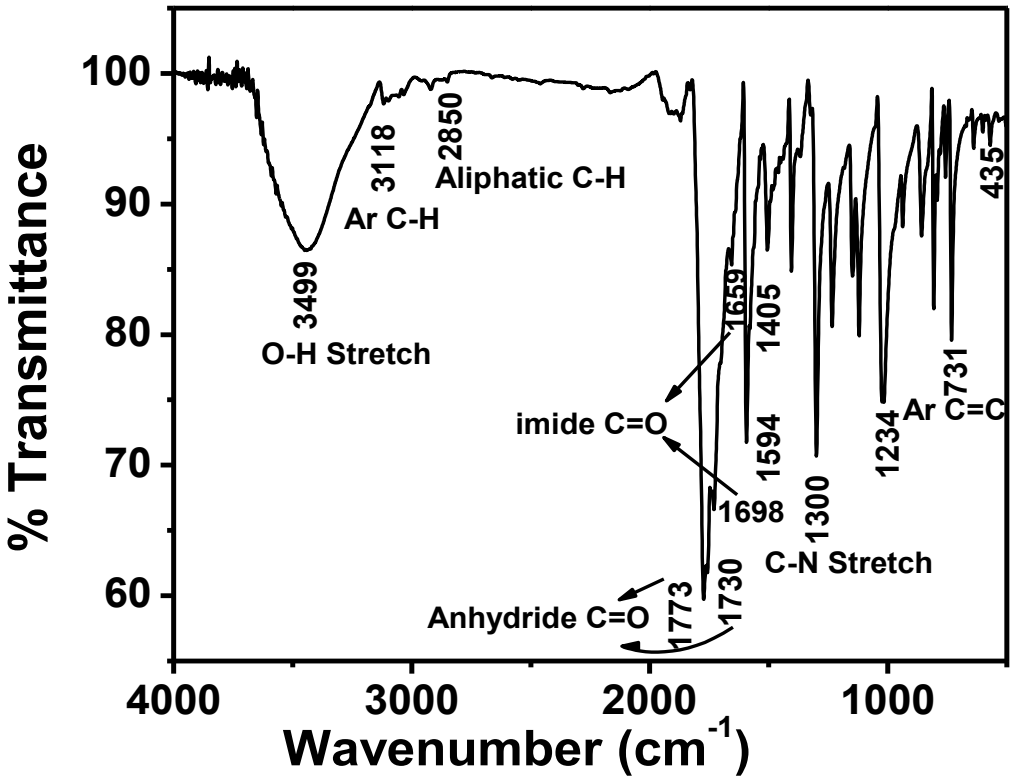

Figure 4.4 FT-IR Spectrum of OH-PMI

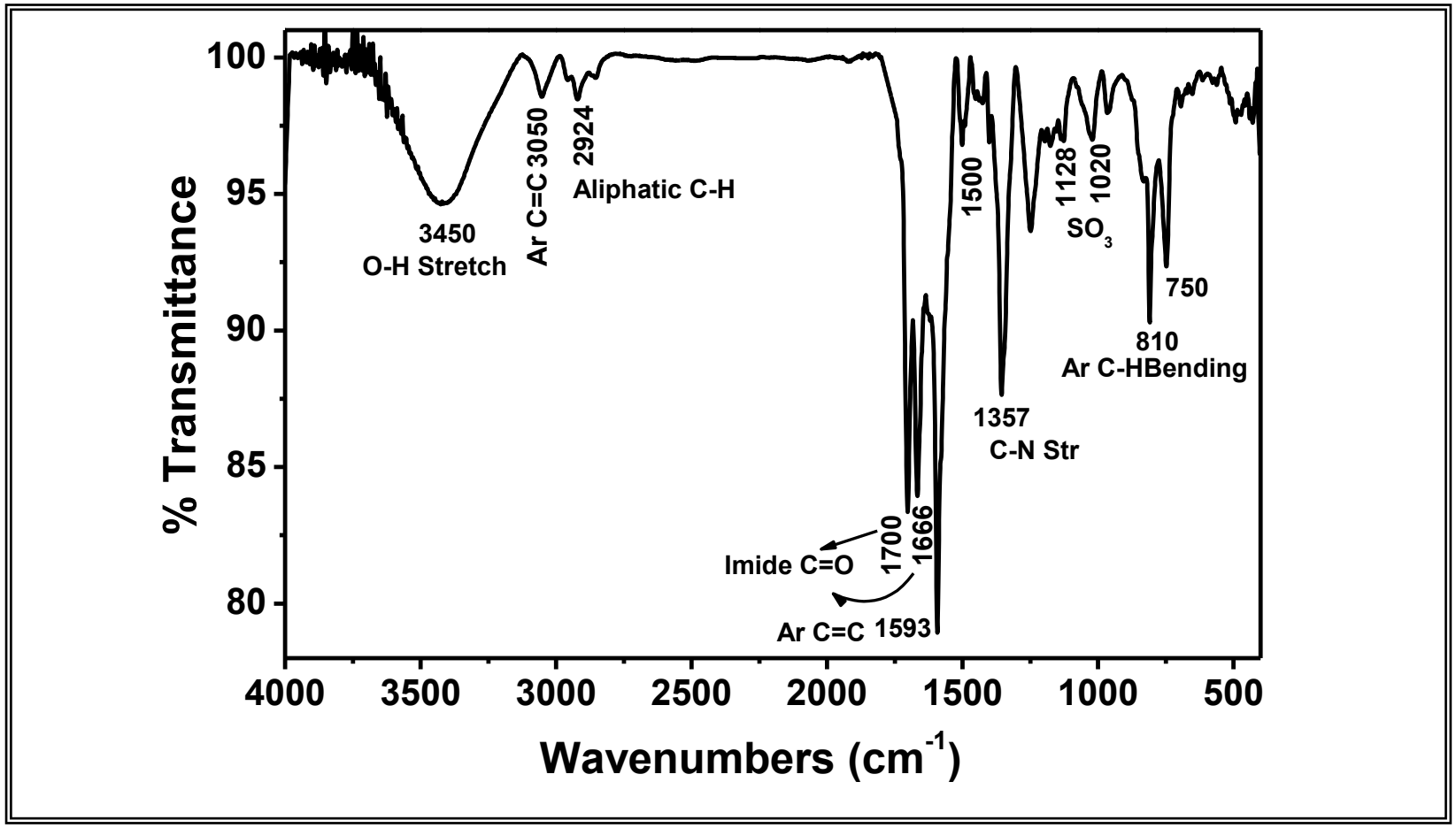

Figure 4.5 FT-IR Spectrum of BP-OHPDI

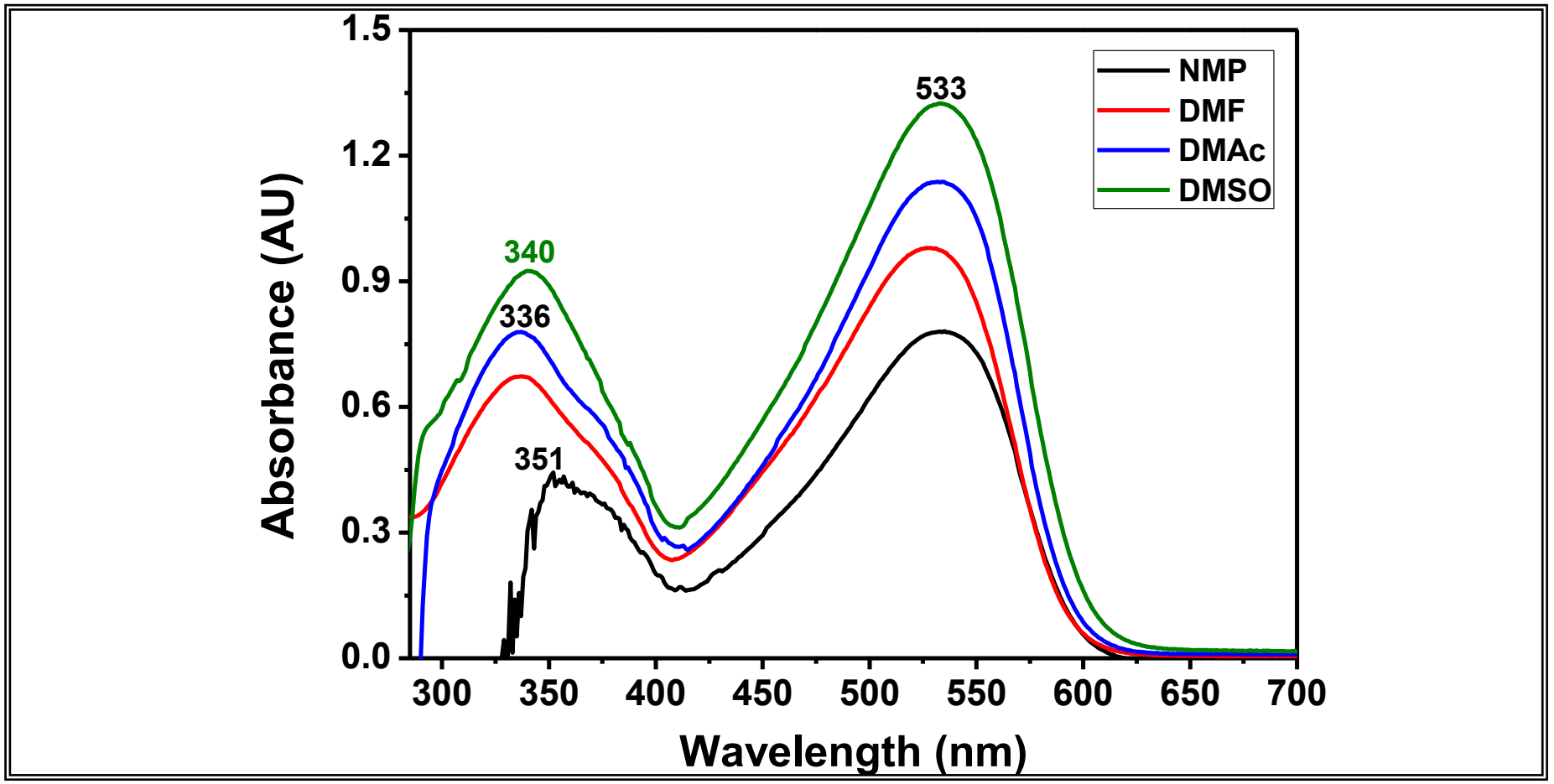

Figure 4.6: Comparison of UV-vis Absorption Spectra of Bp-4B in Dipolar Aprotic Solvents

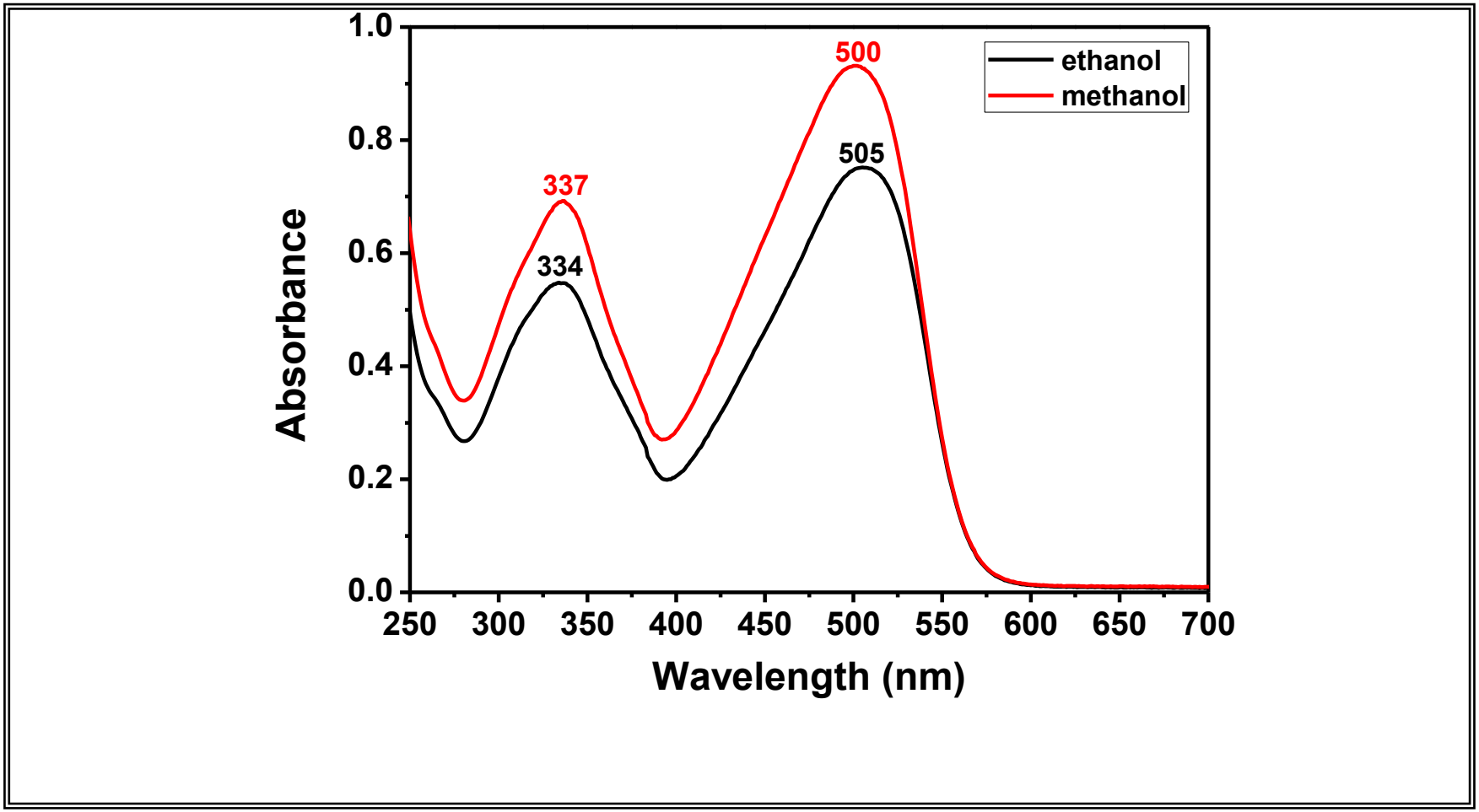

Figure 4.7: Comparison of UV-vis Absorption Spectra of Bp-4B in Polar Protic Solvents

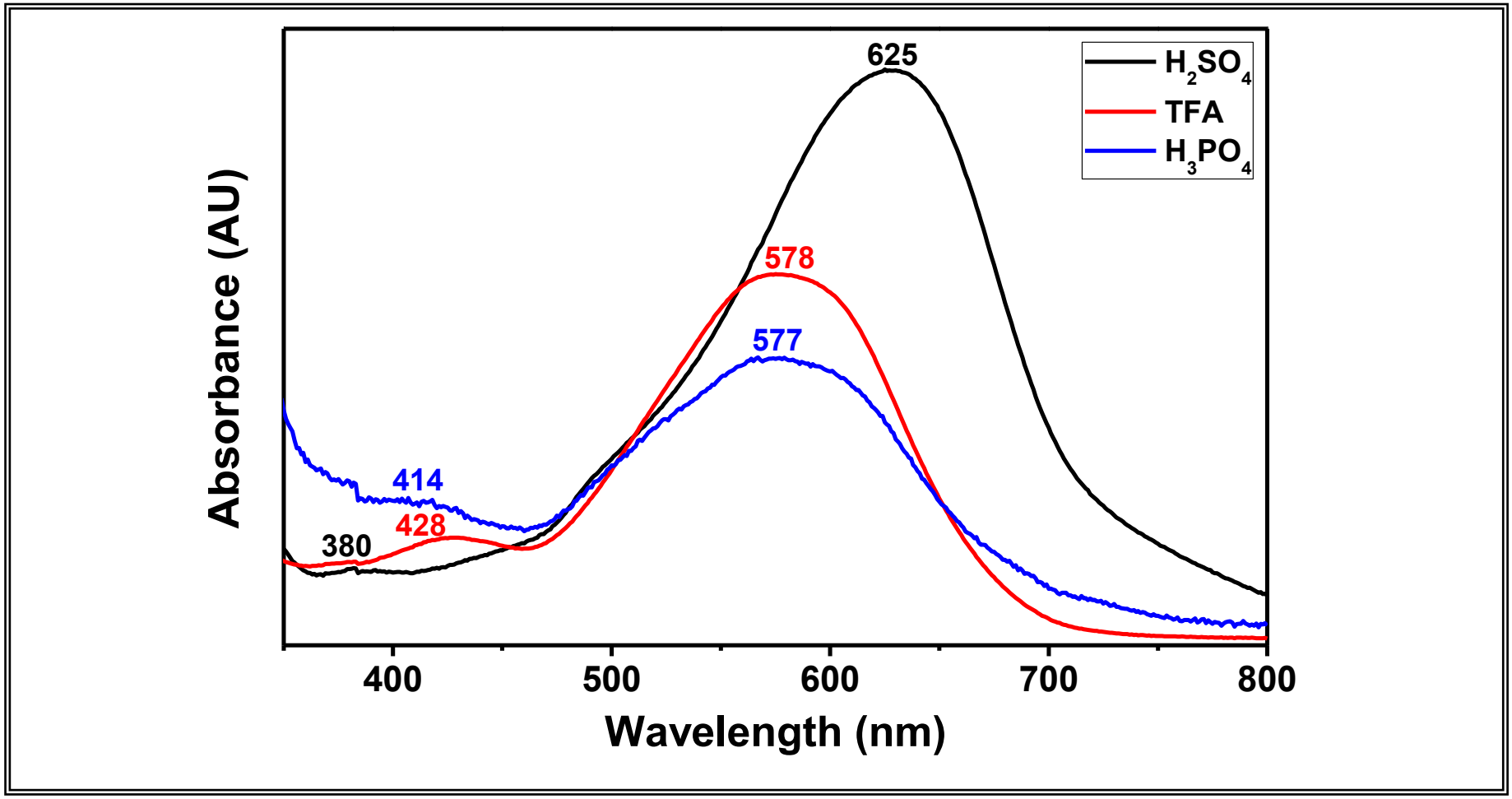

Figure 4.8: Comparison of UV-vis Absorption Spectra of Bp-4B in Various Acids

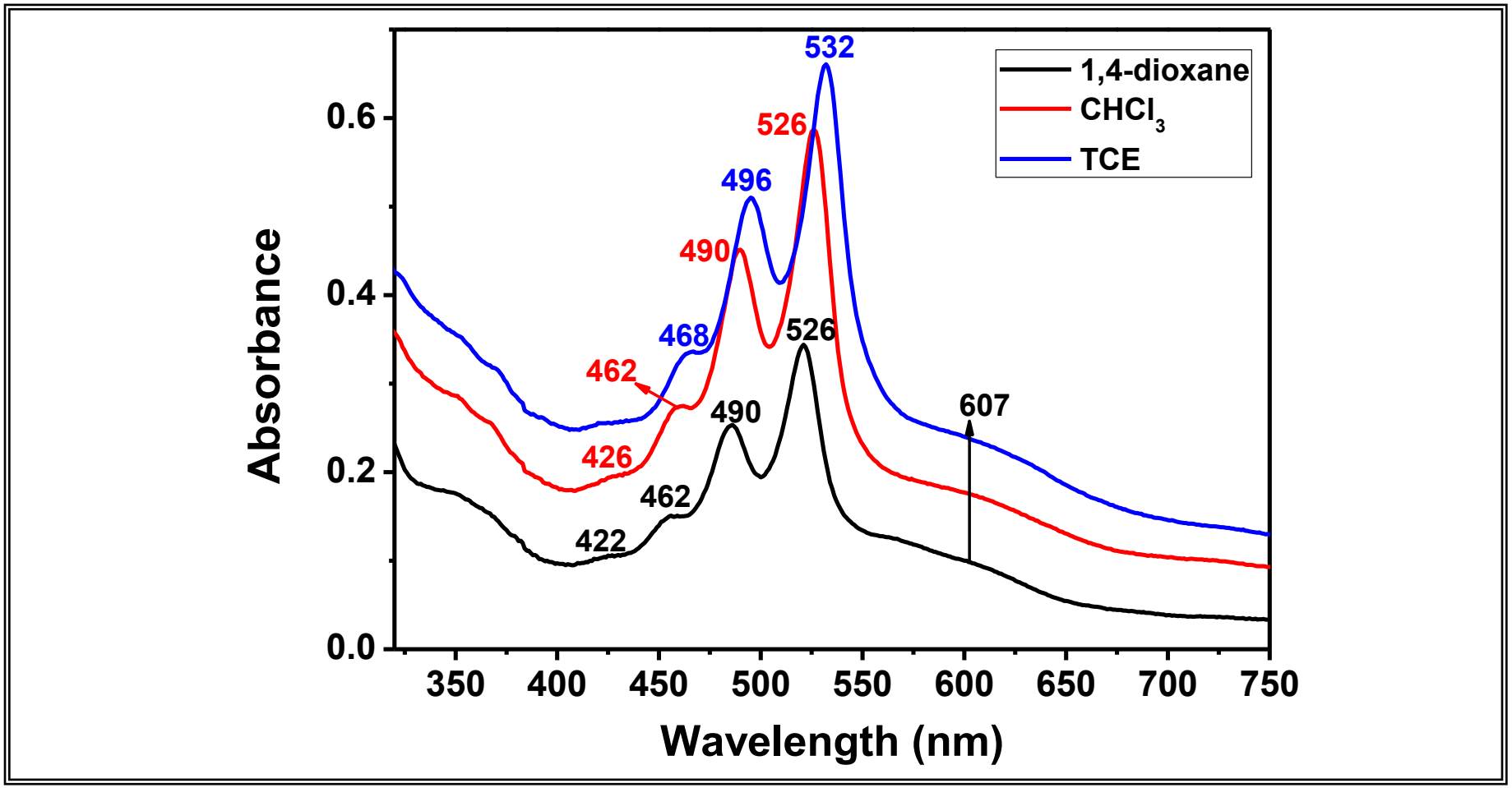

Figure 4.9: Comparison of UV-vis Absorption Spectra of BP-OHPDI in Nonpolar Solvents

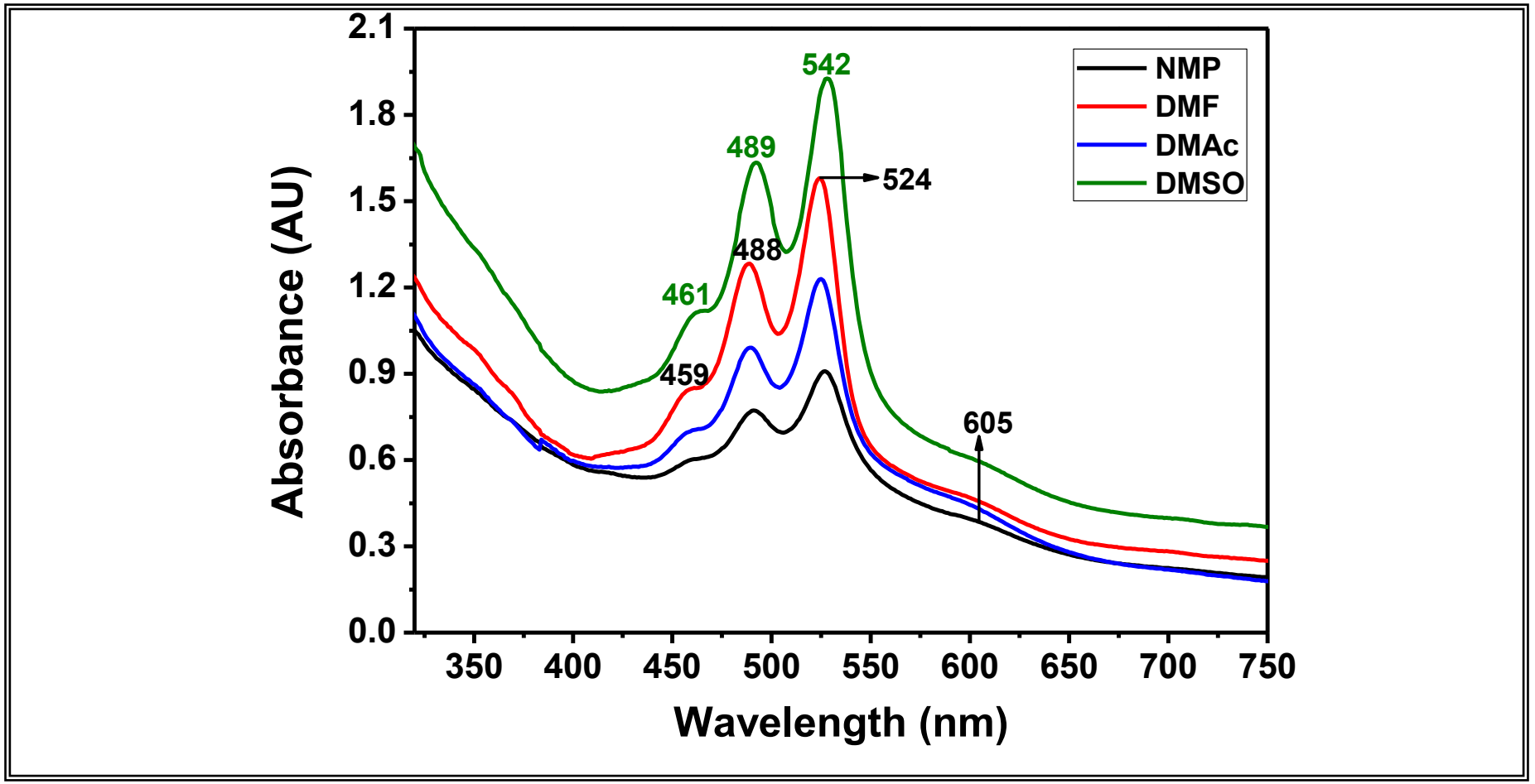

Figure 4.10: Comparison of UV-vis Absorption Spectra of BP-OHPDI in Dipolar Aprotic Solvents

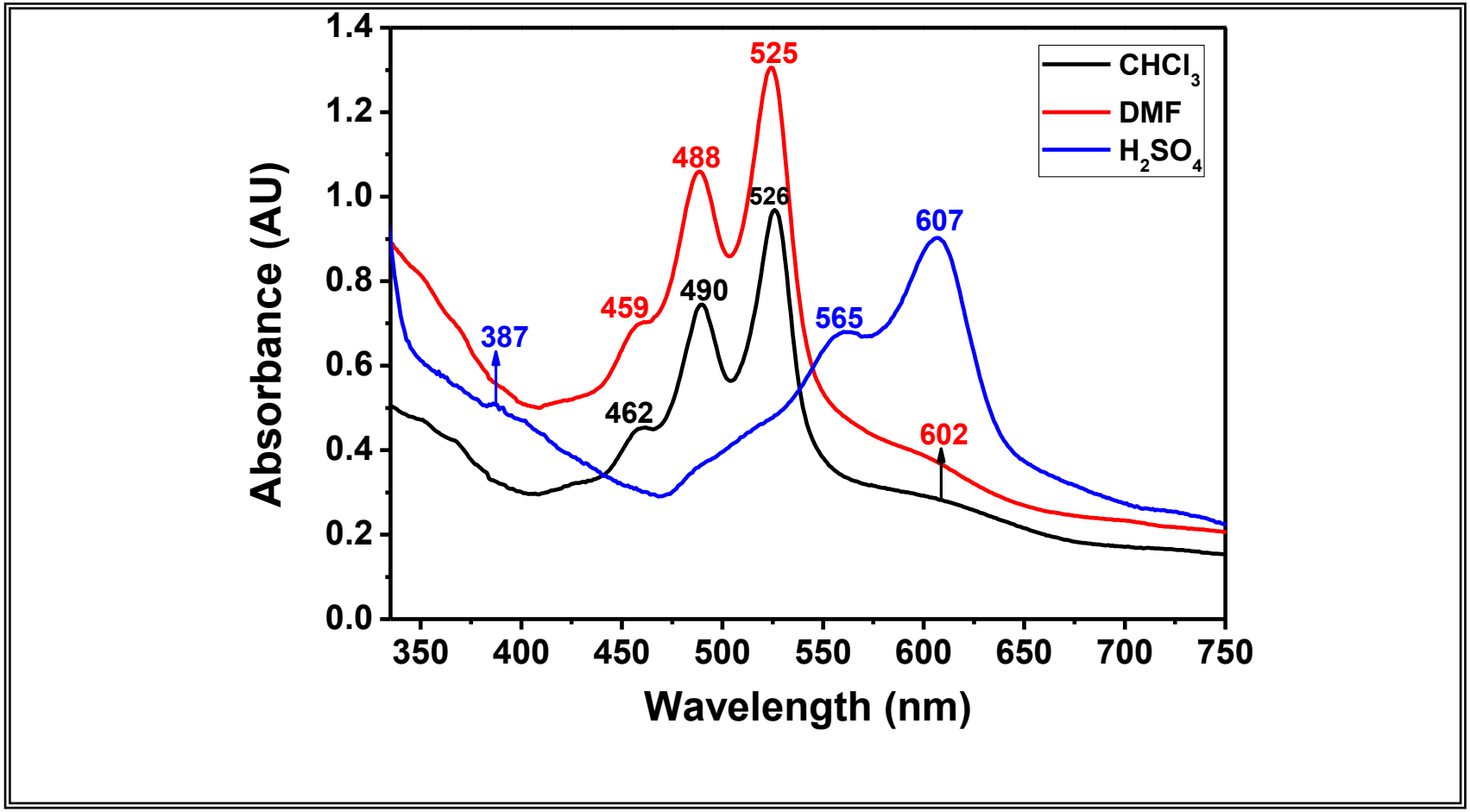

Figure 4.12: Comparison of UV-vis Absorption Spectra of BP-OHPDI in Nonpolar, Dipolar Aprotic, and Acidic Solutions

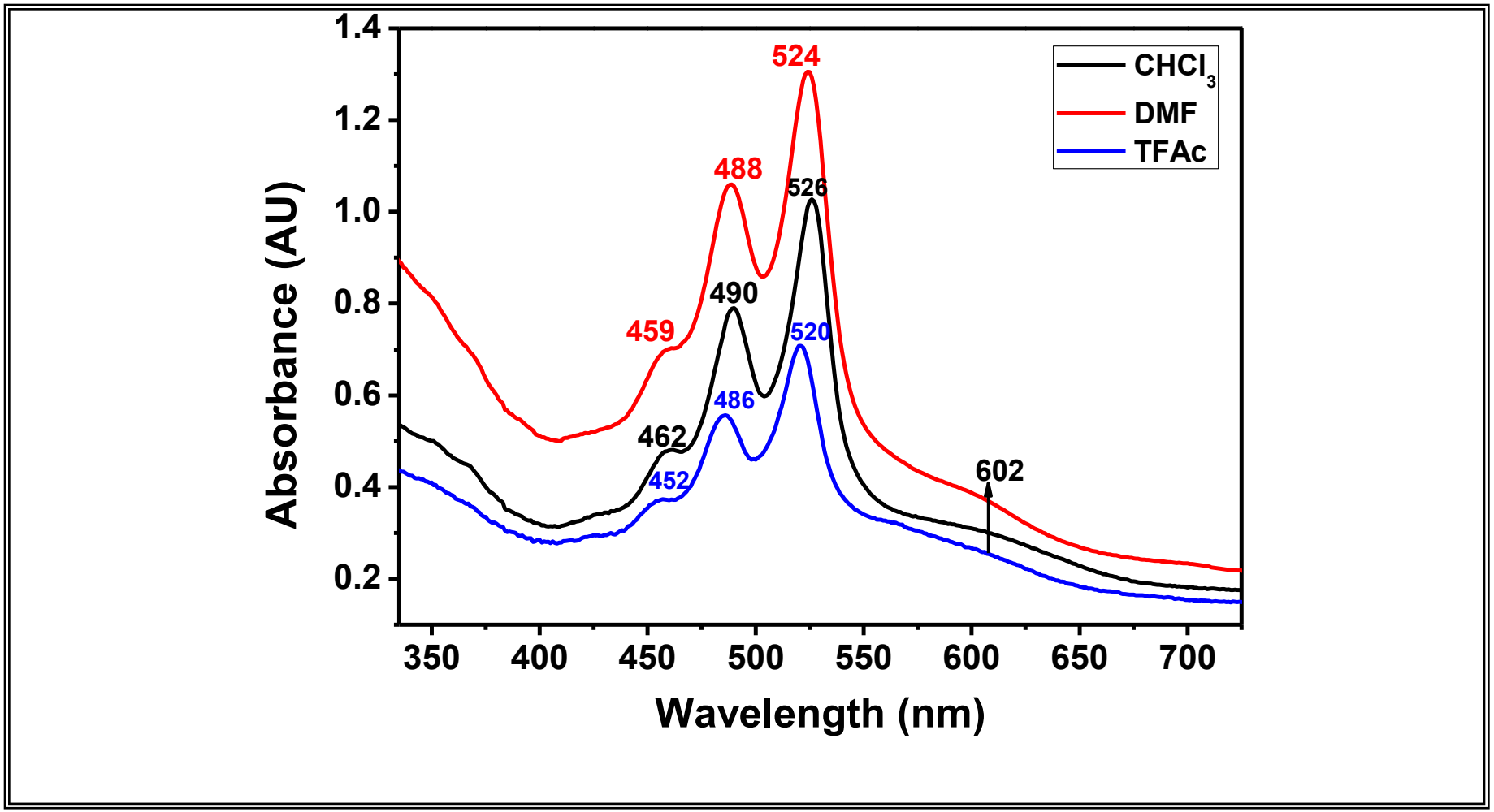

Figure 4.13: Comparison of UV-vis Absorption Spectra of BP-OHPDI in Nonpolar, Dipolar Aprotic, and Acidic Solutions

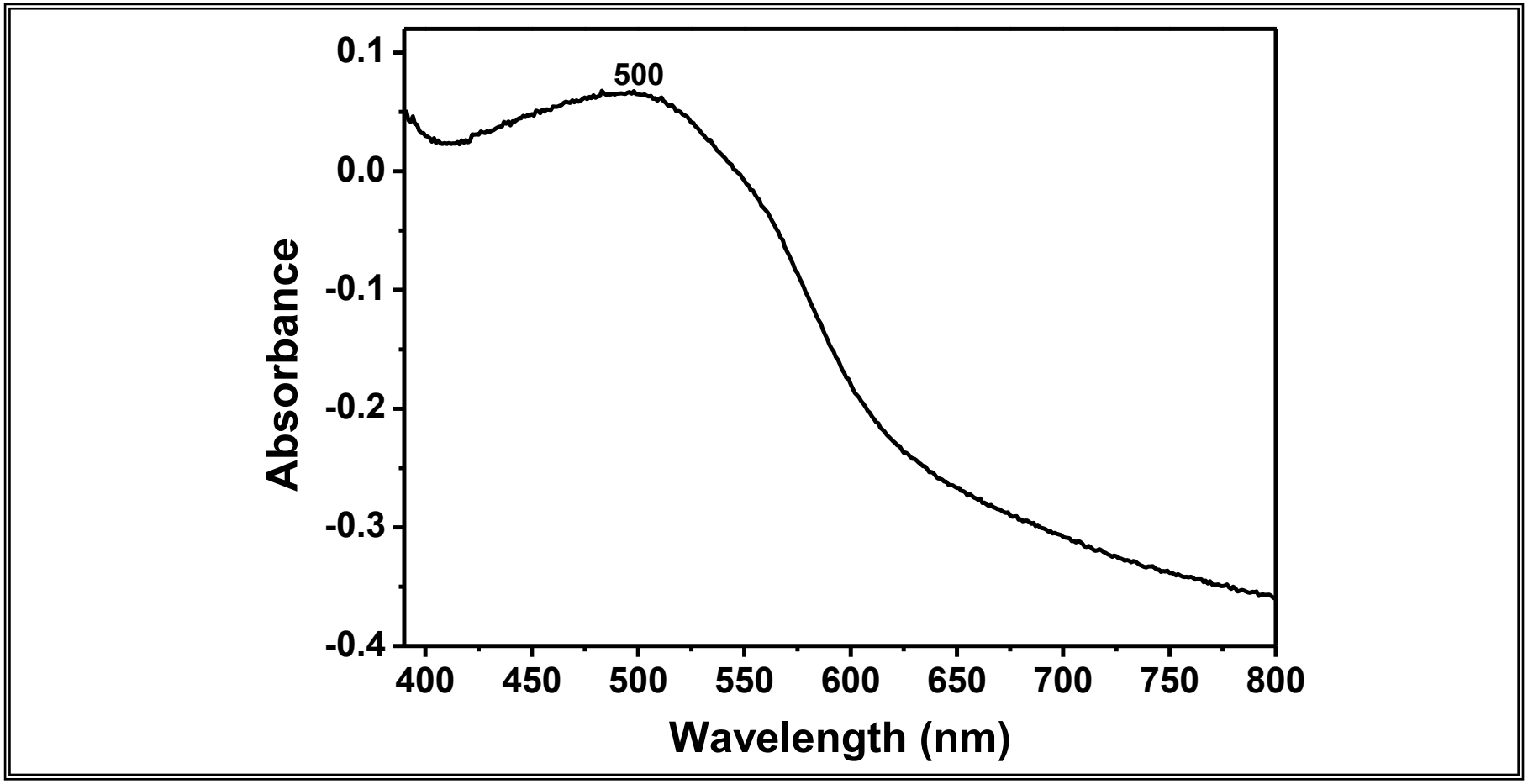

Figure 4.14: UV-vis Absorption Spectrum of Bp-4B at Solid-state

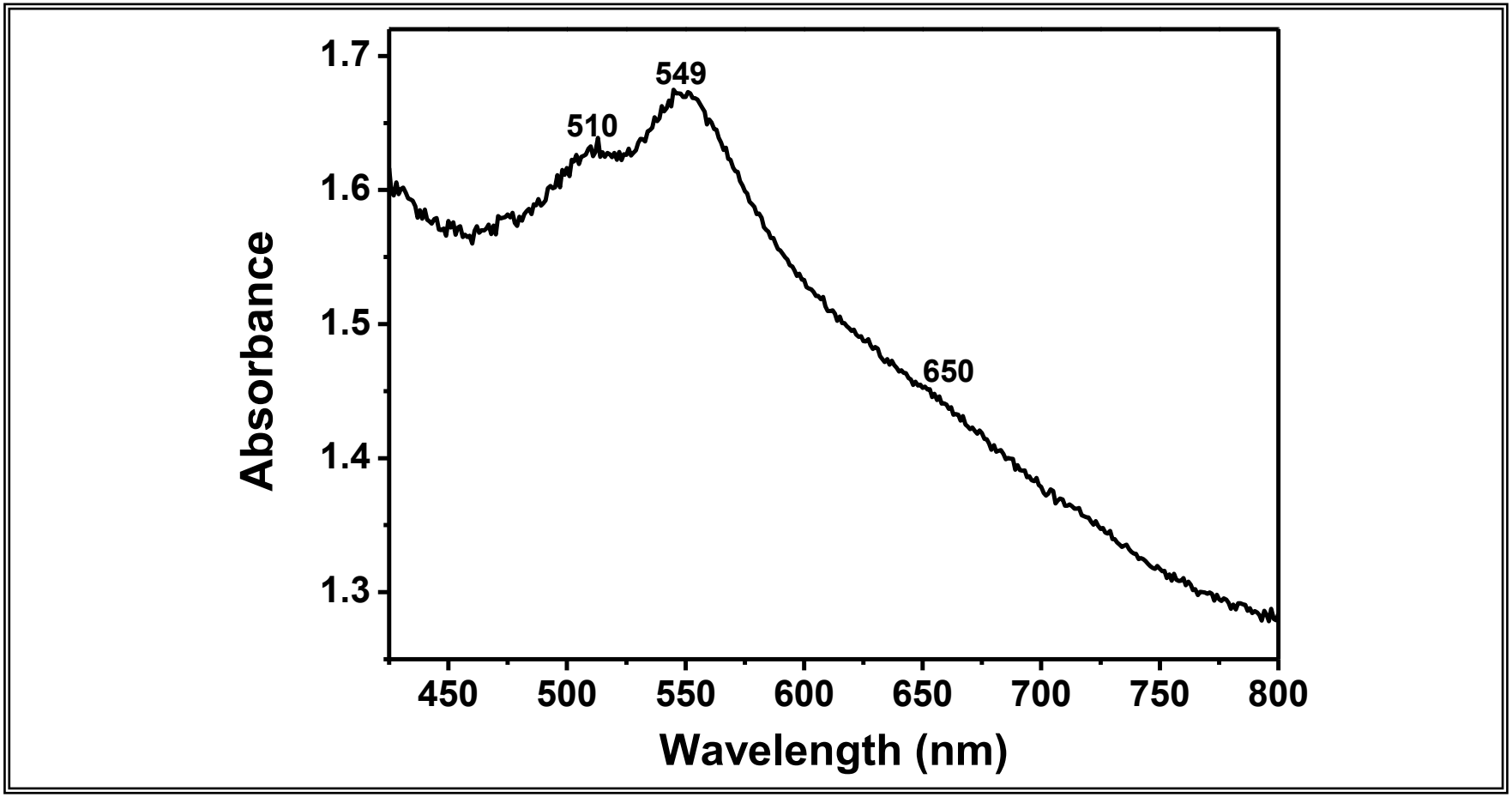

Figure 4.15: UV-vis Absorption Spectrum of BP-OHPDI at Solid-state

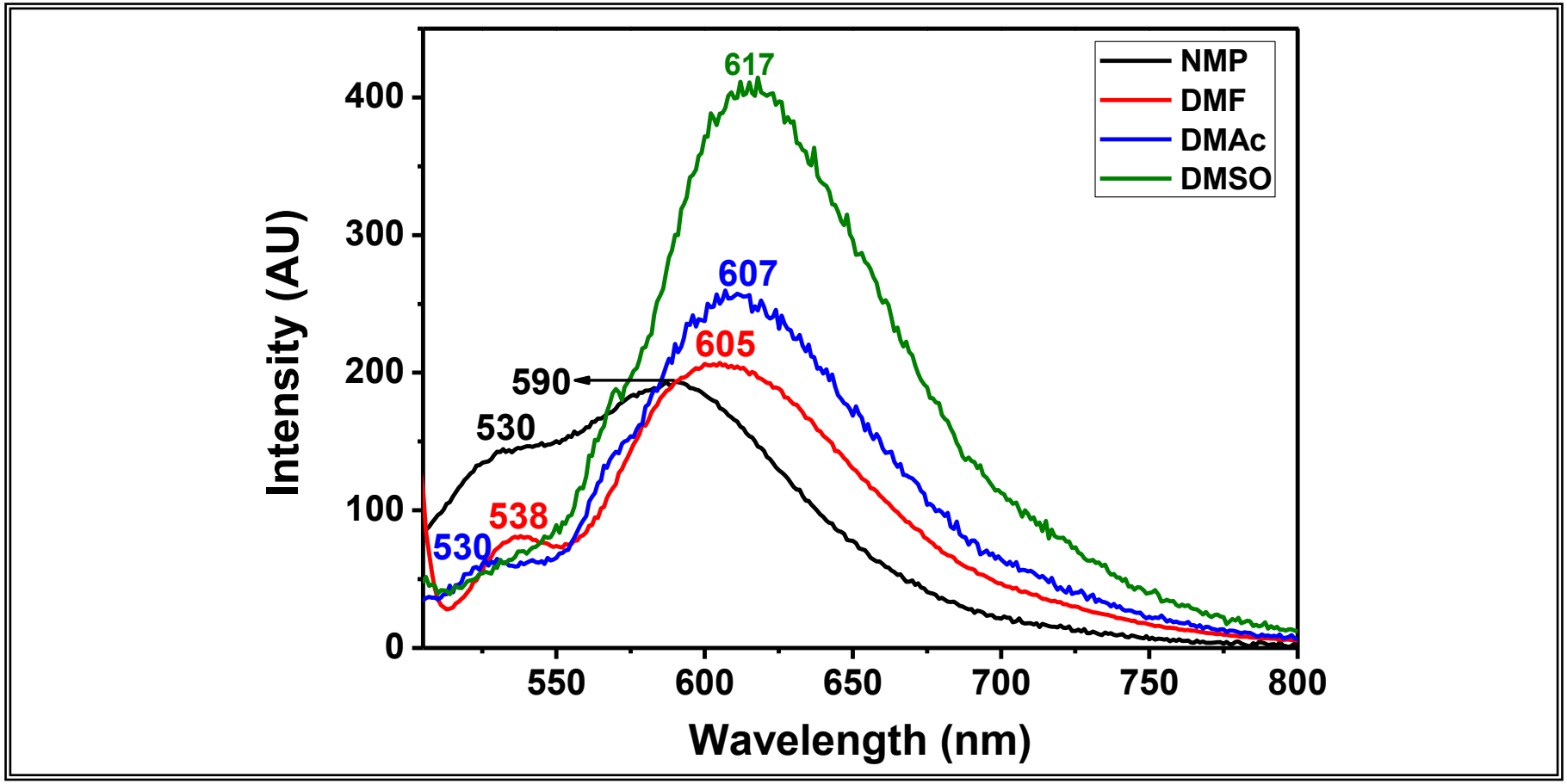

Figure 4.16: Comparison of Emission Spectra (at λ_{max} = 485 nm) of Bp-4B in Dipolar Aprotic Solvents

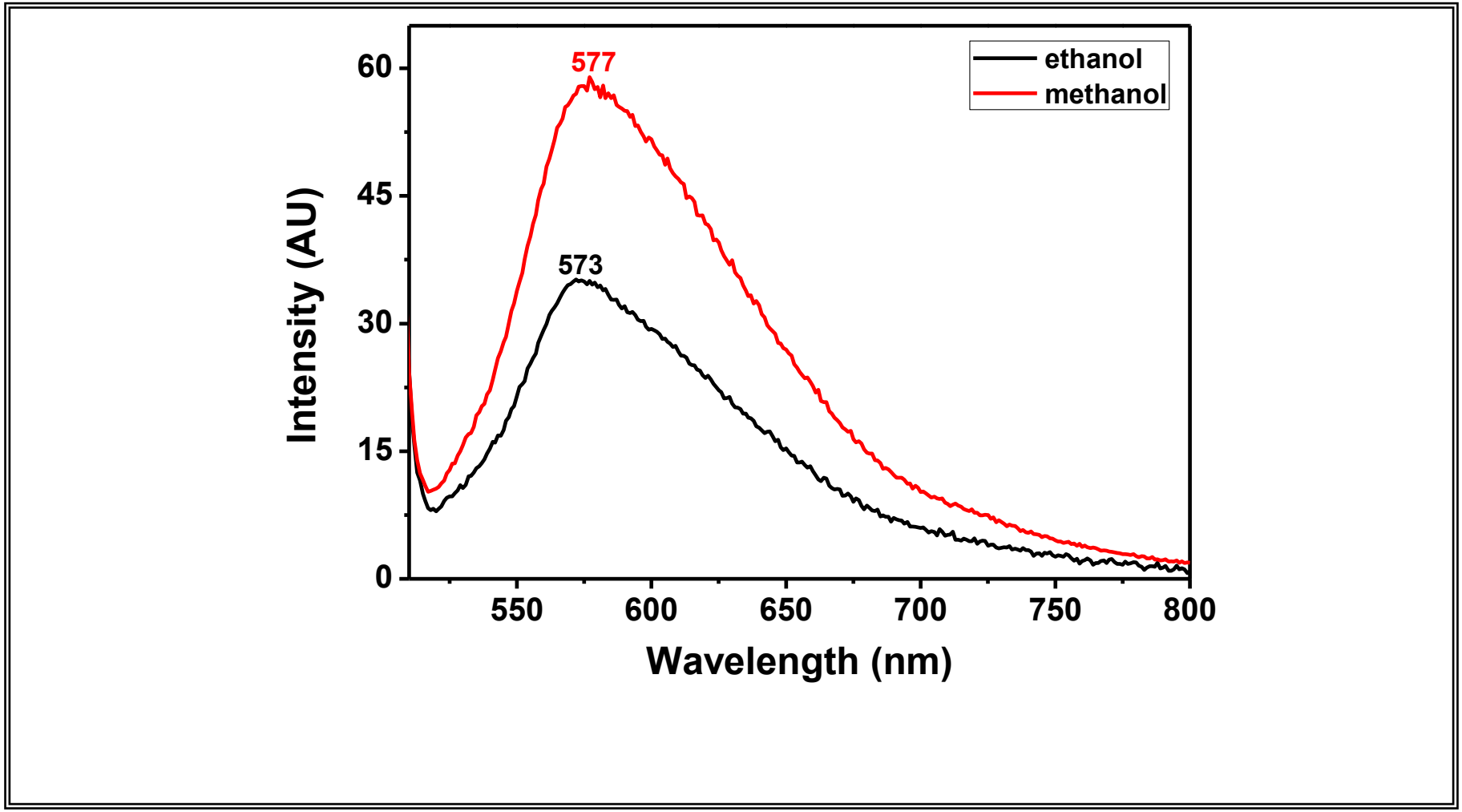

Figure 4.17: Comparison of Emission Spectra (at λ_{max} = 485 nm) of Bp-4B in Polar Protic Solvents

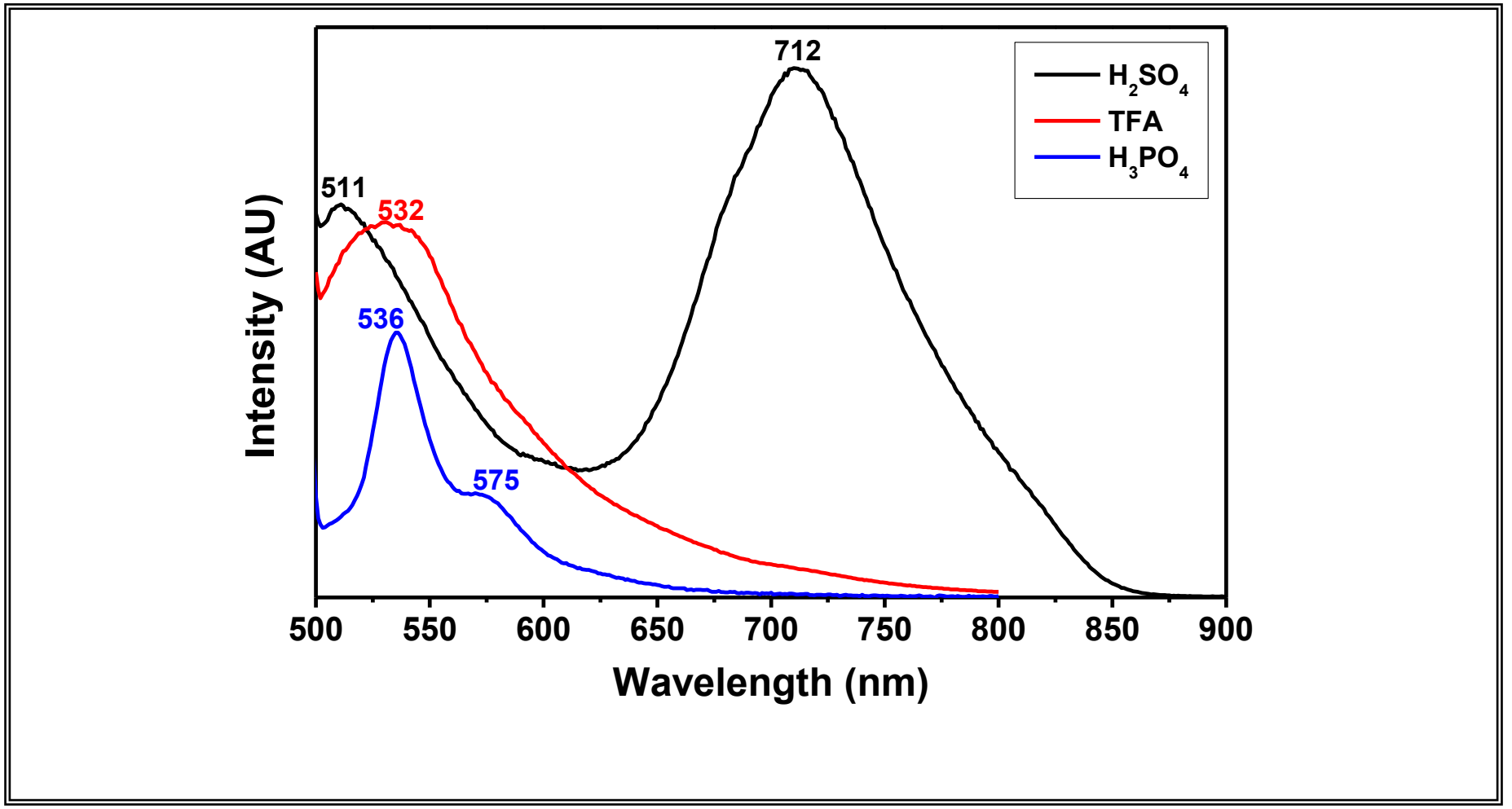

Figure 4.18 Comparison of Emission Spectra (at λ_{max} = 485 nm) of Bp-4B in Various Acids

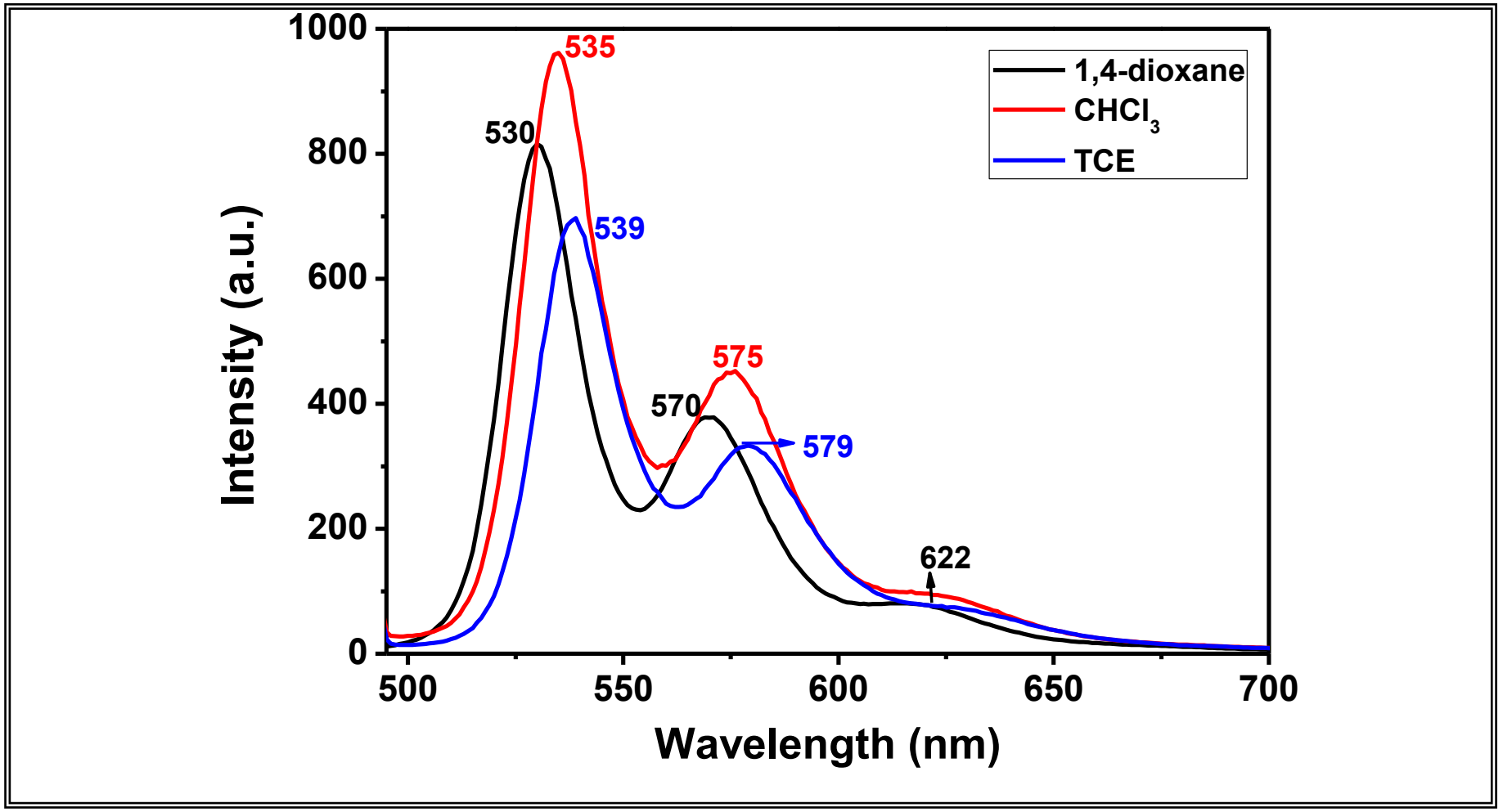

Figure 4.19: Comparison of Emission Spectra of BP-OH-PDI (at λ_{max} = 485 nm) in Nonpolar Solvents

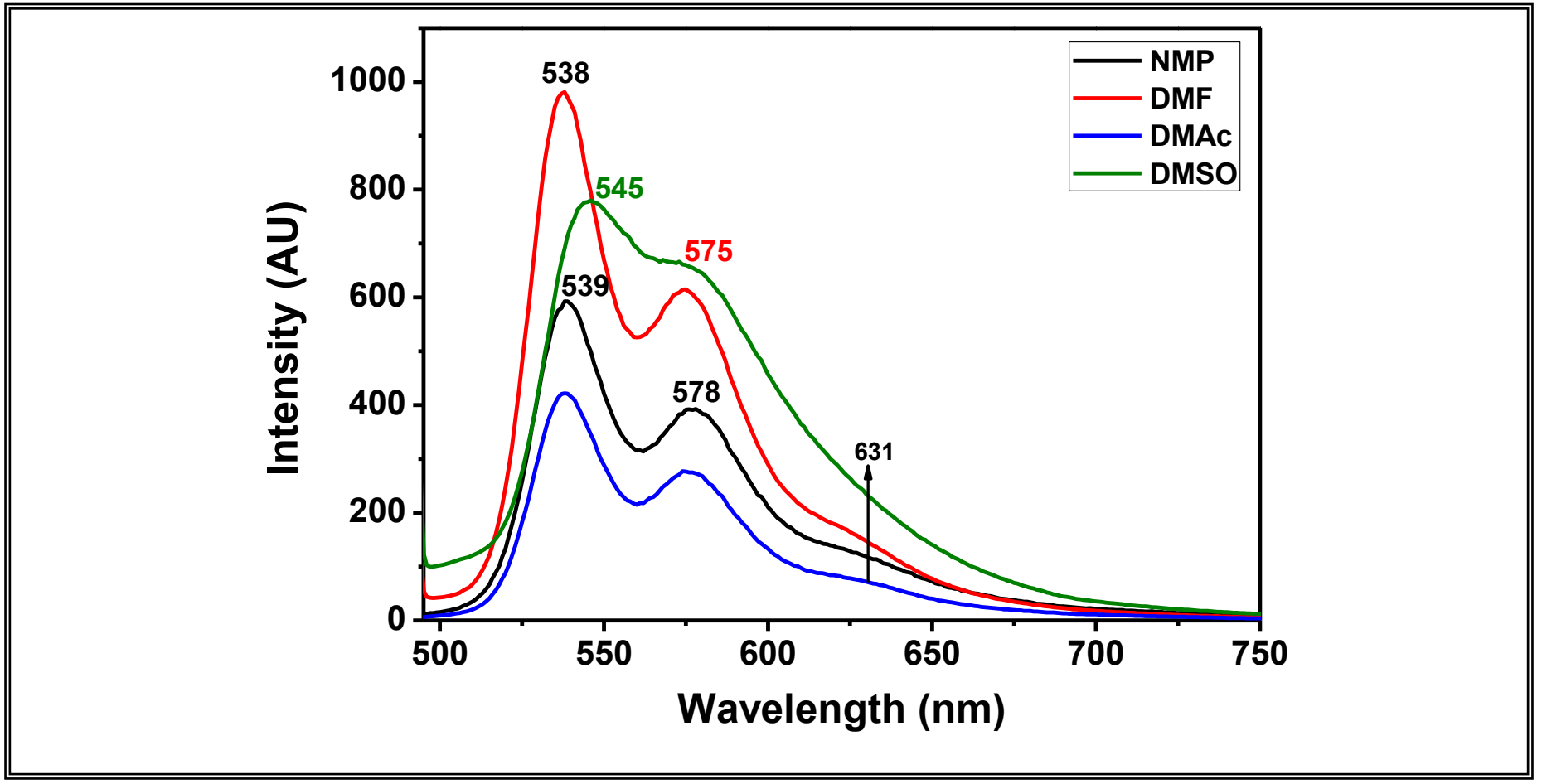

Figure 4.20: Comparison of Emission Spectra of BP-OHPDI (at λ_{max} = 485 nm) in Dipolar Aprotic Solvents

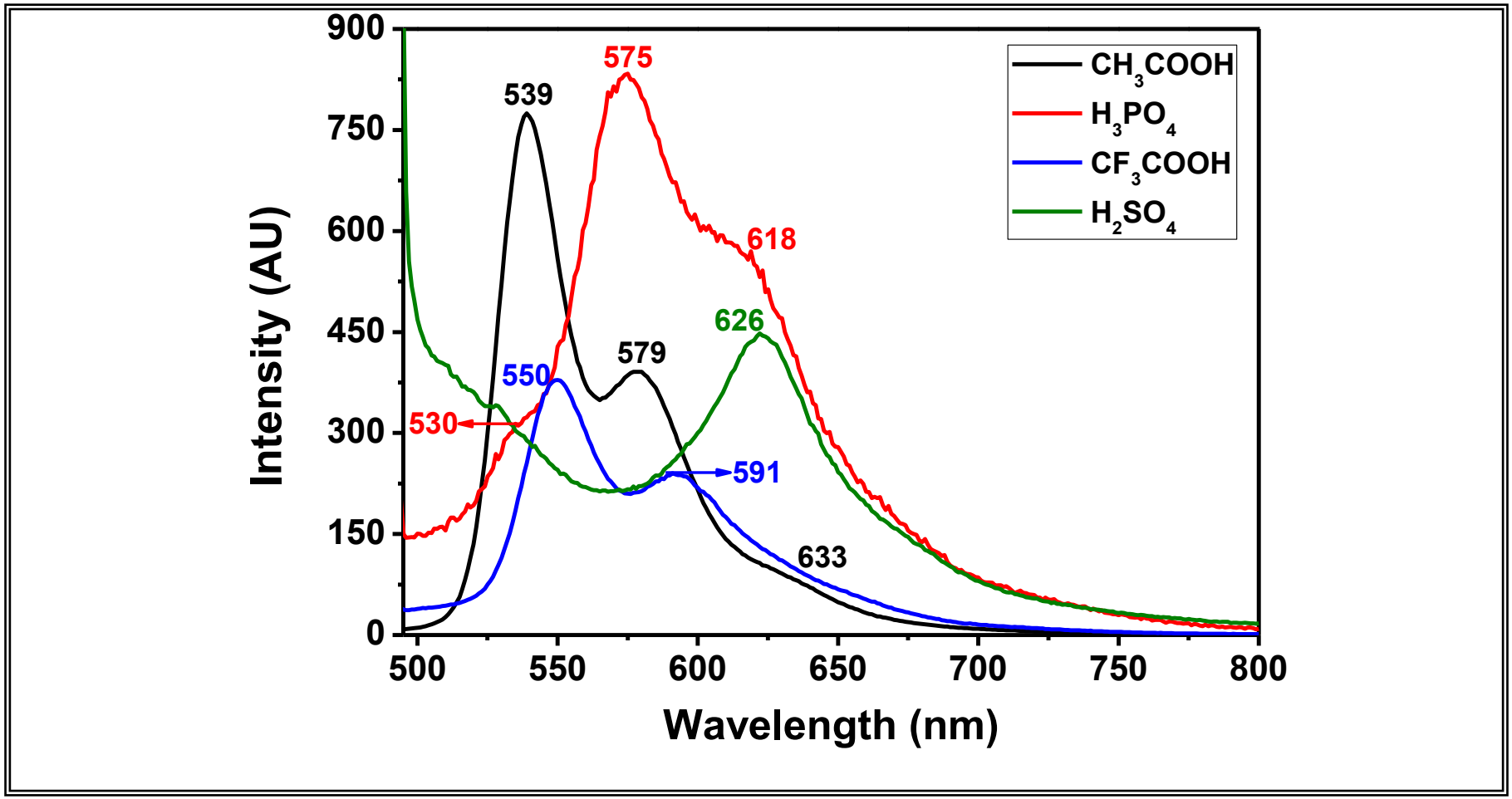

Figure 4.21: Comparison of Emission Spectra of BP-OHPDI (at λ_{max} = 485 nm) in Various Acids

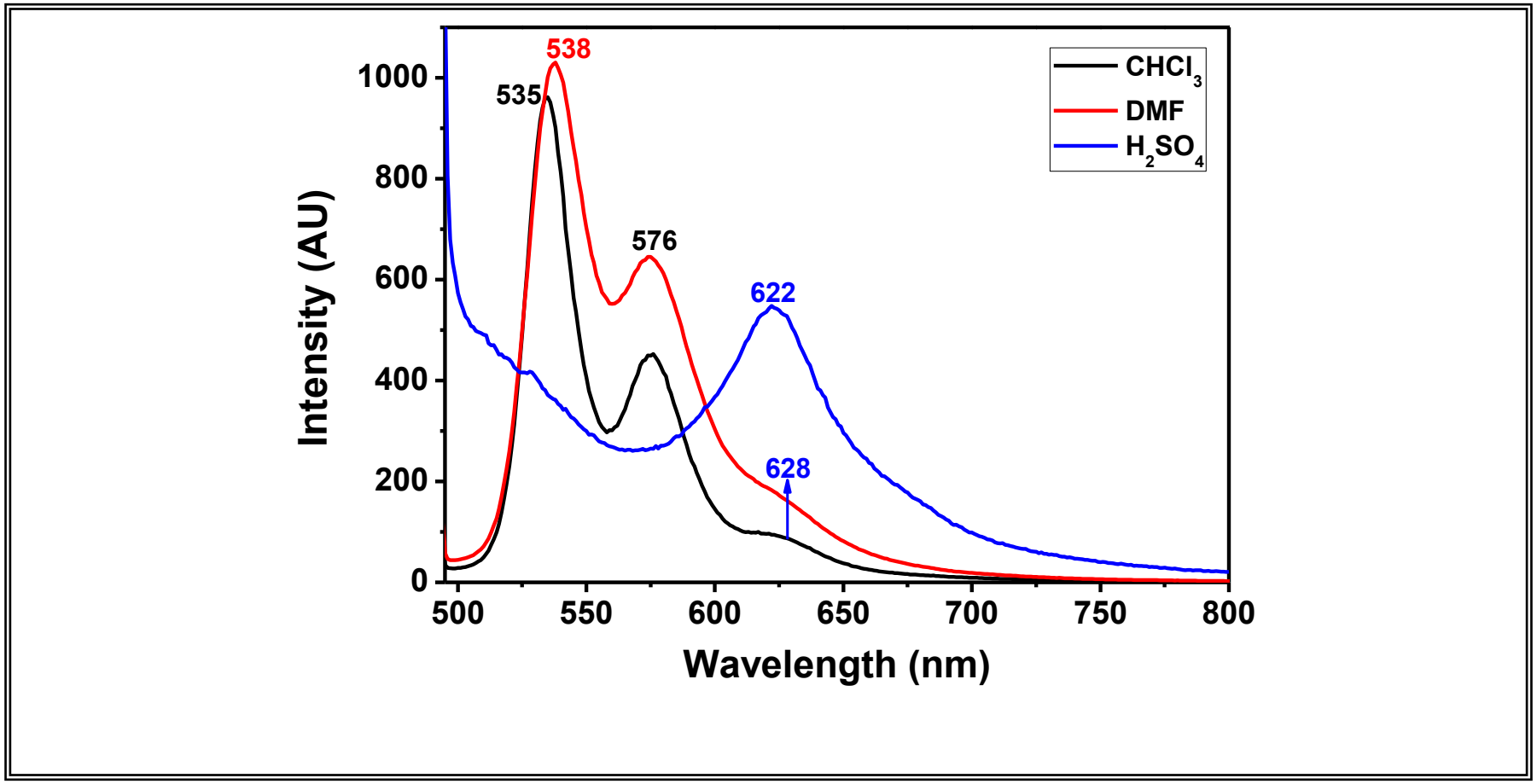

Figure 4.22: Comparison of Emission Spectra of BP-OH-PDI in Nonpolar, Dipolar Aprotic, and Acidic Solutions

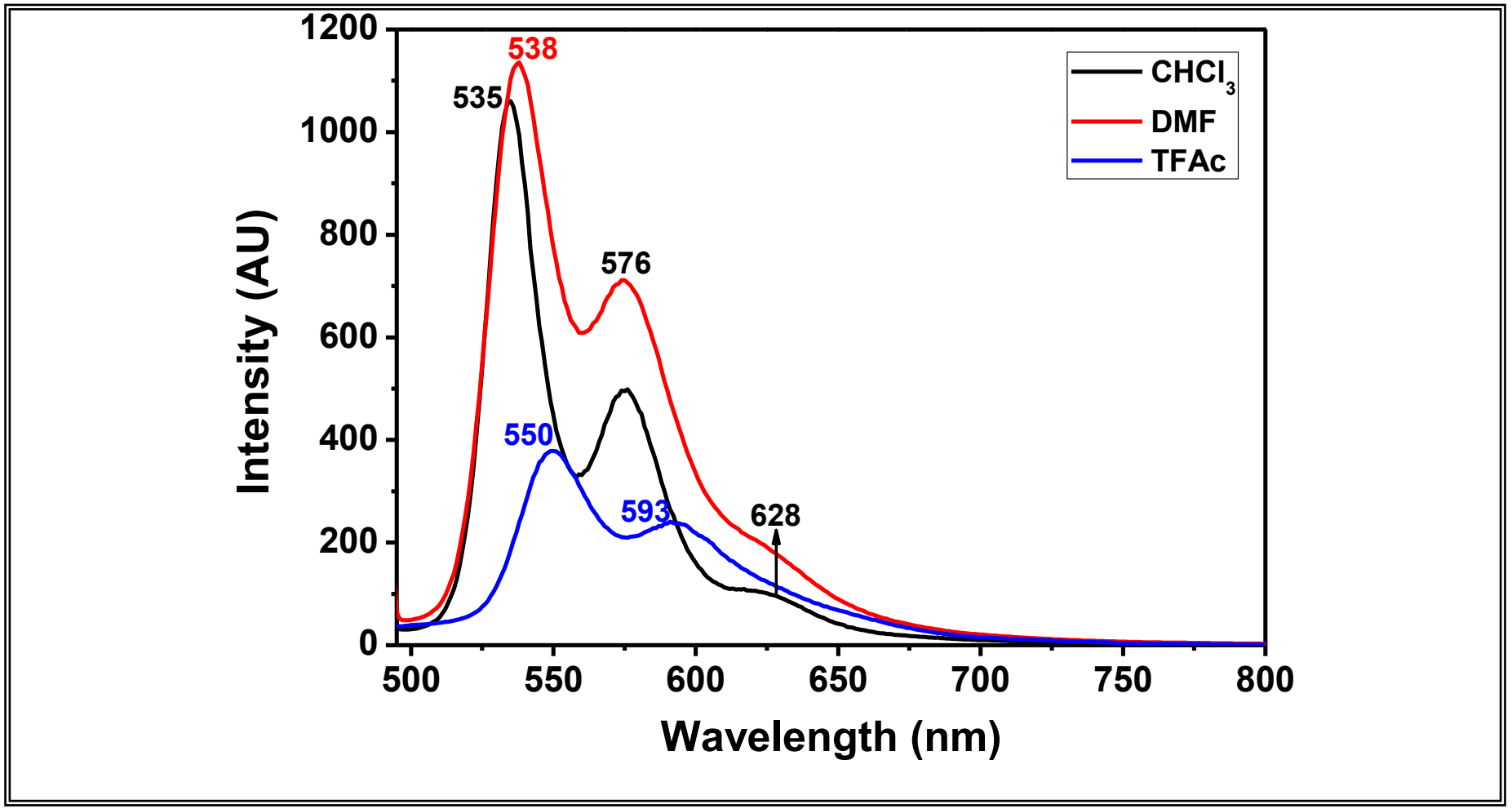

Figure 4.23: Comparison of Emission Spectra of BP-OHPDI in Nonpolar, Dipolar Aprotic, and Acidic Solutions

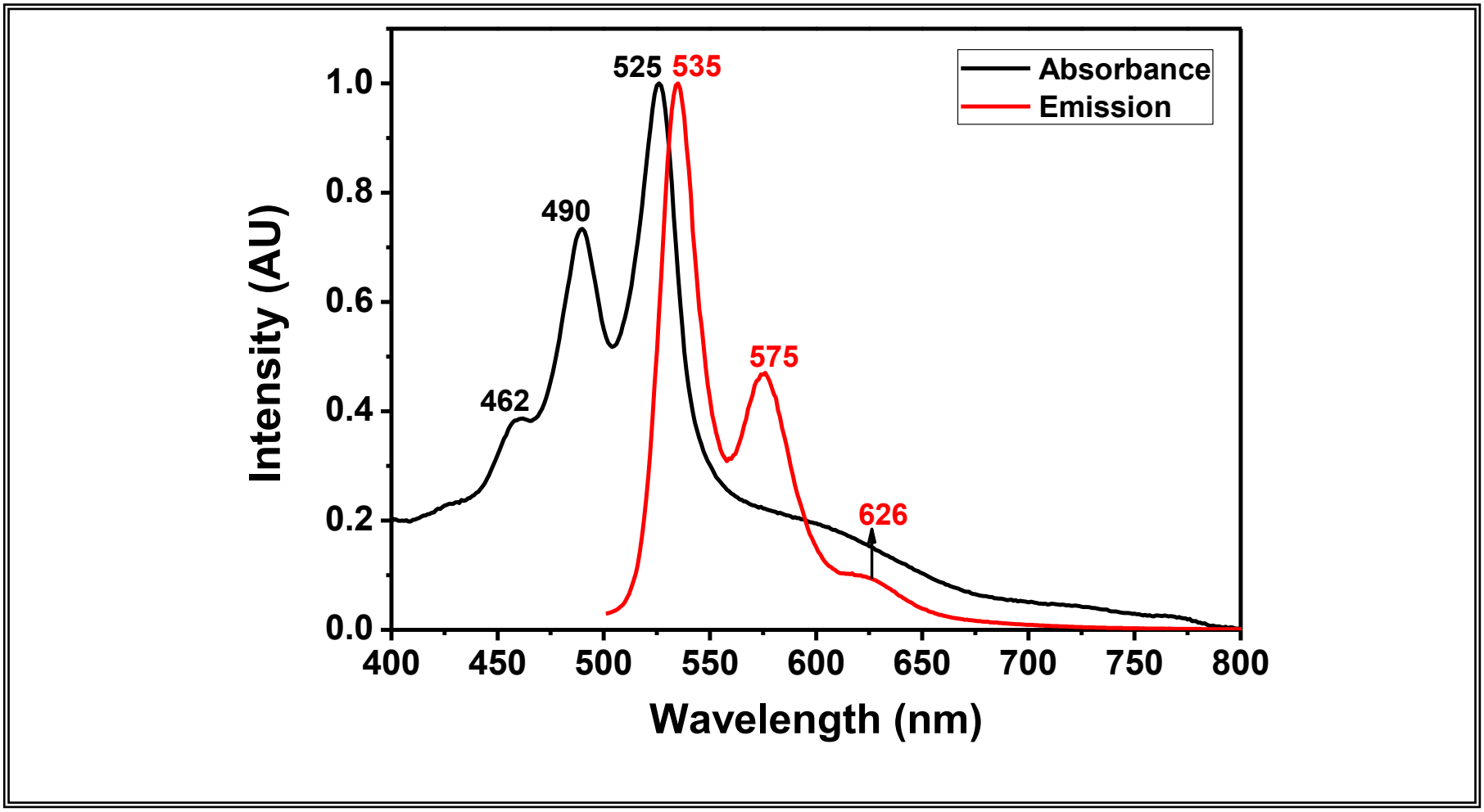

Figure 4.24: Comparison of Absorbance and Emission of BP-OHPDI in $CHCl_3$

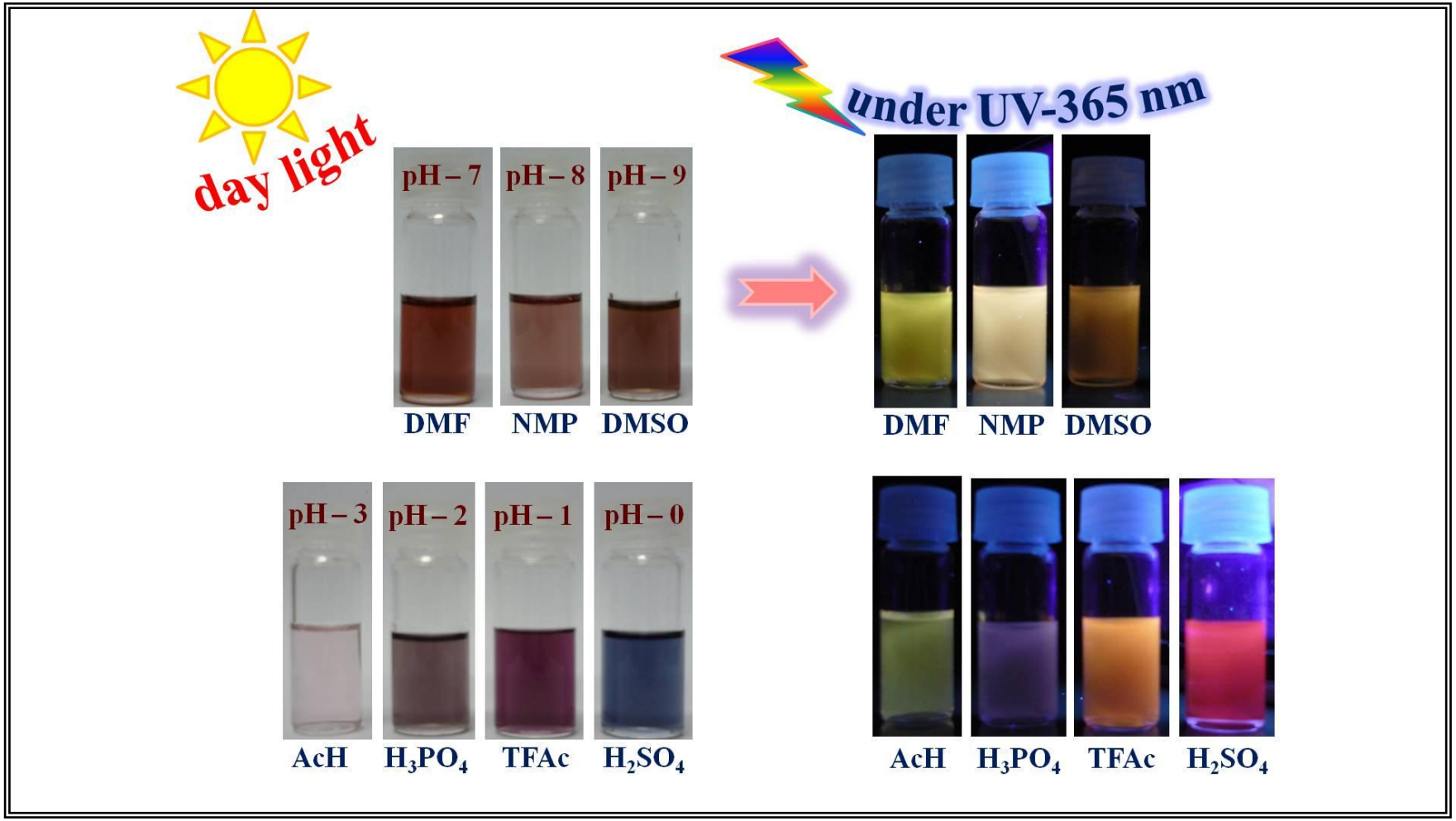

Figure 4.25: pH Sensing and the Fluorescence of BP-OHPDI

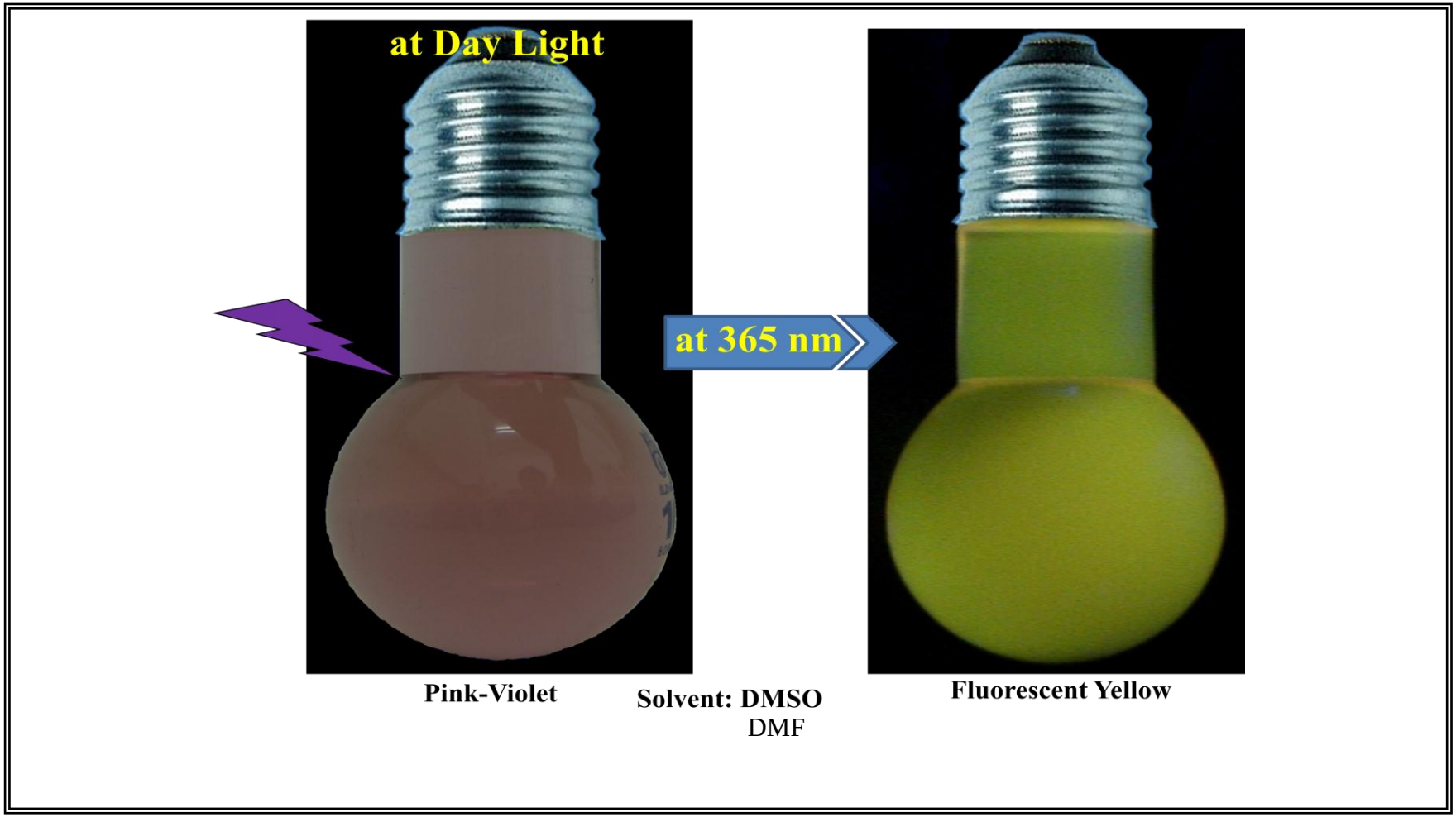

Figure 4.26: Fluorescence of BP-OHPDI and the Color Variation from Pink-Violet to Yellow in DMF

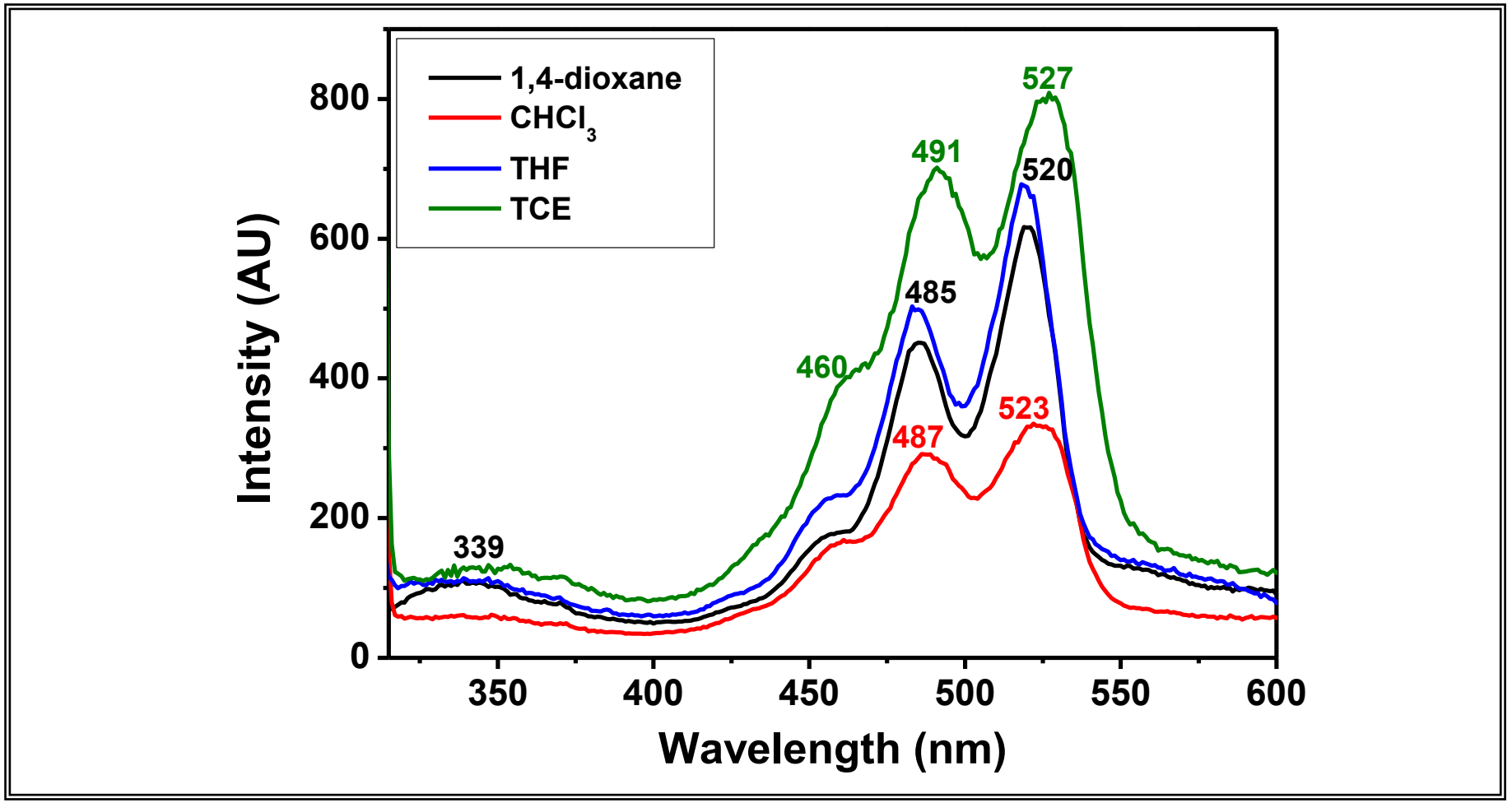

Figure 4.27: Comparison of Excitation Spectra of BP-OHPDI (at λ_{em} = 620 nm) in Nonpolar Solvents

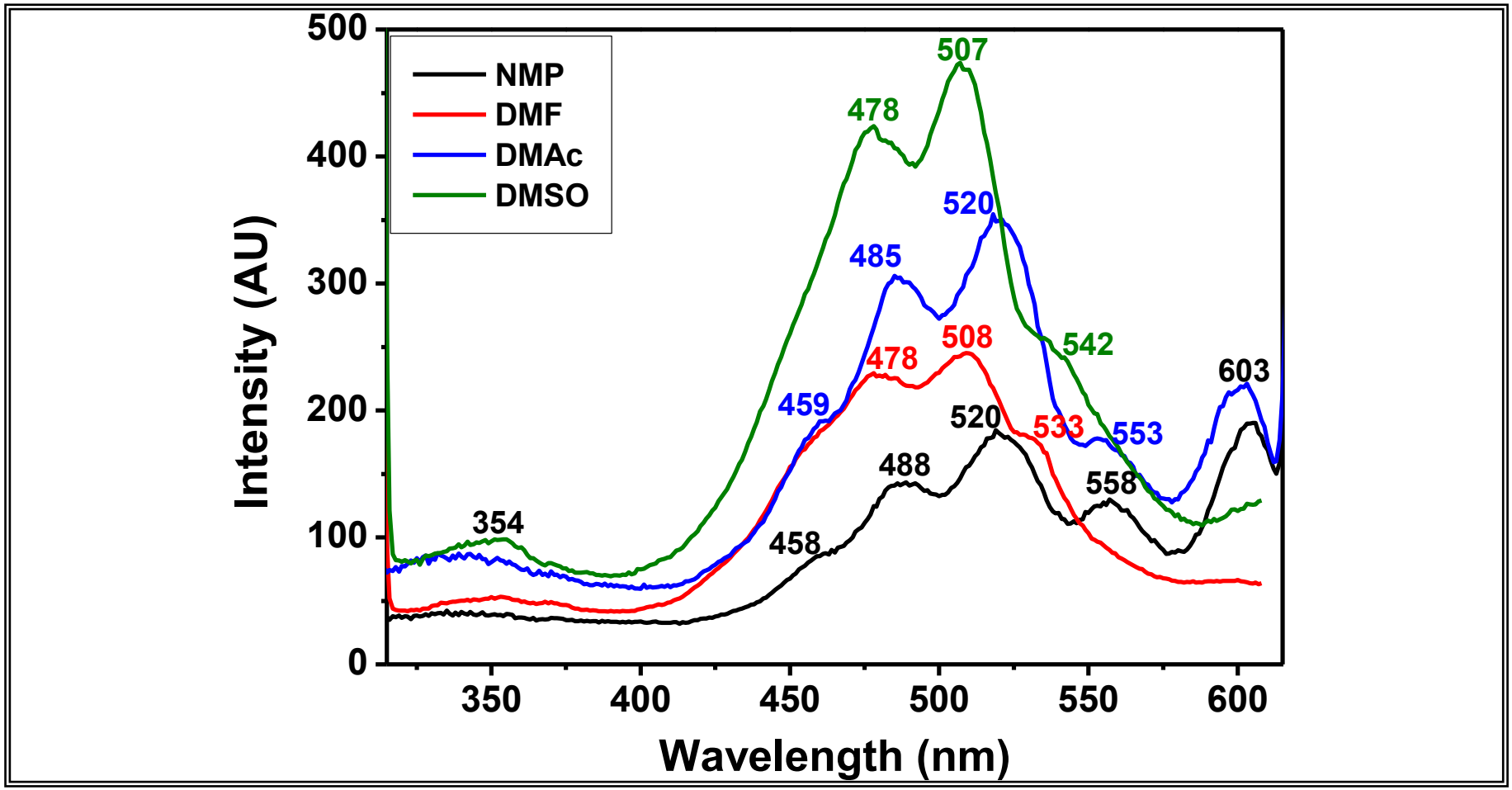

Figure 4.28: Comparison of Excitation Spectra of BP-OHPDI (at λ_{em} = 620 nm) in Dipolar Aprotic Solvents

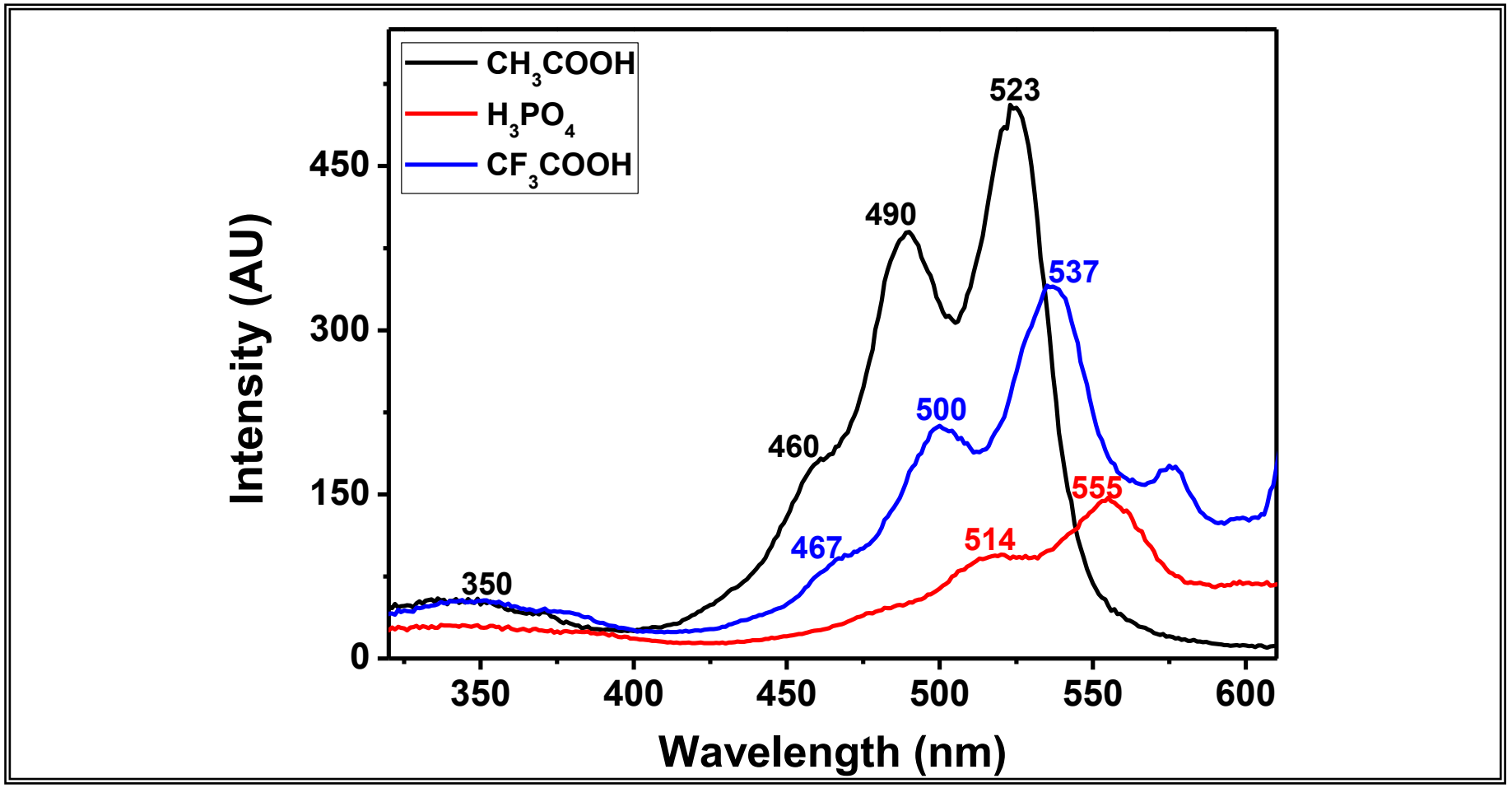

Figure 4.29: Comparison of Excitation Spectra of BP-OHPDI (at λ_{em} = 620 nm) in Various Acids

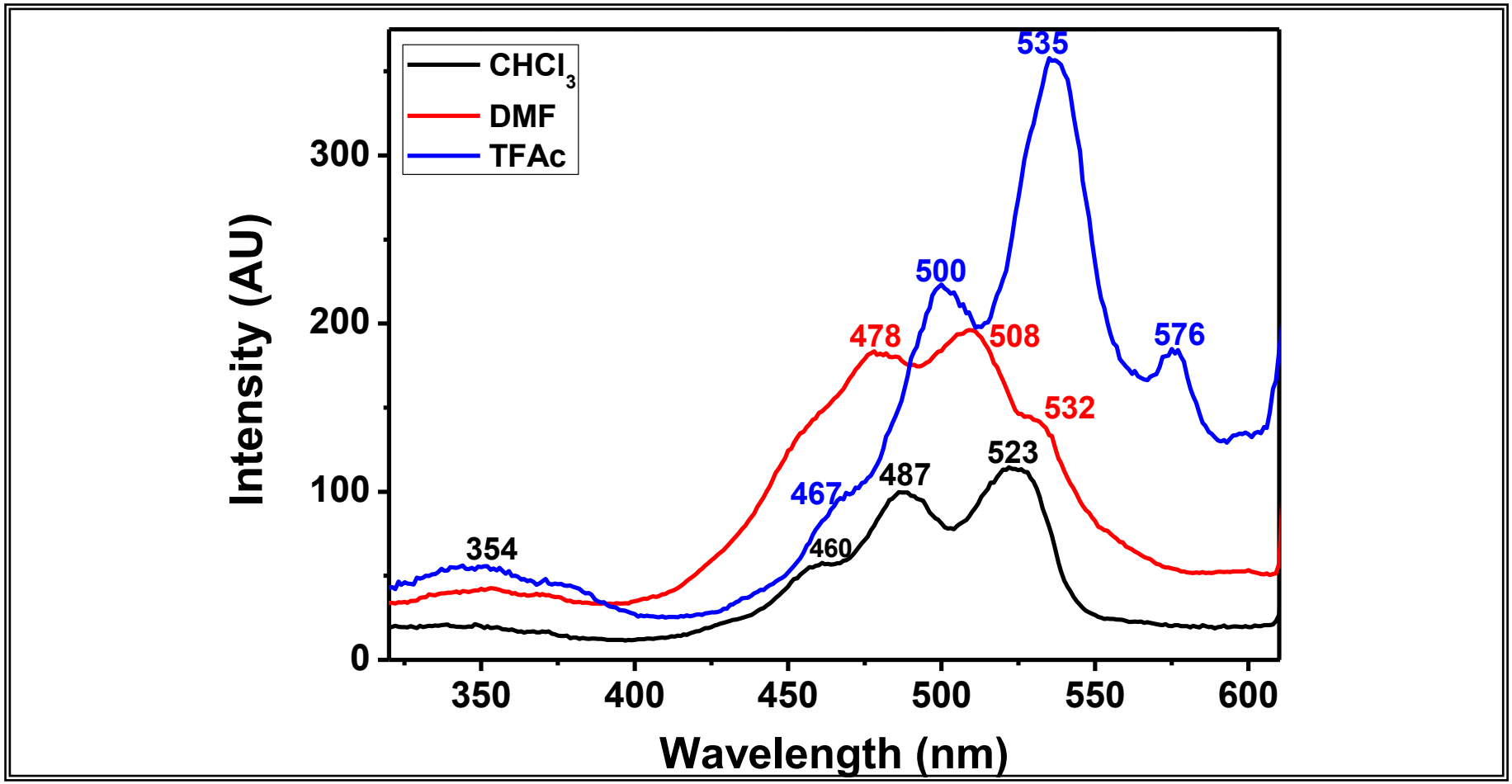

Figure 4.30: Comparison of Excitation Spectra of BP-OHPDI in Nonpolar, Dipolar Aprotic, and Acidic Solutions

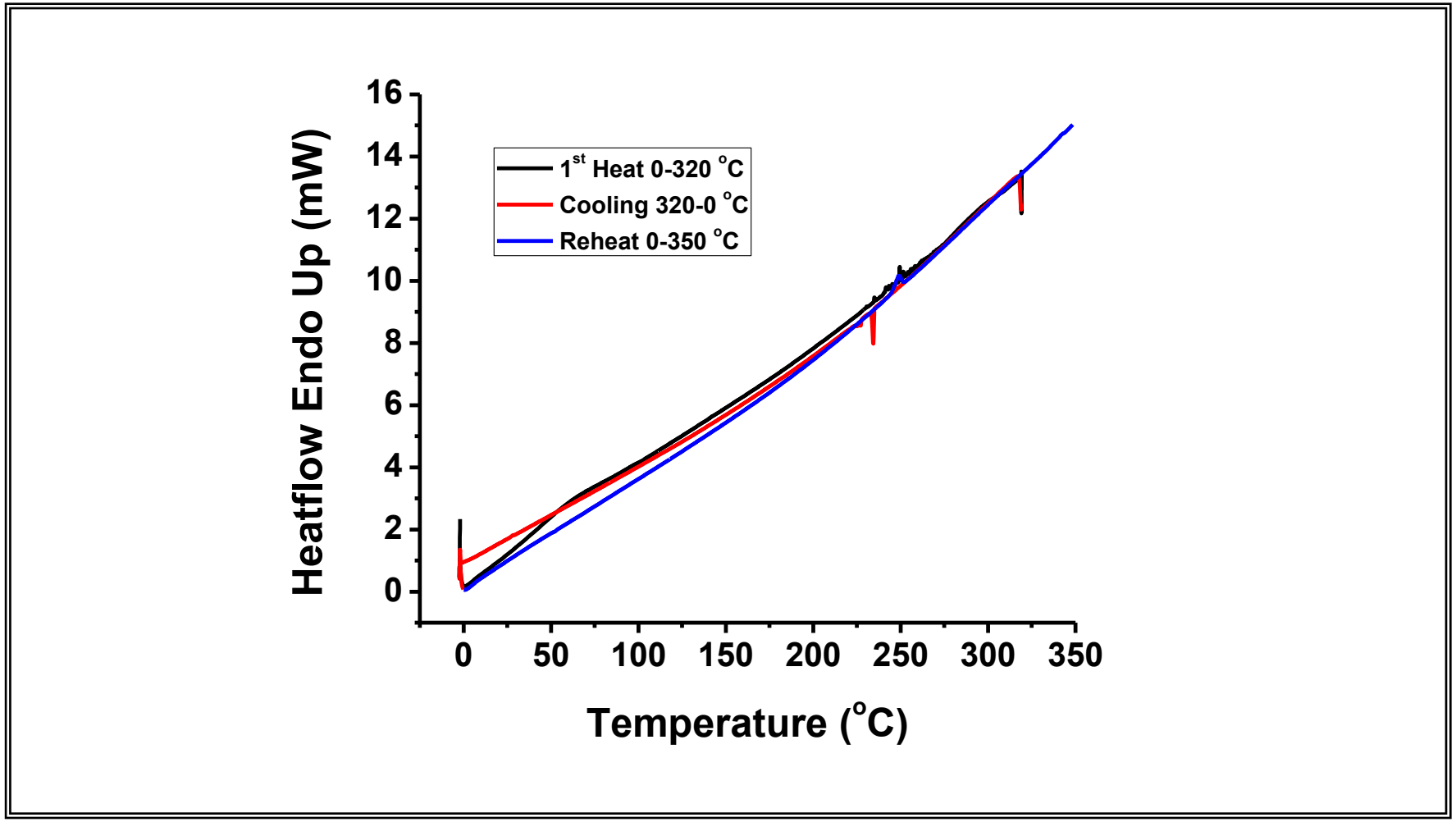

Figure 4.31: DSC Curves of Bp-4B at a Heating Rate of 10 °C/min under Nitrogen Atmosphere

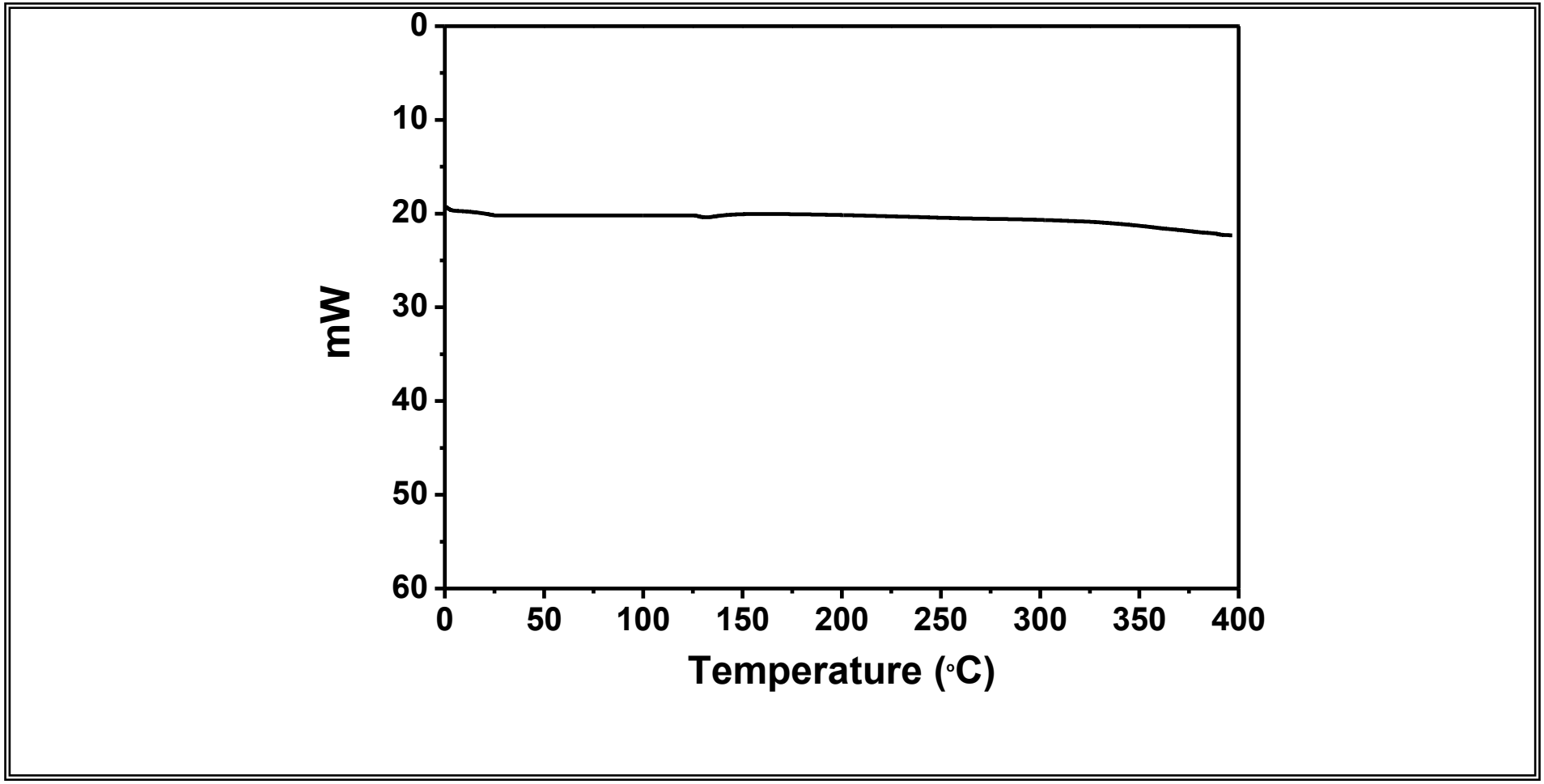

Figure 4.32: DSC Curve of BP-OHPDI at a heating rate of 10°C/min in nitrogen

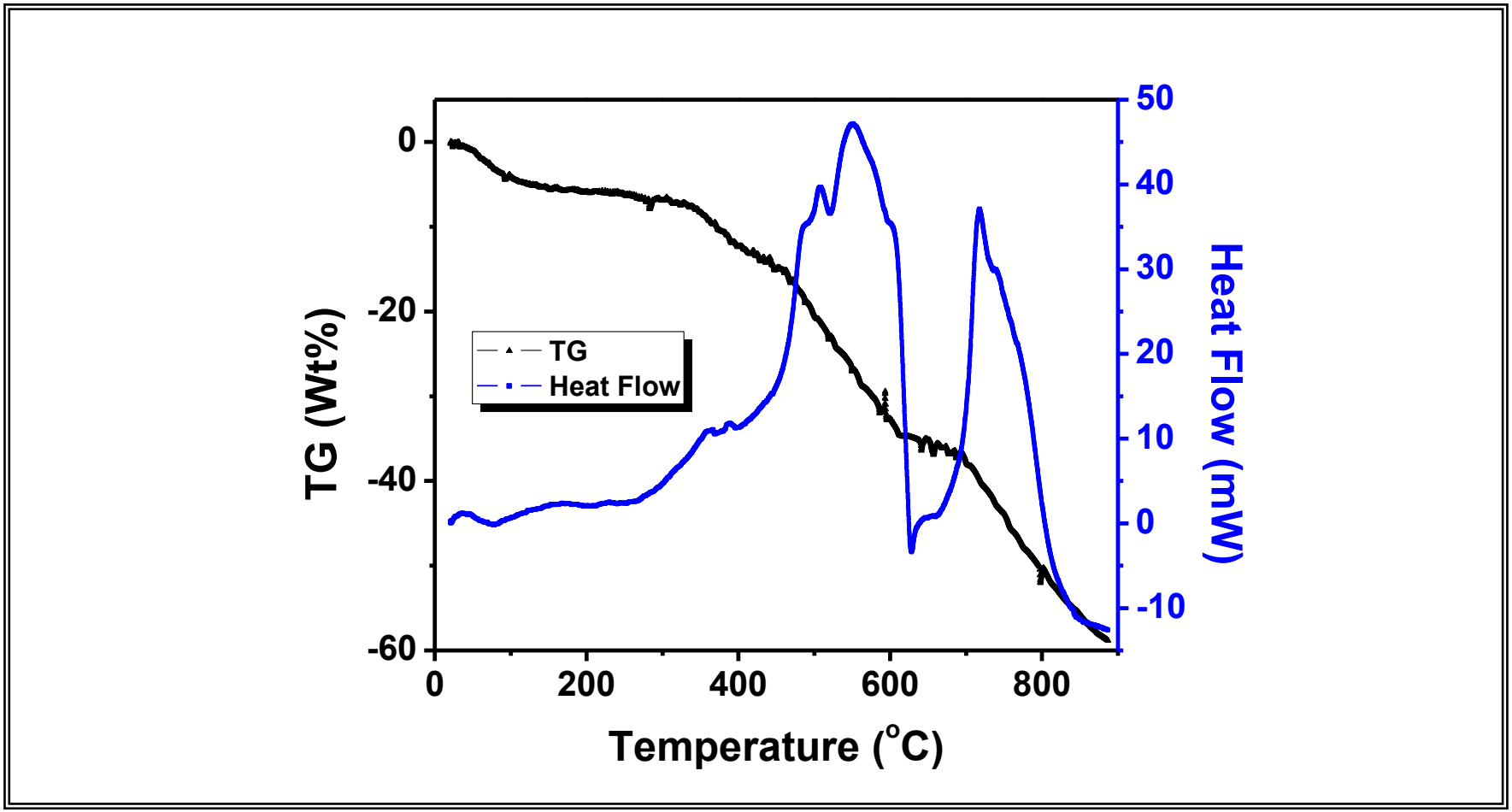

Figure 4.33: TGA Thermograms of Bp-4B at a Heating Rate of 10 ^{o}C/min under Oxygen Atmosphere

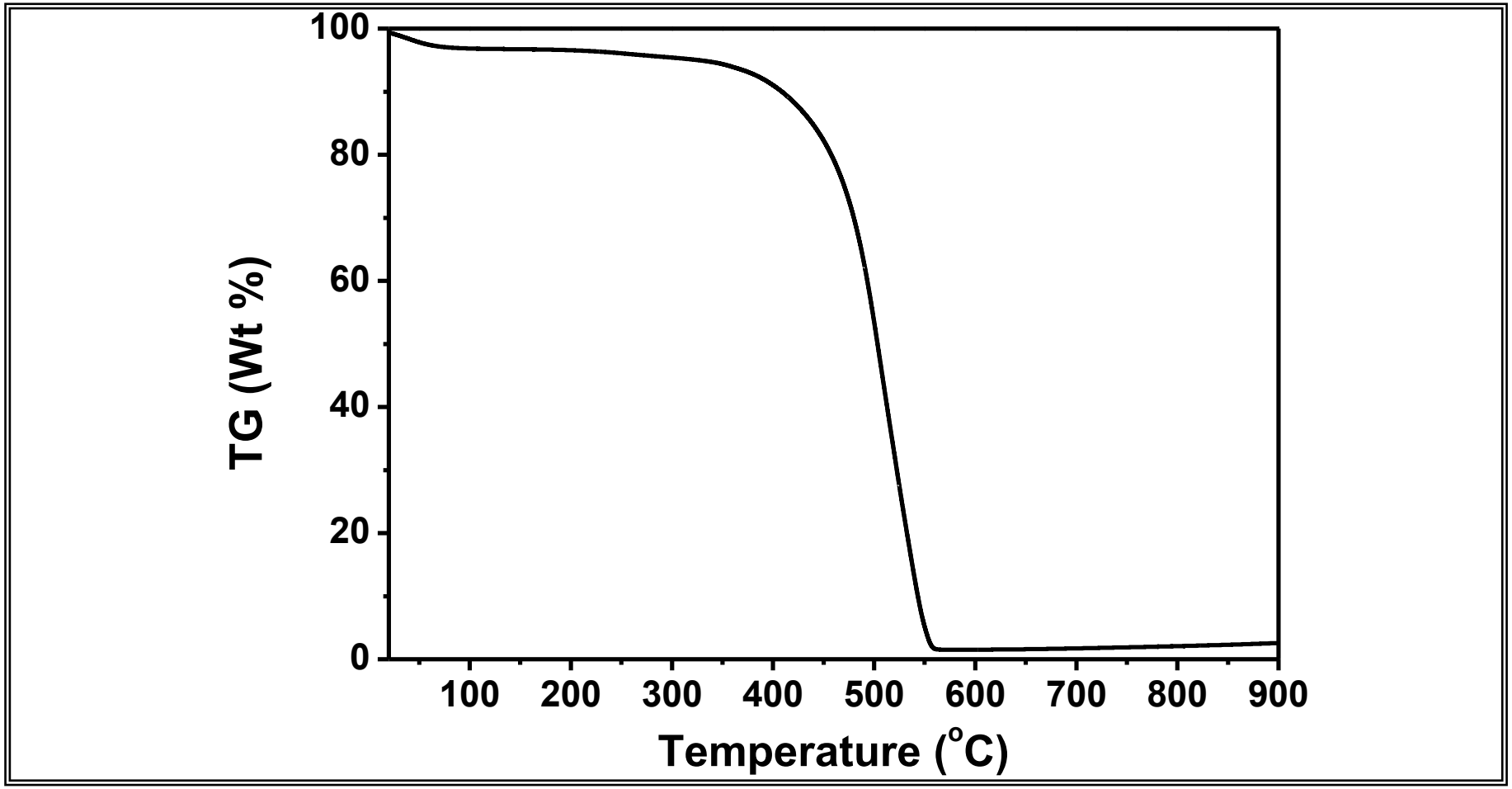

Figure 4.34: TGA Curve of BP-OH-PDI at a Heating Rate of 10 ^{o}C/min under Oxygen Atmosphere

Chapter 5

RESULTS AND DISCUSSION

5.1 Synthesis Analyses and IR Spectra

The synthesis of an unsymmetrical perylene dye by Nur Pasaogullari was considered as references for the present study and *N*-(4-Hydroxyphenyl)-3, 4, 9, 10-perylene tetracarboxylic-3, 4-anhydride-9, 10-imide (OH-PMI) was synthesized again by the reported synthesis procedure. In general, an unsymmetrical perylene derivative is prepared by a three-step reaction mechanism reported. The similar mechanism was also shown in Scheme 3.1. At first, perylene-3,4,9,10-tetracarboxylic acid monoanhydride monopotassium carboxylate was synthesized successfully. At the second step, *N*-alkyl(aryl)-3,4,9,10-perylenetetracarboxylic monoanhydride monoimide was prepared. After the preparation of OH-PMI, finally, the unsymmetrical perylene dye (BP-OHPDI) was synthesized via condensation of selected amine, benzopurpurin 4B and OH-PMI in presence of dried high boiling point solvents, *m*-cresol and isoquinoline. A careful observation of the reaction in terms of mole ratios of the reactants has given high attention to yield the desired product (Scheme 3.2).

The synthesized products were characterized by solid state FT IR spectra in solid-state using KBr pellets (Figure.4.3–4.5). The obtained FT-IR spectra of the new compounds represent all the main functional groups present in their structures. The detailed analyses of the FT-IR spectra are given below.

From the IR spectrum of Figure 4.3, -NH_2 asymmetric and symmetric stretches at 3424 cm^{-1}, aromatic C–H stretch at 3060 cm^{-1}, aliphatic C–H stretch at 2963 cm^{-1} and 2925 cm^{-1}, conjugated C=C stretches at 1600 cm^{-1}, C–N stretch at 1366 cm^{-1}, sulfur dioxide and S-O absorptions at 1176 and 1112 cm^{-1}, aromatic C–H bend at 744 cm^{-1} prove the functional groups present in BP.

From the IR spectrum of Figure 4.4, -OH stretch at 3499 cm^{-1}, aromatic C–H stretch at 3118 cm^{-1}, anhydride C=O stretch at 1773 cm^{-1} and 1730 cm^{-1}, imide C=O stretch at 1698 cm^{-1} and 1659 cm^{-1}, conjugated C=C stretch at 1594 cm^{-1}, C–N stretch at 1300 cm^{-1}, phenolic C-OH absorption at 1234 cm^{-1}, aromatic C–H bend at 809 cm^{-1} and 731 cm^{-1} prove the functional groups present in OH-PMI.

From the IR spectrum of Figure 4.5, -OH stretch at 3450 cm^{-1}, aromatic C–H stretch at 3050 cm^{-1}, aliphatic C–H stretch at 2924 cm^{-1}, imide C=O stretches at 1700 cm^{-1} and 1666 cm^{-1}, conjugated C=C stretch at 1593 cm^{-1}, C–N stretch at 1357 cm^{-1}, weak stretches at 1128 and 1020 cm^{-1} indicating the sulfur dioxide and S-O absorptions, aromatic C–H bend at 810 cm^{-1} and 750 cm^{-1} prove the major functional groups present in BP-OHPDI.

When we compared the IR spectra of three compounds aromatic C-H stretch and aliphatic C-H stretches were observed in all the three spectra. The main functional

group, anhydride carbonyls were noticed only for OH-PMI but do not exist for BP-OHPDI. Weak imide carbonyls (1698 cm^{-1} and 1659 cm^{-1}) were observed for OH-PMI because of the monoimide; whereas existence of two strong imide peaks (1700 cm^{-1} and 1666 cm^{-1}) and absence of anhydride peaks were noticed for BP-OHPDI. On the other hand, no imide peaks were noticed for Bp-4B except an overlap of Ar C=C and NH_2 bending around 1700 – 1600 cm^{-1} region. Furthermore, NH_2 stretch exists in the reactant Bp-4B was lost and only –OH stretch was appeared for BP-OHPDI.

5.2 Solubility of BP-OHPDI

Table 5.1 The solubility, color, and pH details of BP-OHPDI

SOLVENTS	**SOLUBILITY**	**COLOR** Day-Light	**pH**	**COLOR** Under 365 nm
DMSO	Partly soluble	pink violet	9	orange-yellow
DMAc	Partly soluble	pink- violet	7	yellowish
DMF	Partly soluble	Pink violet	7	greenish-yellow
NMP	Slightly soluble	pink violet	8	orange - yellow
PYRIDINE	Slightly soluble	pink -violet	7	greenish-yellow
CH_2Cl_2	Slightly soluble	pink -violet	7	yellow
1,1,2,2-TCE	Partly soluble	violet	7	yellow
THF	Slightly soluble	pink violet	7	pale yellow
$CHCl_3$	Slightly soluble	pink violet	7	greenish- yellow
CONC. H_2SO_4	Soluble	dark blue	0	Red
TFAc	Soluble	dark violet	1	orange
PHOSPHORIC	Partly soluble	violet	2	orange-yellow
ACETIC ACID	Slightly soluble	pale pink violet	3	greenish- yellow

In most of the organic and aqueous acidic solvents, the designed BP-OHPDI has shown partial solubility. On the other hand, the commercially available benzopurpurin 4B has shown good solubility, mostly in dipolar aprotic solvents. Partial solubility was noticed in protic solvents and in acids. OH-PMI has also shown partial solubility in a very few solvents namely, DMF, DMSO, in alkaline solutions such as 5% KOH and NaOH.

The comparison of solubility data of the three compounds was presented in the following table, Table 5.2.

Table 5.2 Solubility[a] details of BP, OH-PMI, and BP-OHPDI

Solvents	OH-PMI	Color Day light	BP-4B	Color Day light	BPOH-PDI	Color Day light
DMSO	(++++)	Pale brown	(++++)	Cherry red	(++ - -)	Pink violet
DMAc	(++++)	Pale brown	(++++)	Cherry red	(++ - -)	Pink violet
DMF	(++++)	Pale brown	(++++)	Cherry red	(++ - -)	Pink violet
MeOH	(- - - -)	Colorless	(+++ -)	Red-orange	(- - - -)	Colorless
NMP	(++++)	Pale brown	(++++)	Cherry red	(+ - - -)	Pink violet
EtOH	(- - - -)	Colorless	(+++ -)	Red-orange	(- - - -)	Colorless
Pyridine	(- - - -)	Coalorless	(++ - -)	Cherry red	(+ - - -)	Pink violet
m-Cresol	(+ - - -)	Pale purple	(++ - -)	Dark purple	(++ - -)	Dark purple
CH_2Cl_2	(- - - -)	Colorless	(- - - -)	Colorless	(++ - -)	Pink violet
TCE	(- - - -)	Colorless	(- - - -)	Colorless	(++ - -)	Violet
THF	(- - - -)	Colorless	(- - - -)	Colorless	(+ - - -)	Pink violet
$CHCl_3$	(- - - -)	Colorless	(- - - -)	Colorless	(+ - - -)	Pink violet
1,4-Dioxane	(- - - -)	Colorless	(- - - -)	Colorless	(+ - - -)	Yellow
HCl	(- - - -)	Colorless	(- - - -)	Colorless	(- - - -)	Colorless
H_2SO_4	(+ +++)	Blue	(++++)	Dark blue	(++++)	Dark blue
TFAc	(+ - - -)	Pale violet	(++ - -)	Blue	(+++ -)	Dark violet
H_3PO_4	(- - - -)	Colorless	(++ - -)	Pale blue	(++ - -)	Violet
CH_3COOH	(- - - -)	Colorless	(- - - -)	Colorless	(+ - - -)	Pale Pink violet

[a] 0.1 mg in 1 mL of solvent. (++++): soluble at RT, (+ + - -): partly soluble (0.4 – 0.6 mg/mL), (+ - - -): slightly soluble (0.2 – 0.4 mg/mL), (- - - -): insoluble

5.3 Analyses of UV-vis Absorption Spectra

5.3.1 UV-vis Absorption Spectra of Bp-4B

Figures 4.6–4.8 show the UV-vis spectra of benzopurpurin 4B in different solvents. The UV-vis absorption spectra of Bp-4B in dipolar aprotic solvents have shown two characteristic absorption bands around 340 nm and 533 nm (Figure 4.6). It can be noticed that the absorption spectra are more resolved as the polarity of the solvent increased gradually from NMP to DMSO.

Similar to the UV spectra of dipolar aprotic solvents, UV spectra of Bp-4B in polar protic solvents (Figure. 4.7) give two absorption peaks with a 30 nm blue shift in the longer absorption peak. This can be due to the solvent effects where the solute-solvent interactions are stronger in dipolar aprotic solvents and better solvation can be resulted.

The absorption spectra of Bp-4B in acids (Figure 4.8) are quite different from the UV-vis spectra of the compound in dipolar aprotic and protic solvents (Figures 4.6 and 4.7). The first absorption peak (higher energy peak) appeared in dipolar aprotic and protic solvents was diminished in acids and the second absorption at longer wavelength was red shifted describing the effect of hydrogen bonding and probable protonation in acidic solutions.

Figure 4.14 shows the UV-vis absorption spectrum of Bp-4B in solid-state. Unlike the absorption in solutions (Figure 4.6–4.8), absorption in solid-state is completely different indicating different intermolecular interaction in solid-state. The two specific absorption peaks in solution were changed to a broad and single absorption peak at 500 nm caused by the strong π-π stacking intermolecular interactions in solid- state.

5.3.2 UV-vis Absorption Spectra of BP-OHPDI

Figures 4.9–4.13 show the UV-vis spectra of BP-OHPDI in different solvents. In order to compare better, overlap was made for all the recorded UV-spectra and categorized.

The UV-vis absorption spectra of BP-OHPDI in nonpolar solvents were shown in Figure 4.9. In all the nonpolar solvents, the compound has shown three well resolved absorption peaks at around 462, 490, and 526 nm respectively. A high energy shoulder around 350 nm indicates the presence of trace amounts of benzopurpurin in the designed structure of BP-OHPDI. Another shoulder around 607 nm was noticed for BP-OHPDI in all the three solvents indicating the possibility of charge transfer. It can be noticed that the absorption spectra show another small high energy shoulder around 420 nm. When the polarity of the solvent is increased gradually from dioxane to TCE, a considerable red shift was observed by 7 nm. This indicates that the compound is more stabilized by polar salvation.

Absorption spectra of BP-OHPDI in dipolar aprotic solvents (Figure. 4.10) show some similarities in the absorption peaks except the shoulders appeared in the spectra of nonpolar solvents. The two high energy shoulders noticed for the absorption spectra in non-polar solvents (350 nm and 420 nm) were disappeared. The higher wavelength shoulder at 607 nm was also diminished and the perylene chromophoric groups were more resolved and were intensified as the polarity of the solvent increased gradually from NMP to DMSO. In the high polar solvent DMSO, there was a considerable red shift noticed.

UV spectra of BP-OHPDI in acids are somewhat different from the other UV-vis spectra (Figure 4.11). Except in phosphoric and sulfuric acids, the compound has shown three absorption peaks similar to the spectra in nonpolar and polar aprotic solvents. The higher energy shoulders noticed before were diminished and the longer wavelength shoulder was appeared in trace amounts in trifluoroacetic acid solution. In phosphoric acid solution, BP-OHPDI exhibited only two absorption peaks, whereas, in sulfuric acid solution, the compound exhibited completely red shifted absorption peaks. These changes can be attributed to the effect of hydrogen bonding and probable protonation.

A fine overlap of UV-vis spectra of BP-OHPDI in three kinds of solvents (Figures 4.12–4.13), namely, nonpolar, dipolar aprotic and acidic/protic solvents explore the above properties in a better understandable way. Especially, the comparison including trifluoroacetic acid shows the differences in molecular interactions of the compound in three different kinds of solvents presented.

Figure 4.15 shows the UV-vis absorption spectrum of BP-OHPDI in solid-state. Unlike the absorption in solutions (Figure 4.9 – 4.13), absorption in solid-state has shown a great change indicating the differences in intermolecular interactions both in solution and in solid-state. The three absorption peaks noticed in solution (in chloroform: 426, 490, 526) were changed to two red shifted absorption peaks at 510, 549 nm and a very weak shoulder at 650 nm respectively, caused by the strong intermolecular interactions in solid- state.

From Table 4.2, molar absorptivity values of BP-OHPDI show interesting absorbance characteristics. In nonpolar solvents such as chloroform, THF, TCE, and 1,4-Dioxane; and in acidic solutions, molar absorptivity is considerably low when compared to dipolar aprotic solvents. This could be attributed to the low solubility of

the compound in respective solutions. In dipolar aprotic solvents, relatively the solubility is increased owing to the corresponding solute-solvent interactions in high polar solvents. Therefore, the molar absorptivity is increased correspondingly.

Table 4.6 reveals the energy needed for BP-OHPDI to enter to the singlet excited state (singlet energy). As expected, in most of the solvents the values were in the same range.

5.4 Analysis of Emission Spectra

5.4.1 Emission spectra of Bp-4B

The emission spectra of Bp-4B were shown in Figures 4.16 to 4.18. Corresponding to their absorption spectra, emission spectra were also compared in different kinds of solvents by categorizing the types of solvents. In order to compare the emission spectra with the synthesized compound, emission spectra were recorded at the same excitation wavelength λ_{ex} = 485 nm.

In nonpolar solvents, emission spectra were not recorded like the absence of absorption spectra because of poor solubility. Emission spectra of Bp-4B in dipolar aprotic solvents show the excimer emission around 605 nm (Figure. 4.16). When the polarity of the solvent is increased, the excimer emission was red shifted considerably. It is clear from the emission spectrum of NMP that the excimer emission is not well resolved like in other solvents. Provided, there is a high energy emission shoulder was noticed. When the polarity was increased, in DMF, a better excimer emission was observed comparing to the emission in NMP together with a similar high energy shoulder emission. The increase in polarity of a dipolar aprotic solvent enhances the solute-solvent molecular interactions and stabilizes the medium better (Figure. 4.16).

In protic solvents, Bp-4B has shown excimer emission around 573 nm (Figure. 4.17). Like the emission spectra in dipolar aprotic solvents, there were no high energy emission peaks noticed around 535 nm. Emission spectra in acids (Figure. 4.18) are quite different from other emission spectra recorded in various solutions. Similar to the results of absorption spectra, emission spectrum in sulfuric acid is completely red shifted and in other two acids there were high energy emission peaks noticed around

532 nm. The differences mainly arise due to the strong acidity of solution in sulfuric acid and therefore corresponding strong hydrogen bonding interactions.

5.4.2 Emission spectra of BP-OHPDI

All the emission spectra were measured with same excitation wavelength, 485 nm for a better comparison with the reactant spectra. Similar to the absorption spectra reported, emission spectra of BP-OHPDI (Figures 4.19–4.23) were taken in the same solvents and categorized them to understand the photophysical processes occurring for the compound.

Emission spectra in nonpolar solvents were shown in Figures 4.19. Spectra indicate the three emission peaks with wavelength maxima 530, 535, and 539 nm respectively. With a gradual increase in polarity of the solvent, it can be noticed that the emission is red shifted by 5 nm with each increase in polarity from dioxane to TCE indicating the solvent polarization effect discussed previously.

Except in DMSO, the emission spectra measured in dipolar aprotic solvents (Figure. 4.20) were similar to the emission spectra recorded for nonpolar solvents. Three emission peaks were noticed and a little red shift in emission was observed for dipolar aprotic solvents comparing to the emission in nonpolar solvents indicating the better stability of the compound by polar salvation effect when the polarity is increased. Interestingly, in high dipolar aprotic solvent, DMSO, an excimer like emission was observed. The results are in good agreement with the corresponding absorption spectra of the solutions.

Emission spectra of BP-OHPDI in acids (Figure. 4.21) were in well support of related absorption spectra. Similar to the previous results, except in phosphoric acid and sulfuric acids, BP-OHPDI exhibited two well resolved emission peaks followed by a weak shoulder around 630 nm. In fact, trifluoroacetic acid solution shows very

weak shoulder at the same longer wavelength (630 nm). In phosphoric acid solution, the compound delivered excimer like emission. Similarly, in sulfuric acid solution, a completely red shifted excimer emission was noticed at 626 nm.

A better clarity can be observed from the overlap emission spectra of BP-OHPDI solutions in the reported three different kinds of solutions (Figure. 4.22–4.23). It is very clear that increase in polarity causes increase in red shift of emission. In chloroform solution the 0→0 emission peak was observed at 535 nm, whereas, in DMF it is 538 nm and in trifluoroacetic acid, the emission maximum was observed at 550 nm. Starting from nonpolar solution to acidic solution, a red shift of 15 nm was observed.

The fluorescence quantum yields measured in three different kinds of solvents (nonpolar, dipolar aprotic and acidic solutions) were interesting and the values were 0.25, 0.157, and 0.062 respectively (Table 4.1). As it is expected for a dipolar aprotic solvent, the fluorescence quantum yield decreased in DMF and the unusual decrease in acidic solutions can be explained by possible protonation interactions of the compound with the solvent.

The theoretical radiative lifetimes of the compound in many solvents (Table 4.3) reveal that in acidic solutions longer lifetimes were noticed attributing to the probable hydrogen bonding and corresponding protonation interactions. Interestingly, in dipolar aprotic solvents lower theoretical radiative lifetimes were observed as expected revealing the high polarity of the solvents. On the other hand, moderate values were obtained in nonpolar solvents. It is noted in Table 4.4 that the theoretical fluorescence lifetimes were 0.25, 0.157, and 0.062 in three different kinds of solutions (nonpolar, dipolar aprotic and acidic solutions) respectively. The

corresponding theoretical fluorescence rate constant values were also presented in Table 4.5.

A comparison on absorbance and emission of BP-OHPDI in chloroform solution was shown in Figure 4.24. The emission was not a complete mirror image of the absorbance. A Stoke's shift of 10 nm was noticed from the absorbance and emission spectra of the compound.

5.5 pH Sensing Property

The designed pH sensor has shown mostly two colors at day light in most of the solvents (Table 5.1). In lowest pH, sulfuric acid, at day light the color of the solution is dark blue. On the other hand, the color was changed to violet in acidic solutions within pH range 0–3. With a gradual increase in pH, the violet became lighter and became pink-violet when the pH was increased up to 9 (Table 5.1).

Under UV light at 365 nm, except in acidic solutions the color was mostly fluorescent yellow and fluorescent greenish-yellow. Interestingly, in acidic solutions under 365 nm, the color was intense orange (Table 5.1).

A representation of the color variation at pH = 7 of BP-OHPDI in DMF was shown in Figure 4.25 and Figure 4.26. At day light, the color of the solution in DMF was pink-violet and changed to fluorescent green-yellow at 365 nm (under UV light).

Different fluorescent colors at different wavelengths in day light and under UV light of BP-OHPDI can make it a potential pH sensor.

5.6 Analysis of Excitation Spectra

Excitation spectra for benzopurpurin 4B were not measured due to the inconvenience arised with the selection of standardizing emission wavelength.

On the other hand, excitation spectra of the synthesized BP-OHPDI were measured by fixing the emission wavelength at 620 nm. The spectra obtained were well resolved and were shown in Figures 4.27–4.30.

In nonpolar solvents, the excitation spectra of BP-OHPDI were similar to the absorption spectra (Figure. 4.27) even with a better benzopurpurin traces around 339 nm. Three peaks were obtained at around 460 nm, 485 nm, and 520 nm respectively, where the wavelength maxima were very close and even equal to the absorption wavelength maxima. Similar results were noticed in dipolar aprotic solvents (Figure. 4.28) except the longer wavelength peak around 603 nm in NMP and DMAc. Interestingly, the wavelength maxima were blue shifted considerably (by 15 nm) in high polar solvent, DMSO. Excitation spectra in acids were also well resolved and three peaks were obtained with an appreciable red shift (Figure. 4.29).

A better clarity can be observed from the overlap excitation spectra of BP-OHPDI solutions in the reported three different kinds of solutions (Figure. 4.30).

5.7 Analysis of DSC Curves and TGA Thermograms

Thermal properties of the synthesized compound were studied by DSC and TGA measurements (Figures 4.31–4.34).

DSC curves of Bp-4B in three different runs (heat, cool, and re-heat) show no glass transition temperature and melting up to 400 ^{o}C (Figure 4.31).

DSC curve of BP-OHPDI shown in Figure 4.31 indicates the absence of glass transition temperature and melting processes up to 400 ^{o}C (Figure. 4.32).

TGA thermogram of Bp-4B indicates that the starting decomposition temperature is 350 ^{o}C (Figure. 4.33).

TGA thermogram shown in Figure 4.33 indicates that the decomposition starts at 390 ^{o}C. Only one step of weight loss was noticed and up to 600 ^{o}C, weight loss of 95% was observed. At 900 ^{o}C, the compound possessed a char yield of about 2.5% (Figure. 4.34). The high thermal stability is attributed to the rigidity of the compound arising from two perylene chromophores attaching to a benzopurpurin system.

Chapter 6

CONCLUSION

The goal of this thesis is to synthesize and characterize a novel fluorescent perylene derivative consisting of benzopurpurin 4B for sensing applications, as a pH sensor. To reach the target compound, the work was started with the synthesis of a perylene monoimide via a two step reaction mechanism. Later, the targeted compound was achieved by a one step condensation reaction mechanism.

The results of this thesis include:

(i) The synthesis of the fluorescent perylene derivative (BP-OHPDI) consisting of benzopurpurin 4B was successfully carried out.

(ii) The optical, photophysical, and thermal properties of the novel BP-OHPDI were studied in detail. Spectral studies were carried out for benzopurpurin 4B for comparison.

(iii) To explore the pH sensing ability of the synthesized compound, optical properties based on pH were studied.

(iv) The synthesized BP-OHPDI has shown partial solubility in nonpolar, dipolar aprotic solvents, and in acidic solutions. On the other hand, benzopurpurin 4B has shown good solubility in dipolar aprotic solvents and moderate solubility in protic solvents like methanol and ethanol.

(v) Whereas, OH-PMI has shown solubility in very few solvents such as DMF, DMSO, and in alkaline solutions (5% KOH and NaOH).

(vi) Absorption spectra of BP-OHPDI in nonpolar solvents showed a charge transfer peak along with the perylene chromophoric absorption peaks, some high energy shoulders and traces of benzopurpurin absorption. Increasing the polarity of solvent resulted in considerable red shift in absorption (7 nm).

(vii) Absorption spectra of BP-OHPDI in dipolar aprotic solvents showed mainly the peaks of perylene cromophore unlike the absorption in nonpolar solvents. But, similar to the absorption in nonpolar solvents, red shift in absorption was notified by increasing the polarity of the solvent.

(viii) Absorption spectra of BP-OHPDI in acids showed similar results except in phosphoric acid and sulfuric acid. In sulfuric acid, especially, a complete red shifted absorption was noticed.

(ix) Emission spectra of BP-OHPDI in nonpolar solvents showed three emission peaks relating to the perylene chromophore. In dipolar aprotic solvents, similar result was noticed and interestingly in high polar solvent, DMSO, excimer emission was observed. Increase in polarity resulted in appreciable red shift in emission, which is in support of absorption spectra measured. Emission spectra in acids were also similar to the emission spectra in other solvents except the excimer like emissions observed in phosphoric and sulfuric acids.

(x) The absorption spectra of the synthesized BP-OHPDI and Bp-4B in solution and in the solid state show extreme differences in view of peak shapes which is attributed to intermolecular π interaction in the solid-state.

(xi) BP-OHPDI has shown interesting pH sensing property. Mostly it has shown two colors at day light; violet in acidic solutions (pH=1–3) and pink-violet in organic

solvents with a gradual increase in pH (up to 9). On the other hand, in sulfuric acid (pH=0) the color of the solution is dark blue. This itself shows that the compound is a potential pH sensor.

(xii) Under UV light at 365 nm, except in acidic solutions the color was mostly fluorescent yellow and fluorescent greenish-yellow. Interestingly, in acidic solutions under 365 nm, the color was intense orange. On the other hand, in sulfuric acid intense red color was observed.

(xiii) Thermogravimetric analysis of BP-OHPDI shows higher thermal stability of the compound. Additionally, exhibit no glass transition temperature in DSC curve.

REFERENCES

Acemioglu, B., Adsorption of Congo red from aqueous solution onto calcium-rich fly ash. *J.Colloids Interface Sci.274 (2004): 371- 379.*

Agostiano, A., Mavelli, F., Milanoa, F., Giottac, L., Trotta, M., Nagyd, L., Maroti, P.pH-Sensitive Fluorescent Dye as Probe for Proton uptake in Photosynthetic Reaction Centers. Bioelectrochemistry 63 (2004):125– 128.

Ahmad, M., & Tan, T.W.Optical pH Sensing Material Prepared From Doped Sol-Gel Film For Use in Acid- Base Titration. *Asean* Journal *on Science and echnology for Development 18(2001).*

Ahrens, M. J., Fuller, M. J., Wasielewski, M. R. Cyanated Perylene-3-4-dicarboximides and Perylene-3,4:9,10-bis(dicarboximide): facile Chromophoric Oxidants for Organic Photonics and Electronics. *Chemistry of Materials.* 15 (2003): 2684-2686.

Amiralaei, S., Uzun, D., & Icil, H. Chiral Substituent Containing perylene Monoanhydride Monoimide and its Highly Soluble Symmetrical diimide: Synthesis, Photophysics and Electrochemistry from Dilute solution to solid state. *Photochemical and Photobiological Sciences.7 (2008): 936-947*

Asir, S., Demir, A. S., & Icil, H. The Synthesis of Novel, Unsymmetrically substituted, Chiral Naphthalene and perylene Diimides: photophysical, Electrochemical, Chiroptical and Intermolecular Charge Transfer properties. *Dyes and pigments. 84 (2009): 1- 14.*

Austin, E., Dakin, J. Interrogation of Optical pH Sensor Based on Sol-GEL Doped New Luminescent Chelate with Compact Photo Counting System.

Bhat S, Otsuka T, Srinivasan A. Benzopurpurin and related compounds inhibit the binding of gp120 to galactosyl ceramide/sulfatide and infection of human immunodeficiency virus. *DNA Cell Biol. 13 (1994): 211-6.*

Bodapati, J B (2005) Ms Thesis, Eastern Mediterranean University.

Chen, Y., Kong, Y., Wang, Y., Ma, P., Bao, M., & Li, X., Supramolecular self-Assembly study of a flexible perylenetetracarboxylic diimide dimer in Langmuir And Langmuir–Blodgett films. Journal of Colloid and Interface Science.330 (2009): 421–427

Dinçalp, H., kizilok S., & Icli, S., Fluorescent macromolecular perylene diimides containing pyrene or indole units in bay positions. *Dyes and pigments. 86 (2010): 32- 41.*

Icil, H., & Arslan, E., Synthesis and Properties Spectroscopic properties OF Highly Pure Perylene Fluorescent Dyes. *Spectroscopy Letters, 34(3), 355–363 (2001).*

Icil, H., & Icil, S. Synthesis and Properties of a new Photostable Polymer: Perylene - 3, 4, 9, 10-tetracarboxylic Acid-bis-(N, N- dodecylpolyimide). *J.poly.sci. A: polym.Chem.35 (1997):2137-2142.*

Lakwicz, J.R. Principle of Fluorescence Spectroscopy (2006).

Langhals, H., & Pust, T., Axially Extended Perylene Dyes. *Eur. J. Org. Chem. (2010): 3140–3145.*

Lau, K.T., Shepherd, R., Diamond, D., & Diamond, D. Solid State pH Sensor Based on Light Emitting Diodes (LED) As Detector Platform. *Sensors 6: (2006)* 848-859.

Lee1, S.T., Gin,G., Nampoori, V. P. N., Vallabhan1, C, P, G., Unnikrishnan N,V., & Radhakrishnan, P. A sensitive fibre optic pH sensor using multiple sol–gel coatings.J. Opt. A: Pure Appl. Opt. 3 (2001): 355–359.

Maruthamuthu, M., & Subramanian, E., Binding of Benzopurpurin 4B to poly (N-vinyl-2-pyrrolidone): A spectral study on the mechanism of dye binding. *Colloid & Polymer Science (1990): 256-263.*

Misra, V., Mishra, H., Joshi, H.C., & Pant, T.C. An Optical PH Sensor based on Excitation Energy Transfer in Nafian Film. *Sensors and Actuators B82 (2002): 133-141.*

Misra, V., Mishra, H., Joshi, H.C., & Pant. Excitation Energy Transfer between a Criflavine and Rhodamine 6G as a pH Sensor .*Sensors and Actuators B 63(2000):18–23.*

Mckitterick, C. B., Erb-Satullo, N. L., LaRacuente, N. D., Dickinson, A. J., & Collings, P. J. Aggregation Properties of the Chromonic Liquid Crystal Benzopurpurin 4B *J. Phys. Chem. B(* 2010):1888-1896.

Pasaogullari, N., Icil, H., & Demuth, M. Symmetrical and unsymmetrical perylene diimides: Their synthesis, photophysical and electrochemical properties. *Dyes and Pigments 69 (2006): 118-127.*

Posch, H.E., & Wolfbeis, O.S., Optical Sensors, 13: Fibre-Optic Humidity Sensor based on Fluorescence Quenching. *Sensors and Actuators*. *15 (1998): 77-83*.

Rashwan, F.A., Mohran H. S., & El-samahy A.A., Electrochemical Characteristics of Some Purpurins in Aqueous and Nonaqueous Solutions. *American Journal of Applied Sciences 2 (7) (2005): 1174-1177.*

Safavi, A., & Bagheri, M., Novel Optical pH Sensor for High and Low pH Values *Sensors and Actuators B 90: (2003) 143–150.*

Scaiano, J.C. (1989) (Ed.) Handbook of Organic Photochemistry, CRC Press.

Shi, W., He, S., Wei, M., Evans, D. G., & Duan, X. Optical pH Sensor with Rapid Response Based on a Fluorescein- Intercalated Layered Double Hydroxide. *Advanced Functional Materials. (2010).*

Shtykov, S. N., Rusanova, T. Yu., Smirnova, T. D., & Gorin, D. A. Sensing Element of a Benzopurpurin 4B-Based Optical Sensor for Determining the Acidity of Etch Solutions. *Journal of Analytical Chemistry, Vol. 59, No. 2, 2004, pp. 175–178.*

Turro, N.J. (1965) Molecular Photochemistry, Benjamin, London, 44.

Zohra, B., Aicha, K., Fatima, S., Nourredine, B., & Zoubir, D., Adsorption of Direct Red 2 on bentonite modified by cetyltrimethylammonium bromide. *Chemical Engineering Journal. 136 (2008): 295–305.*

Wencel, D.,Higgins, C.,Klukowska, A.,Maccraith, B.D.,& Mcdonagh, C.Novel Sol-gel Derived Films for Luminescence- based Oxygen and pH Sensing. *Materials Science-Poland 25: (2007).*

Wen-Ke, F., Yi-Yu, F., Shu-Feng, W., Wei, F., Wen-Hui, Yi., & Qi-Huang Gong. Intramolecular Photoinduced Electron-transfer in Azobenzene-perylene Diimide. C*hin. Phys. B 19: (2010)* .

Würthner, F. Perylene Bisimide Dyes as Versatile Biulding Blocks for Functional Supramolecular Architectures. *Chemical Communications. (2004): 1564-1579*.

Xiong, Yan., Huang, Ying., Ye, Zhongbin., & Guan, Yafeng. Flow Injection Small-volume Fiber-optic pH Sensor Based on Evanescent Wave Excitation and Fluorescence Determination Springer. Science Business Media, LLC (2010).